Modeling of Complex Electrolytes

A Numerical Simulation Study

Von der Fakultät Energie-, Verfahrens und Biotechnik der Universität Stuttgart und dem Stuttgart Center for Simulation Science (SC SimTech) zur Erlangung der Würde eines Doktors-Ingenieurs (Dr.-Ing.) genehmigte Abhandlung

Vorgelegt von
Anand Narayanan Krishnamoorthy
aus Delhi

Hauptberichter : Prof. Dr. Christian Holm
Mitberichter : apl. Prof. Dr. -Ing. Niels Hansen
Prof. Dr. -Ing. Joachim Gross
Prof. Dr. Joachim Dzubiella

Tag der mündlichen Prüfung: 14. Juli 2020
Institut für Computerphysik der Universität Stuttgart

2021

I would like to dedicate this thesis to my loving parents, wife and friends …

Declaration

I hereby declare that except where specific reference is made to the work of others, the contents of this dissertation are original and have not been submitted in whole or in part for consideration for any other degree or qualification in this, or any other university. This dissertation is my own work and contains nothing which is the outcome of work done in collaboration with others, except as specified in the text and acknowledgements. I also declare no conflict of interest and any included publications are the my own work, except where indicated throughout the thesis and summarised and clearly identified on the declarations page of the thesis.

Anand Narayanan Krishnamoorthy

2021

Acknowledgements

This thesis is a compilation of my research work done in the group of Prof. Christian Holm in Institute for Computational Physics (ICP) - University of Stuttgart during the years 2014-2018. I would like to convey my gratitude to Prof. Christian Holm and Dr. Jens Smiatek for granting me an opportunity to work in their group and also for their sincere guidance. I would like to specially thank my funding consortia SFB716 and SIMTECH excellent cluster - University of Stuttgart for funding this research project during my tenure at ICP, also SIMTECH graduate school for accepting me as a graduate student for 'Atomistic and Mesoscopic Simulations of Polyelectrolytes' project.

I am grateful to Prof Timo Jacob for hosting me as a guest researcher for few months in University of Ulm in the department of electrochemistry to provide useful insights on reactive forcefields, also would like to convey my regards to my fellow colleagues in the department of electrochemistry in Ulm who made my stay confortable and knowledgable there.

I would like to thank all my experimental collaborators Dr. Klaus Dieter Kreuer, Dr. Andreas Wohlfarth, Kristina Oldiges, Prof. Dr. Martin Winter, Dr. Isidora Cekic-Laskovic for useful discussions and providing interesting insights on experimental observations. Also would like to convey my regards to Prof. A Heuer, Prof J Belher and Dr. Matthias Rupp for their interesting discussion during the course of this work. Furthermore I wish to thank my doctoral committee members Prof. Jochaim Gross, Prof. Schmauder for providing useful comments on my thesis. I also thank my co-workers J. Zeman, M Baur, Dr. F Uhlig for sharing their respective expertise to this research project.

This is a special journey in my life, with lots of special people who made my life memorable and interesting during the course of my research. I convey my sincere thanks to my current, and former colleagues especially the administrative staff at the ICP, for the pleasant working environment. Last but not the least I thank all the special people my friends, my family and my wife for their support and making my life in Germany a joyful ride.

Anand Narayanan Krishnamoorthy

Publications

This thesis is based on the following publications:

- A. Narayanan Krishnamoorthy, J. Zeman, C. Holm and J. Smiatek, Preferential solvation and ion association properties in aqueous dimethyl sulfoxide solutions, Phy. Chem. Chem. Phys 18 (45), 31312-31322 (2016).
- A. Narayanan Krishnamoorthy, C. Holm and J. Smiatek, Influence of cosolutes on chemical equilibrium: a Kirkwood–Buff theory for ion pair association–dissociation processes in ternary electrolyte solutions, J. Phys. Chem. C 122 (19), 10293-10302 (2018).
- A. Narayanan Krishnamoorthy, C. Holm and J. Smiatek, Specific ion effects for polyelectrolytes in aqueous and non-aqueous media: the importance of the ion solvation behavior, Soft matter 14 (30), 6243-6255 (2018).
- A Narayanan Kirshnamoorthy, K Oldiges, M Winter, A Heuer, I Cekic-Laskovic, C Holm and J Smiatek, Electrolyte solvents for high voltage lithium ion batteries: ion correlation and specific anion effects in adiponitrile, Phys. Chem. Chem. Phys 20, (40) 25701-25715 (2018).
- G Sivaraman, A Narayanan Krishnamoorthy, M Baur, C Holm, M Stan, G Csányi, C Benmore, and Á Vázquez-Mayagoitia, Machine Learning Inter-Atomic Potentials Generation Driven by Active Learning: A Case Study for Amorphous and Liquid Hafnium dioxide, arXiv preprint arXiv:1910.10254.

Other publications:

- A. Narayanan Krishnamoorthy, Influence of antifreeze proteins on local water dyanmics in presence of osmolytes, Task Quaterly, 17 (1-2), 5-42 (2013).
- A. Narayanan Krishnamoorthy, C. Holm and J. Smiatek, Local water dynamics around antifreeze protein residues in the presence of osmolytes: the importance of hydroxyl and disaccharide groups, J. Phys. Chem B 118 (40), 11613-11621 (2014).

Abstract

Electrolytes are chemical substances when dissolved in solvents produce conductive solutions by dissociating into cations and anions. Under an applied potential positively charged ions move towards the electrode having abundance of electrons and the negatively charged ions move towards the other electrode. This motion of ions is measured via ionic conductivity in the system, an important property for applications in standard lithium ion batteries (LIB), PEM fuel cells and in the development of other novel battery materials. Electrolytes solution show extreme variations in thermodynamic and dynamical properties upon change in concentration, temperature, pressure and chemical environments. Understanding the structural and dynamical properties of these complex electrolytes in solution and solutions mixtures are very important to further enhance the efficiency of future batteries. Experiments provide interesting insights on conductivites, mass densities, diffusion behavior under various concentrations and stabilities of solutes in solutions and solution mixtures but mostly fail to provide strong understanding of underlying molecular picture and mechanism of these occurences.

Using numerical simulations and statistical thermodynamical approaches we try to address the potentially relevant scientific questions with regard to the choice of suitable electrolytes for highly efficient battery applications. In this thesis we discuss these following problems:

- What are the factors affecting ion dissociation and association behvior. How can we rationalize ion-ion interactions in these systems and how do they affect the corresponding charge transport behavior?
- What are the descriptors for optimum choice of solvents, and which solvents increase the ion mobility and excess salt solubilities?
- Do the molecular properties of the solvent influence ion solvation effects?
- Do co-solvents and further components change the ion dissociation behavior?

- What about the validity of standard electrostatic mean field theories for these kind of systems?

This thesis provides some insights and solutions to these questions and our results will be also relevant for molecular level understanding of some experimental research on these complex solutions. Specifically the first chapter lists several factors affecting ion association behaivor in these complex systems using standard electrolyte complexes. Here we study the dynamic and structural properties of promising novel elctrolytes that consist of lithium conducting salts (LiBF4 and LiTFSi in organic solvent by a combination of atomistic molecular dynamics (MD) simulations. The simulations outcome reveals an increased tendency of ion complex formation in LiBF4 in comparison to LiTFSI from measured ionic conductivities. These results can be mainly attributed to the solvation behaviour of the individual anions. It is also revealed that the ion association and dissociation behavior does not just dependent on the dielectric property of solvents but that also the specific chemical interactions of ions and solvent play a major role.

To further elucidate the importance of specific ion effects with relevance to ion solvation and ion pairing effects, we study a reference system by introducing rigid and rod-like models of polyanions and polycations in combination with alkali metal cations and halide anions as counterions in water, methanol and N,N-dimethylacetamide (DMAc) solvents. Pronounced specific ion effects can be observed in terms of the individual anion and cation condensation behavior towards polyions in different solvents. A detailed investigation of the individual energy contributions shows that ion–dipole interactions play a pivotal role in rationalizing the findings. The outcome of our simulations thus reveal significant deviations from standard electrostatic mean-field theories. This deviation highlights the importance of solvent–ion interactions in addition to electrostatic attraction. Our findings are also in agreement with standard empirical concepts like donor and acceptor number of solvents. All our findings highlight the crucial importance of specific ion effects in combination with molecular details of solvation for specific ion association behavior.

Since organic solvents play an important role in battery technology it is crucial to understand the influence of additives and cosolutes on the ion assocation and ion solvation behavior. To enunciate this fact we study the solvation and the association properties of ion pairs in non ideal aqueous dimethyl sulfoxide (DMSO) solution by atomistic molecular dynamics (MD) simulations. The ion pair consists of two lithium and a single sulfonated diphenyl sulfone ion which are dimeric units of novel polyelectrolytes of PEM fuel cells whose properties are studied under the influence of different DMSO concentrations. Our simulation outcomes reveal an aqueous homoselective solvation of the ion species which fosters the occurrence of pronounced ion association constants coupled with reduced conductivites at higher DMSO

mole fractions. As in this case the presence of a cosolute influences the ion association behavior, it is necessary to understand the generic behavior of ion pairing in ideal and non ideal solution mixtures.

For this we use the Kirkwood Buff theory, which is introduced to describe the influence of cosolutes on the chemical equilibrium between dissociated and associated ion pairs in ternary electrolyte solutions. This approach makes use of Kirkwood Buff integrals and the introduction of a local bulk partition model. Kirkwood-Buff (KB) theory provides a theoretical route to analyze the specific interactions between the solute and the cosolutes in terms of the preferential solvation or preferential binding coefficients. It is an approach derived from fluctuation theory of solutions to measure macrosopic thermodynamic entities from microscopic quantities that can be calculated via numerical simulations. For this approach, the cosolute species can be either charged or uncharged, and our approach is applicable for ideal and weak non-ideal solutions in combination with low ion concentrations. As the main result, the theory reveals that differences in the local cosolute accumulation behavior around the ions induces a shift of the chemical equilibrium either to the associated or the dissociated state. All results are verified by atomistic molecular dynamics simulations in terms of sodium chloride ion pairs in dimethylacetamide (DMAc) water mixtures.

Although molecular dynamics simulations provide understanding of the chemical interaction mechanisms, structure and dynamics of a electrolyte systems at a molecular level, they are confronted with many challenges related to the limitations in understanding chemical reactions and ion transport mechanisms in detail since the empirical potentials used in these methods are rigid and reactions cannot be included. Though quantum mechanical methods can still be used, are constrained in system size and the available computational power. To bridge this gap between the scales and accuracies in numerical simulations, this thesis provides a outlook towards machine learning based potentials (Gaussian based aprroximated potentials - GAP) and compare the accuracies of other forcefields for ideal noble liquid mixtures of argon and krypton. These methods can further be used to model and study bulk systems with quantum mechanical accuracies which can provide a deeper understanding of ion transports mechanisms in complex electrolyte solutions.

Zusammenfassung

Die vorliegende Dissertationsschrift beschäftigt sich mit grundlegenden Solvatationsvorgängen in mehrkomponentigen Elektrolytlösungen. Die Ergebnisse dieser Arbeit zielen insbesondere auf ein vertieftes Verständnis von ionenspezifischen Effekten, als auch den Einfluss von Ko-Soluten und Ko- Lösungsmitteln auf das Dissoziationsverhalten von Polyelektrolyten und Ionenpaaren. Die entsprechenden Ergebnisse von atomistischen Molekulardynamik-Simulationen werden mittels der molekularen Theorie von Lösungen (Kirkwood-Buff-Theorie) in grundlegende Beschreibungen der statistischen Physik der Flüssigkeiten eingeordnet. Des Weiteren liegt ein großer Schwerpunkt dieser Schrift auf der Auswertung des dynamischen Verhaltens der Ionen als auch der Entwicklung von verbesserten Kraftfeldern mittels verschiedener Algorithmen aus dem Kanon des maschinellen Lernens.
In einer ersten Studie werden anionen-spezifische Effekte von zwei Lithiumsalzen in Adiponitril untersucht, wobei gezeigt wird, dass insbesondere verschiedene Solvatationscharakteristika der beteiligten Ionen einen entscheidenden Einfluss auf das Dissoziationsverhalten und dementsprechend auch auf die ionische Leitfähigkeit haben. Die vorliegenden Ergebnisse erweitern dabei das Grundlagenverständnis von neuen Lithium-Ionen-Batterieelektrolytlösungen.
Das Solvatationsverhalten von Polyelektrolyten mit verschiedenen Alkali- und Halidionen in drei unterschiedlichen Lösungsmitteln wird in einer weiteren Studie dieser Dissertationsschrift untersucht. Die entsprechenden Erkenntnisse deuten darauf hin, dass neben elektrostatischen Wechselwirkungen auch die chemische Natur des Lösungsmittels im Rahmen von Dispersions- und Polarisationswechselwirkungen einen massiven Einfluss auf das Dissoziationsverhalten hat. Basierend auf diesen Erkenntnissen können Lösungsmittel als eher Kationen- oder Anionen-spezifisch charakterisiert werden, wobei die molekularen Eigenschaften des Solvens die Dissoziation des Polelektrolyten entweder fördern oder unterdrücken können. Zusätzlich zum Haupt-Lösungsmittel beinhalten modere Elektrolytlösungen in technischen Anwendungen auch zusätzliche Ko-Solute oder Ko-Lösungsmittel um z. B. die elektrochemische Stabilität des Gemischs zu erhöhen. Die Auswirkungen dieser zusätzlichen Komponenten im Hinblick auf das Ionendissoziationsverhalten werden in einem weiteren Kapitel untersucht. Dabei zeigt sich, dass insbesondere das Bindungsverhalten

des Ko-Lösungsmittels einen großen Einfluss auf das Dissoziationsverhalten hat. Ähnliche Resultate zeigen sich auch bei den Auswirkungen von Lösungsmittelgemischen auf komplexe Salze. Bei bestimmten Konzentrationen entstehen unterschiedliche Zusammensetzungen der ersten Solvatationsschalen, welche die Affinität der Ionen zu den Gegenionen entweder fördern oder unterdrücken können. Im Ausblick dieser Arbeit wird der Einsatz von Algorithmen des maschinellen Lernens im Hinblick auf die Elektrolytforschung erläutert und am konkreten Beispiel einer Kraftfeldparametrisierung demonstriert.
Die Ergebnisse dieser Arbeit vertiefen dabei den gegenwärtigen Stand der Grundlagenforschung und erweitern unser Verständnis von modernen Elektrolytmischungen.

Table of contents

Publications **ix**

Abstract **xi**

Zusammenfassung **xv**

List of figures **xxi**

List of tables **xxvii**

1 Introduction **1**

2 Adiponitrile as electrolyte solvents for high voltage batteries **5**

2.1 Introduction 5

2.2 Theoretical Background 7

2.3 Kirkwood Buff Theory 9

2.3.1 Derivatives of chemical activities 10

2.3.2 Thermodynamic and structural properties of the solution 11

2.4 Simulation details 12

2.4.1 Atomistic molecular dynamics simulations 12

2.5 Results 13

2.5.1 Structural and thermodynamic properties of ions 13

2.5.2 Dynamic properties of the electrolyte solution 20

2.6 Summary and conclusion 21

2.7 Acknowledgement 23

3 Specific ion effects for polyelectrolytes in aqueous and non-aqueous media **25**

3.1 Introduction 25

3.1.1 Counterion condensation theory 27

3.1.2 Fraction of condensed counterions and coordination numbers 27
3.1.3 Calculation of the dielectric constant 28
3.2 Simulation Details 29
3.3 Results 31
3.3.1 Counterion distribution 31
3.3.2 Ion solvation behavior 34
3.3.3 Enthalpic contributions to specific ion effects 38
3.3.4 Ion solvation and counterion distributions in connection with the donor and acceptor number concept 41
3.4 Summary 42
3.5 Acknowledgement 43

4 Preferential solvation and ion association properties in aqueous dimethyl-sulfoxide 45
4.1 Introduction 45
4.2 Theoretical Background 47
4.3 Simulation Details 48
4.4 Results 49
4.4.1 DMSO/water mixture without ions 49
4.4.2 Properties of ion pairs in aqueous DMSO solutions 51
4.4.3 Ion pairing and ionic conductivity 55
4.5 Summary and Conclusion 57
4.6 Acknowledgement 57

5 Influence of co-solutes on chemical equilibrium 59
5.1 Introduction 59
5.2 Theoretical Background 61
5.2.1 Chemical reaction: Ion pair dissociation-association equilibrium . . 61
5.2.2 The influence of co-solutes on the chemical equilibrium 62
5.2.3 Implications for dissociation-association reactions 65
5.3 Simulation results 67
5.4 Summary and conclusion 71
5.5 Acknowledgement 73

6 Outlook 75
6.1 Introduction 75
6.2 Training data 78
6.3 GAP Parameters 78

6.4 Machine learning simulation setup 79
6.5 Results 80
6.6 Summary 81

7 Conclusion 83

References 87

Appendix A Influence of co-solute on ion assocation-dissociation chemical equilibrium 103
A.1 Details of the simulated systems 103
A.2 Radial distribution functions for sodium and chloride ions 105
A.3 Distance-dependent ion association constant in pure water without constraints on ion positions 107
A.4 Analysis of m-value for different associated ion pair reference states 109
A.5 Analysis of the derivative of the chemical activity for different associated ion pair reference states 111
A.6 Polyion-solvent and polyion-counterion coordination numbers 111
A.7 Potential of mean force between ions and solvent molecules 114
A.8 Total energies: ion-solvent and ion-polyelectrolyte interactions 114
A.9 Interaction energies between ions 116
A.10 Ratio between LJ and electrostatic energies including ion-polyelectrolyte and ion-solvent interactions 117
A.11 Closest contact distance between ions and polyion 119
A.12 Closest contact distance between ions and solvent molecules 120

Appendix B Additional Information 121
B.1 CHELPG partial charges for atoms of adiponitrile 121
B.2 Mass densities: experimental and simulation results 121
B.3 Coordination number of adiponitrile molecules around lithium ions 123
B.4 Center-of-mass radial distribution functions between lithium ions and anions 123
B.5 Radial distribution functions for LiTFSI: lithium ions and nitrogen atoms of $TFSI^-$ and adiponitrile 124
B.6 Radial distribution functions for $LiBF_4$: lithium ions and fluorine atoms of BF_4^- and nitrogen atoms of adiponitrile 124
B.7 Relative coordination numbers in $LiBF_4$-ADN mixtures: local environment around lithium and BF_4^- ions 126

B.8 Relative coordination numbers in LiTFSI-ADN mixtures: local environment around lithium and $TFSI^-$ ions 126
B.9 Potentials of mean force between ions 129
B.10 Ion self-diffusion coefficients 129
B.11 Correlation between relaxation time scales 129

List of figures

2.1 Chemical structure of adiponitrile ($NC(CH_2)_4CN$). The two terminal nitrile groups (C≡N) are main locations for lithium ion coordination[1]. 6

2.2 Molecular snapshots of BF_4^- anions (left side), ADN molecules (middle panel) and TFSI anions (right side). Fluorine atoms are colored in light blue, carbon atoms in grey, nitrogen atoms in dark blue, sulfur atoms in red, hydrogen atoms in white, and boron atoms in pink. 7

2.3 Values for the derivative of the chemical activity $a_{\alpha\alpha}$ for LiTFSI (red line with squares) and $LiBF_4$ (black line with circles) at various salt concentrations c_s. The solid lines are guides for the eyes. 14

2.4 Transfer free energies ΔF_{tr}^* for ions of LiTFSI (red line with squares) and $LiBF_4$ (black line with circles) at various salt concentrations c_s. The solid lines are guides for the eyes and the transfer free energies are calculated by the indistinguishable ion approach, as it is in more detail outlined in the main text. 15

2.5 Left: Center-of-mass coordination number $n_-(r)$ of TFSI anions around lithium ions for different salt concentrations as denoted by the color code in the legend. Right: Center-of-mass coordination number $n_-(r)$ of BF_4^- anions around lithium ions for different salt concentrations as denoted by the color code in the legend. 16

2.6 Left: Center-of-mass radial distribution function for ADN molecules around TFSI anions for different salt concentrations as denoted in the legend. Right: Center-of-mass radial distribution function for ADN molecules around BF_4^- anions for different salt concentrations as denoted in the legend. 18

2.7 Left: Local/bulk partition coefficients $K_+^p(r)$ at different distances r around lithium ions for different concentrations of LiTFSI (nitrogen as reference atom) as indicated by different colors. Right: Local/bulk partition coefficients $K_+^p(r)$ at different distances r around lithium ions for different concentrations of $LiBF_4$ (fluoride as reference atom) as indicated by different colors. . . . 19
2.8 Ideal Nernst-Einstein (blue lines with triangles) and effective Einstein-Helfand ionic conductivities (red lines with circles) for varying concentrations of LiTFSI (left panel) and $LiBF_4$ (right panel) in ADN. Experimental results are shown as squares with black lines. The solid lines are guides for the eyes. 21
2.9 Schematic representation of anion solvation by ADN molecules. The ellipsoidal TFSI anion and the spherical tetrafluoroborate anion are colored in blue, whereas ADN molecules are colored in red. 22

3.1 Molecular snapshots of methanol (left side) and DMAc (right side). Carbon atoms are colored as green spheres, nitrogen atoms as blue spheres, hydrogen atoms as white spheres, and all oxygen atoms are colored in red. 26
3.2 Snapshots of the simulation box with typical configurations for lithium (left) and iodide (right) ions (light red spheres) in the presence of water and the model polyanion (left) and the model polycation (right), respectively (both represented by light blue spheres). 31
3.3 Fraction $Q(\ln(r/r_0)$ of condensed cations (top) and anions (bottom) around the oppositely charged and rod-like model polyelectrolyte in a) water (left side), b) methanol (middle) and c) DMAc (right side). The value of r_0 for each ion corresponds to the closest contact distance between the polyelectrolyte and the specific ion. The circles at the lines denote the corresponding values of $\ln(\lambda_B/r_0)$, which are used for the evaluation of the fraction of condensed counterion Q^{M} in Fig. 3.4. 32
3.4 Fraction of condensed counterions Q^M at the Bjerrum length in water (top), in methanol (middle) and in DMAc (bottom). The blue lines denote the values of θ in accordance with standard MO counterion condensation theory (Eqn. (3.3)). 33
3.5 Coordination numbers $\mathrm{CN_s}(r/r_s)$ (Eqn. (3.6)) of solvent molecules around the cations in water (top), methanol (middle) and DMAc (bottom). The distance r_s denotes the closest contact distance between ions and solvent molecules. 35

3.6 Coordination number $CN_s(r/r_s)$ (Eqn. (3.6) of solvent molecules around the anions for water (top), methanol (middle) and DMAc (bottom). The distance r_s denotes the closest contact distance between ions and solvent molecules. 36
3.7 Top: Excess numbers (Eqn. (3.8)) of water (H_2O) and methanol (MeOH) molecules around the individual ion species. The red line denotes $N^{xs} = 0$ as a help for the eye. Bottom: Excess numbers (Eqn. (3.7)) of DMAc molecules around the individual ion species. All standard deviations are within symbol size. 37
3.8 Lennard-Jones short-range (LJ (SR)) and Coulomb short-range (Coulomb (SR)) energies between ions and water molecules (top), ions and methanol molecules (middle) and ions and DMAc molecules (bottom). 39
3.9 Lennard-Jones short-range (LJ (SR)) and Coulomb short-range (Coulomb (SR)) interaction between ions and the polycation or polycation, respectively, in water (top), in methanol (middle) and in DMAc (bottom). 40

4.1 Snapshot of the sulfonated diphenyle sulfone (SDS^{2-}) and two lithium ions (Li^+). 49
4.2 Diffusion coefficient for DMSO (blue triangles) and water (red circles) in a DMSO-water mixture for different mole fractions x_{DMSO}. 50
4.3 Derivative of the chemical activity a_{ss} for DMSO (red circles) and water (blue triangles) in a DMSO-water mixture for different mole fractions x_{DMSO} for DMSO. 51
4.4 Dielectric constant ε_r of the solution for different mole fractions x_{DMSO}. The black line represents the values for an ideal solution whereas the red circles denote the results for the pure solution and the blue triangles the results for the DMSO-water solution in presence of the ion pair as calculared by Eqn. 4.6. 52
4.5 Radial distribution functions at different mole fractions x_{DMSO} for the center-of-masses of DMSO and water molecules around lithium ions (top) and SDS^{2-} (bottom). The different mole fractions are denoted by the symbols described in the legend. Blue lines correspond to the RDFs between water and the ions whereas all red lines represent the results for the RDFs of DMSO molecules around the ions. 52
4.6 Local/bulk partition coefficient for DMSO (left side) and water (right side) around lithium ions (top) and the SDS^{2-} dimer (bottom) for different DMSO mole fractions x_{DMSO}. 54

4.7 Association constant found in the simulation by the fraction of condensed counterions θ_c for different mole fractions x_{DMSO}. All counterions within the actual Bjerrum length were considered as condensed in the simulations. 56
4.8 Ionic conductivity σ for combined lithium ion and dimer contributions for different DMSO mole fractions x_{DMSO}. The solid line is only a guide for the eye. 56

5.1 Schematic illustration of ion dissociation in presence of co-solutes (black spheres). The cation (blue sphere) and the anion (red sphere) are located in the local region (a) and form a contact ion pair on the left side. The more pronounced binding of co-solutes to the dissociated ions favors a dissociation of the ion pair (right side). The chemical potential in the bulk region (b) remains constant. 63
5.2 Derivative of the chemical activity $a_{\alpha\alpha}$ for the individual components water (α=Water) and DMAc (α=DMAc) in DMAc/water mixtures with different mole fractions of the constituents. 68
5.3 Derivative of the chemical activity of DMAc divided by the bulk number density a_{33}/ρ_3 for different mole fractions of DMAc x_3. 69
5.4 Corresponding values of m in accordance with Eqn. (A.4) for different mole fractions of DMAc. More details on the calculation can be found in the text. 70
5.5 Values for the logarithm of the chemical equilibrium constant for increasing values of the DMAc bulk number density. 71
5.6 Values for the derivative of the chemical activity as obtained from the KB approach according to Eqn. (A.5) in comparison to the values obtained from Eqn. (A.6) for DMAc mole fractions between $x_{\mathrm{DMAc}} = 0 - 0.4$. The solid line represents a linear fit and the correlation coefficient yields $R^2 = 0.98$. . 72

6.1 Energy correlations of pure argon liquid 80
6.2 Force correlations of pure argon liquid 80
6.3 Radial distribution function of a pure argon liquid. 81

A.1 Radial distribution function for sodium and chloride ions in solutions with varying mole fractions of DMAc x_{DMAc} (MD without constraints) as denoted in the legend. 106
A.2 Values of $\ln K^0_{\mathrm{sim}}(r)$ in accordance with Eqn. (A.2) and Eqn. (A.3) for sodium-chloride pairing in pure water ($x_{\mathrm{DMAc}} = 0$). The red solid line denotes the value $\ln K^0 = 6.01$ as obtained by linear regression analysis of the corresponding m-values in the main text. 107

A.3 Values of m in accordance with Eqn. (A.4) for different mole fractions of DMAc and with regard to different associated ion pair reference states (CP, IS and 1SP) as denoted in the legend. More details can be found in the text. 110
A.4 Values for the derivative of the chemical activity $a_{33}(\mathrm{KB})$ (KB approach with Eqn. (A.5)) in comparison to the values for a_{33} as obtained by linear regression (Eqn. (A.6)) for DMAc mole fractions between $x_{\mathrm{DMAc}} = 0.08 - 0.3$. The black solid line corresponds to an exact agreement with slope equals unity on a logarithmic scale. 112
A.5 Coordination numbers $\mathrm{CN}(r)$ between polyion and solvents (solid lines) and between polyion and counterions (lines with datapoints). The left side shows the results for the cations and on the right side the results for the anions are presented. The results for water are shown in the top, methanol in the middle and DMAc in the bottom. 113
A.6 Sum of Lennard-Jones short-range (LJ (SR)) and Coulomb short-range (Coulomb (SR)) energies between ions and polyelectrolyte and ions and solvent in water (top), in methanol (middle) and in DMAc (bottom). 115
A.7 Lennard-Jones short-range (LJ (SR)) and Coulomb short-range (Coulomb (SR)) energies between ions in water (top), in methanol (middle) and in DMAc (bottom). 116
A.8 Ratio of Lennard-Jones to electrostatic interactions concerning the total interaction energy of the ions, including ion-solvent, and ion-polyelectrolyte interactions (top), and between the ions and the solvent molecules (bottom). 117
A.9 Closest contact distance r_0 between ions and polyions for all solvents and all ion species. 119
A.10 Closest contact distance r_s between ions and solvent molecules for all solvents and all ion species. 120

B.1 Mass densities of all simulated adiponitrile-lithium salt electrolyte formulations. Black symbols represent experimental results, whereas red symbols indicate simulation outcomes. The values for LiTFSI and LiBF4 electrolyte solutions with different salt concentrations c_s are marked as squares and circles, respectively. 122
B.2 Left side: Coordination number of adiponitrile molecules $n_{\text{Li-ADN}}(r)$ around lithium ions for various salt concentrations of LiTFSI. Right side: Coordination number of adiponitrile molecules $n_{\text{Li-ADN}}(r)$ around lithium ions for various salt concentrations of $\mathrm{LiBF_4}$. 123

B.3 Left side: Center-of-mass radial distribution functions between lithium ions and TFSI anions for different salt concentrations c_s of LiTFSI in adiponitrile. Right side: Center-of-mass radial distribution functions between lithium ions and BF_4^- anions for different salt concentrations c_s of $LiBF_4$ in adiponitrile. 123

B.4 Left side: Atomic radial distribution functions between lithium ions and nitrogen atoms of TFSI anions for different salt concentrations c_s of LiTFSI in adiponitrile. Right side: Atomic radial distribution functions between lithium ions and nitrogen atoms of adiponitrile for different salt concentrations c_s of LiTFSI in adiponitrile. 124

B.5 Left side: Atomic radial distribution functions between lithium ions and fluorine atoms of BF_4^- anions for different salt concentrations c_s of $LiBF_4$ in adiponitrile. Right side: Atomic radial distribution functions between lithium ions and nitrogen atoms of adiponitrile for different salt concentrations c_s of $LiBF_4$ in adiponitrile. 125

B.6 Relative coordination number for species $n_j(r)/n_{\text{tot}}(r)$ as denoted in the legend for different LiBF4 concentrations of $c_s = 0.14$ mol/L (top), $c_s = 0.30$ mol/L (middle), and $c_s = 0.74$ mol/L (bottom) around lithium (left side) and BF_4^- ions (right side). 127

B.7 Relative coordination numbers for species $n_j(r)/n_{\text{tot}}(r)$ as denoted in the legend for different LiTFSI concentrations from top to bottom with $c_s = 0.15$ mol/L, $c_s = 0.33$ mol/L, $c_s = 0.85$ mol/L, and $c_s = 1.61$ mol/L around lithium (left side) and BF_4^- ions (right side) 128

B.8 PMF values Δ_{PMF} between lithium ions and anions for different concentrations c_s of LiTFSI (left side) and $LiBF_4$ (right side). 129

B.9 Self-diffusion coefficients for all ions at various salt concentrations c_s. The values for lithium ions are shown as circles (red color for lithium ions of LiTFSI and black color for lithium ions of $LiBF_4$). The corresponding results for the anions are shown as squares. The lines are just guides for the eye. . . 130

List of tables

2.1 Coordination numbers $n_{\mathrm{ADN}}(r_{1\mathrm{st}})$ for ADN molecules around BF_4^- and TFSI anions at first minimum position in the radial distribution functions with $r_{1\mathrm{st}} \approx 0.81$ nm for LiTFSI and $r_{1\mathrm{st}} \approx 0.68$ nm for $LiBF_4$. The relative decrease of the coordination number R is calculated with respect to the value for the lowest salt concentration. 18

3.1 Dielectric constant ε_r from the simulations (Eqn. (4.3)) and dielectric constants $\varepsilon_r^{\mathrm{exp}}$ from experiments [68, 167] at 298.15 K, resulting Bjerrum lengths λ_B, Manning parameters ξ, and fractions of condensed counterions θ (Eqn. (3.3)) for the solvents in the simulations. The values for the acceptor (AN) and donor numbers (DN) are presented in Ref. 140 and were derived by standardized experimental procedures. The SPC/E model [18] is used for water, whereas methanol (MeOH) and N,N-dimethylacetamide (DMAc) are modeled as KB force fields published in Refs. 200, 84. The errorbars for the dielectric constant are of the order of the first digit. 29
3.2 Partial charges of atoms for SPC/E water as taken from Ref. 18. 30
3.3 Partial charges of molecular groups for methanol as taken from the KB force field presented in Ref. 200. 30
3.4 Partial charges of molecular groups for DMAc as taken from the KB force field presented in Ref 84. 30

6.1 GAP Parameters 79
6.2 Diffusion coefficients of argon liquid * $10^{-5} cm^2/s$ 81
6.3 Performance of ML potentials 81

A.1 System setup for DMAc-water mixture simulations. 104
A.2 Diameters (taken from Ref. 57) for all ion species [57]. 118

B.1 CHELPG partial charges for atoms of adiponitrile. All other parameters are identical to Ref. 82. 121
B.2 Relaxation τ_{TST} and corresponding ion correlation times τ for distinct concentrations c_s of LiTFSI and $LiBF_4$ in adiponitrile. 130

Chapter 1

Introduction

In the last century, study of electrolyte solutions was one of the central areas of research in physical chemistry[205]. The role of charge species in aqueous chemistry, measuring ion mobility and conductivity was the driving force for this reseach. With the need for advanced and efficient batteries for future transport, electronics and civil amenities, understanding the structural and dynamical nature of complex electrolytes was an absolute necessity. The choice of efficient, system dependent, batteries depended on a suitable choice of these electrolytes. Experimentalists performed numerous measurements on various complex electrolytes to observe different subtle effects and microscopic details to understand the molecular picture of these complex systems which were never understood from coarser measurements on other condensed phase systems. This led to the rapid interest in theoreticians to understand the molecular picture of these systems and to provide a rationale for the experimental findings. This led to the advent of limiting laws for dilute electrolyte solutions, this helped in understanding experimental findings, and also Debye and Hückel's theory of the structure of ionic solutions was one of the first successful usage of self-consistent field ideas. Though there were significant molecular models developed to understand this complex nature of ionic solutions, still some rather fundamental questions like ionic interactions, ion solvation and transport were not very clearly understood for these systems.

Furthermore, standard electrolyte formulations in current energy storage device include organic solvents and combinations of distinct lithium salts with certain additives to attain maximum efficiencies[44]. Despite a long time of intense research, and as a main source for recent incidents , highly flammable liquid electrolytes, which are composed of lithium salts, several organic solvents, and varying amounts of additive molecules are commonly used [206, 207, 32]. Due to their low cost, standard solvents for commercial LIBs most often include distinct alkyl carbonates like propylene carbonate (PC), ethylene carbonate (EC) or

dimethyl carbonate (DMC), whose mixtures show beneficial physicochemical properties like low viscosities and sufficient ionic conductivities [206, 207, 148].

In order to increase the safety and overall performance of LIBs, research focusing on the properties of novel solvents and electrolyte additives in terms of low flammabilities and higher electrochemical stabilities is of prime importance[19, 206, 207, 44, 182, 183, 208]. It is known for a long time that the choice of solvent significantly influences dissociation rates as well as polyelectrolyte conformations[174]. Thus, in order to further improve such electrolytes, a detailed understanding of chemical solvent solute interactions is a pre-requisite.

Also, specific ion effects attracted a lot of attention over the last years [104, 130, 111, 190, 37, 93, 83, 9]. Although already known for more than a century, the literature on specific ion effects has grown rapidly in the last two decades [116]. The recent interest can be mainly rationalized with regard to the broad importance of these effects for distinct systems [104]. For instance, specific ion effects dominate the adsorption behavior at surfaces [158, 159], modify precipitation of macromolecular compounds [104], promote salting in or salting out of proteins [37], or influence the counterion condensation behavior around highly charged polyelectrolytes [71, 12]. Also aqueous electrolyte solutions of simple salts reveal a plethora of specific ion effects and ion pairing mechanisms [113, 189]. One can distinguish between contact, solvent-shared and solvent-separated ion pairs, whereas the theoretical description of ion pair formation is challenging and even nowadays under debate [35, 54, 113, 190]. In order to complement theoretical predictions, computer simulations allow us to achieve deeper insights into the underlying behavior [189] of molecular mechanisms and specific chemical interactions between species in these systems. They also help us to bridge physical concepts to understand experimental findings with proper validations. But this approach comes up with its own technical challenges. Though the computational resources are enormous with the advent of fast supercomputers, it is still improbable to model specific chemical reactions and other bioprocesses. Thus it is necessary to use different approaches of multiscale modeling to study electrochemical interactions. Quantum mechanical based ab0initio methods are used in understanding electrochemical stability and ion transport mechanism in liquid electroyltes. For studying ion specific interactions and ion solvation properties, molecular dynamics approach is used. Although these approaches provide a molecular level picture of liquid electrolytes, a direct comparison of the results to experiments is not straight forward. Here Kirkwood Buff (KB) theory of solutions and KB integrals are used for generating macroscopic thermodynamic properties like activity coefficients, and transfer free energies from microscopic quantities like measured radial distribution fuctions. These quantities can also be obtained from experiments using reverse Kirkwood-Buff theory proposed by Arieh Ben Naim[54]. In this thesis, a modified version of KB theory on an

atomistic scale is used to understand the chemical equilibrium shift of ion dissociation and ion asscociation process under the influence of co-solutes. Here, we address all the aforementioned research questions and provide solutions using advanced numerical methods coupled with standard theoretical models to support our findings.

This thesis outline is as follows: Chapter 2 focusses on current trends in liquid electrolytes and electrolyte solvents for high voltage lithium ion batteries: ion correlation and specific anion effects in adiponitrile based solvents. Chapter 3 discusses on specific ion effects for polyelectrolytes in aqueous and non-aqueous media and the importance of the ion solvation behavior. Influence of co-solutes on ion association properties is studied in Chapter 4 followed by the development of the theory based on KB integrals for understanding the chemical equilibrium shift of ion dissociation and ion asscociation process in ternary electrolyte solutions mixtures. Finally the results are summarized and an outlook for future prospects and methods based on machine learning is given.

Chapter 2

Adiponitrile as electrolyte solvents for high voltage batteries

2.1 Introduction

The suitable choice of electrolytes for potential lithium ion battery technology requires facilitated charge transport in order to enable high battery performance. In this chapter we will look into the influence of solvents and specific ion interactions on ion association and dissociation behviours using simple lithium salts based electrolytes used in fuel cells and high voltage lithium battery applications. Here we also discuss in detail one of the alternatives to linear and cyclic alkyl carbonates are aliphatic dinitriles ($NC(CH_2)_4CN$) (Adiponitrile - ADN), which combine high flash and boiling points with pronounced electrochemical stabilities [160, 1, 77, 58, 26, 48, 207, 103, 49, 51, 67]. It is one of the potential donor solvent due to its low melting temperature and high ionic conductivitites[51].

The structure of adiponitrile is shown in Fig. 2.1. Nucleophilic terminal nitrogen atoms can be regarded as a source of lithium coordination in turn contributing for the solubility of lithium salts which could results in more mobile free ions in turn leading to higher conductivities[1].

With regard to the broad electrochemical stability window of adiponitrile ($\Delta_{ESW} > 6$ V vs. Li^+/Li[1, 58, 48]), it has to be noticed, that ADN does not decompose at the electrodes in the relevant potential range [203], which advocates the use of this solvent in LIBs for high energy density applications [1, 121, 51, 32]. In combination with this property, the limited compatibility of ADN with the anode also prohibits the use of standard graphite electrodes, which require the formation of a solid electrolyte interphase (SEI) by decomposition products of the solvent, the additive molecules, or the anions of the salt [203].

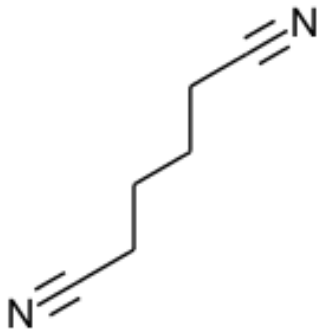

Fig. 2.1 Chemical structure of adiponitrile ($NC(CH_2)_4CN$). The two terminal nitrile groups ($C\equiv N$) are main locations for lithium ion coordination[1].

In contrast to technological progress, molecular insights and combined theoretical as well as numerical studies on solvation and ion pairing processes in ADN and further aprotic organic solvents are relatively scarce. Noteworthy, a series of seminal studies was performed for various concentrations of distinct lithium conducting salts in closely related acetonitrile solutions [165, 164, 163]. The authors observed the following ion association tendency with increasing association strength $LiPF_6 < LiFSI < LiTFSI \leq LiClO_4 < LiBF_4 \ll LiCF_3CO_2$, which remains valid for nearly all concentrations with slight variations. Interestingly, the value of the ionic conductivity decreases accordingly, which highlights the fact, that the amount of unpaired ions contributes significantly to the transport behavior.
Recent computational studies by some of us highlighted the importance of complex mutual correlation processes in terms of ion solvation and ion pair formation processes in mixtures of different solvents [175, 99, 101, 100, 92, 90, 124]. In this regard, molecular theories of solutions in combination with atomistic molecular dynamics (MD) simulations are powerful tools in order to shed more light onto molecular behavior.

The corresponding molecular snapshots of the anions and ADN are shown in Fig. 2.2. Here, we study the behavior of low and moderate lithium salt concentrations up to 1.6 mol/L, depending on the solubility of the salt, which roughly agrees with the corresponding salt concentrations in commercial LIBs [206, 207]. We explicitly focus on ion correlation mechanisms and specific anion effects, which are mostly dominated and influenced by the solvation and molecular properties of ADN. With regard to this aim, we focus on two standard lithium conducting salts with distinct anion sizes and different solvent accessible surface areas. The salt $LiBF_4$ is known to reveal high ionic mobilities, but rather low dissociation constants in organic carbonate solvents with regard to the relatively small tetrafluoroborate anion [206]. In contrast, LiTFSI shows a good dissociation behavior and sufficient ionic

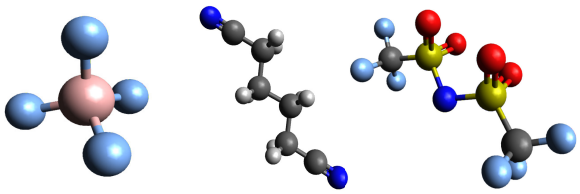

Fig. 2.2 Molecular snapshots of BF_4^- anions (left side), ADN molecules (middle panel) and TFSI anions (right side). Fluorine atoms are colored in light blue, carbon atoms in grey, nitrogen atoms in dark blue, sulfur atoms in red, hydrogen atoms in white, and boron atoms in pink.

conductivities in combination with a bulky $TFSI^-$ anion [206]. Hence, the choice of these two salts allows us to study size effects and the corresponding implications concerning ion association and solvation behavior in more detail. In this context, previous studies on ionic liquids as solvents already showed that the certain physicochemical properties of distinct ions in terms of anion-specific effects have indeed a crucial impact on the properties of the solution [99, 100]. In consequence, our study enlightens main principles of ion solvation in aprotic organic solvents, and provides more insights into ADN-based electrolyte formulations for high voltage applications.

2.2 Theoretical Background

One of the most important values for electrolyte solutions is given by the ionic conductivity, which rationalizes the amount of charge transport.

A simple approach to compute the ideal ionic conductivity relies on the Nernst-Einstein method, which for a $1:1$ salt like LiTFSI or $LiBF_4$ in an electrolyte solution reads

$$\sigma_{\mathrm{id}} = \frac{z^2 e^2 \rho_s}{k_B T} (D_+ + D_-) \tag{2.1}$$

with Boltzmann constant k_B, absolute temperature T, elementary charge e, valency of the ions $z = |z_-| = z_+$, salt number density $\rho_s = \rho_+ = \rho_-$, where ρ_+ and ρ_- denote the corresponding densities of the ion species, and individual cation and anion self-diffusion coefficients D_+ and D_-, respectively. The self-diffusion coefficient can be computed by

$$D_\alpha = \lim_{t\to\infty} \frac{\langle (\mathbf{r}_\alpha(t) - \mathbf{r}_\alpha(t_0))^2 \rangle}{6t} \tag{2.2}$$

where $\mathbf{r}_\alpha$ denotes the center-of-mass position of the considered molecule or ion α at different times t and t_0.

As it was often discussed [92, 202], the Nernst-Einstein ionic conductivity suffers from neglect of ionic correlations, such that Eqn. (2.1) provides the maximum possible or ideal ionic conductivity in absence of ion correlation effects. In order to consider correlations between ion species, a more refined approach has to be introduced. In more detail, the corresponding Einstein-Helfand method provides direct access to the relative static permittivity ε_r and the effective ionic conductivity σ by applying one linear fit to the mean squared displacement $\left\langle \Delta M^2(t) \right\rangle = \left\langle (\langle \mathbf{M} \rangle - \mathbf{M}(t))^2 \right\rangle$ of the total dipole moment $\mathbf{M}$ of the system. The associated dipolar mean-square displacement is calculated from the current autocorrelation function $\langle \mathbf{J}(t)\mathbf{J}(t_0) \rangle$ with the total current of a system $\mathbf{J}$, which is directly related to the dipole moment with regard to $\partial \mathbf{M}/\partial t = \mathbf{J}$. In neglect of vanishing rotational contributions [151], the translational current is composed only of center-of-mass velocities $\mathbf{v}_\mathrm{com}$ for N_M molecules or ions in accordance with the expression

$$\mathbf{J}_\mathrm{trans}(t) = \sum_{\alpha=1}^{N_\mathrm{M}} q_\alpha \, \mathbf{v}_{\mathrm{com},\alpha}(t), \tag{2.3}$$

and

$$\mathbf{M}_\mathrm{trans}(t) = \sum_{\alpha=1}^{N_\mathrm{M}} q_\alpha \, \mathbf{r}_{\mathrm{com},\alpha}(t). \tag{2.4}$$

which represents the total translational dipole moment of the system. Here, the molecular net charge is denoted by $q_\alpha = z_\alpha e$, while $\mathbf{r}_{\mathrm{com},\alpha}$ describes the respective center-of-mass position. As already stated, the Einstein-Helfand relation focuses on the the dipolar mean-square displacement in the limit of $t \gg t_\mathrm{c}$, with t_c being the autocorrelation time of the current [162, 151] in accordance with

$$\begin{aligned} \left\langle \Delta M^2(t) \right\rangle &= \frac{6V\sigma(t_0)}{\beta} t - 2\int_{t_0}^{\infty} \tau \, \langle \mathbf{J}(t)\mathbf{J}(t_0) \rangle \, \mathrm{d}t \\ &= \frac{6V\sigma(t_0)}{\beta} t + 2\left\langle M^2 \right\rangle \\ &= \frac{6V\sigma(t_0)}{\beta} t + \frac{6V\varepsilon_0}{\beta} \left[\varepsilon_\mathrm{r}(t_0) - 1 \right] \end{aligned} \tag{2.5}$$

where $\sigma(t_0) \equiv \sigma$ and $\varepsilon_\mathrm{r}(t_0) \equiv \varepsilon_r$ are the low frequency ($\omega = 0$) limits of the effective ionic conductivity and dielectric permittivity, respectively, with $\beta = 1/k_B T$ for a system with volume V and vacuum permittivity ε_0. The static Einstein-Helfand or effective ionic

conductivity and dielectric permittivity thus can be identified as

$$\sigma = \frac{\beta}{6V} m \tag{2.6}$$

and

$$\varepsilon_{\mathrm{r}} = 1 + \frac{\beta}{6V\varepsilon_0} m_0 \,, \tag{2.7}$$

with m and m_0 being the slope and intercept of a linear fit to $\left\langle \Delta M^2(t) \right\rangle$, respectively. A straightforward and fast calculation approach for the dielectric constant is also given by

$$\varepsilon_r = 1 + \frac{4\pi}{3} \frac{\langle M^2_{\mathrm{trans}} \rangle}{V k_B T} \,, \tag{2.8}$$

which is applicable for single solvents [127]. This method is used for the computation of the dielectric constant for pure ADN without ions.

2.3 Kirkwood Buff Theory

The Kirkwood-Buff (KB) theory of solutions is one of the most powerful theories related to solvation thermodynamics and other properties of solutions. The theory introduced by Kirkwood and Buff in 1951 relates thermodynamic properties of solutions to molecular pair-distribution functions of the solutions without making any assumptions regarding the non-covalent interaction operative between the atoms/molecules [85]. This theory is exact, it does not assume any pair-wise additivity of the interaction potentials and it is applicable to any number of molecular species of any type and shape. KB theory uses the integrals of the radial distribution functions (RDFs) between the molecular species present in the solutions and relates them to the thermodynamic properties of the solutions such as compressibility, partial molar volumes or the derivatives of the chemical potentials with changing solution compositions which can also be found from experimental studies. The integrals, named as Kirkwood-Buff integrals (KBIs), can also be calculated alternatively from the crossfluctuations of the particle-numbers in solutions. Inversion of the Kirkwood-Buff theory, derived by Ben-Naim, relates the thermodynamic quantities of the solutions to the individual KBIs between the molecular species present in the solutions. By this means, experimental thermodynamic results can be analysed on the basis of KBIs and on the other hand KBIs obtained from theoretical or simulations studies can directly be compared with the experimental results. A detailed derivation of the Kirkwood-Buff theory and molecular distribution functions can be found in the literature [66]. In this chapter important thermodynamic relations regarding

KB theory and the relations between the KBIs and the thermodynamic quantities of the solutions are presented briefly. Elaborate use of this theory and derivations to study the effect of cosolute is discussed in Chapter 5.

2.3.1 Derivatives of chemical activities

From a thermodynamic point of view, ion correlation effects also directly influence the chemical activity of the species in regards of [7, 20]

$$a_\alpha = \exp(\mu_\alpha - \mu_\alpha^*)/RT \tag{2.9}$$

including the chemical potential μ_α of species α, the standard chemical potential μ_α^*, and the molar gas constant R. The deviation from an ideal liquid behavior can be expressed by the activity coefficient[7, 20]

$$\gamma_\alpha = \frac{a_\alpha}{x_\alpha} \tag{2.10}$$

with the mole fraction x_α of species α in the solution. The presence of an ideal solution is expressed by $\gamma_\alpha = 1$ whereas non-ideal behavior can be observed for $\gamma_\alpha \neq 1$. The derivative of the chemical activity in NpT ensemble with constant temperature and pressure p for a binary solution in terms of the indistinguishable ion approach [95, 137, 177, 172] for a 1 : 1 salt is defined as

$$a_{\alpha\alpha} = \left(\frac{\partial \ln a_\alpha}{\partial \ln \rho_\alpha}\right)_{T,p} \tag{2.11}$$

in accordance with an equivalent expression in regards of the KB theory [85, 15, 178, 137, 172]

$$a_{\alpha\alpha} = \frac{1}{1+\rho_\alpha(G_{\alpha\alpha} - G_{\alpha\beta})}, \tag{2.12}$$

including the KB integrals

$$G_{\alpha\beta} = 4\pi \int_0^\infty r^2 \left[g_{\alpha\beta}(r) - 1\right] \mathrm{d}r \tag{2.13}$$

with the radial distribution function $g_{\alpha\beta}(r)$ between individual components α and β of the solution. With regard to Eqn. (A.5), it becomes clear, that an ideal mixture is represented by $a_{\alpha\alpha} = 1$, due to the condition $G_{\alpha\beta} = G_{\alpha\alpha}$, whereas deviations from an ideal behavior are highlighted by $a_{\alpha\alpha} \neq 1$, and hence $G_{\alpha\beta} \neq G_{\alpha\alpha}$. The values of the KB integrals can be interpreted as excess (or deficiency) of particle β around particle α [199]. Hence, assuming that cations and anions contribute equally, one can compute $G_{\alpha\alpha}$ for a salt α according to

[199, 57, 53]

$$G_{\alpha\alpha} = \left(\frac{N_+}{N_\pm}\right)^2 G_{++} + \left(\frac{N_-}{N_\pm}\right)^2 G_{--} + \frac{N_+ N_-}{N_\pm^2}(G_{+-} + G_{-+}) \tag{2.14}$$

with $N_\pm = N_+ + N_-$, where N_+ and N_- denote the number of corresponding ion species in the salt association-dissociation reaction under the constraint $G_{+-} = G_{-+}$ for cations $(+)$ and anions $(-)$ due to reasons of symmetry [16, 95, 172, 177]. The corresponding expression for ion-solvent interactions with solvent molecules of type β is defined by

$$G_{\alpha\beta} = G_{\beta\alpha} = \frac{N_+}{N_\pm} G_{+\beta} + \frac{N_-}{N_\pm} G_{-\beta} \tag{2.15}$$

with $G_{\alpha\beta} = G_{\pm\beta} = G_{\beta\pm}$. It has to be noted that KB theory was originally formulated for the grand canonical μVT ensemble [85, 15, 178, 137], whereas the applicability for isothermal and isobaric ensembles in computer simulations was in detail discussed in Refs. 16, 177, 137. Hence, approximate KB integrals at large but finite distances r_c can be also obtained from NVT or NpT ensemble simulations [137, 172] in accordance with

$$G_{\alpha\beta} \approx G_{\alpha\beta}(r_c) = 4\pi \int_0^{r_c} r^2 \left[g_{\alpha\beta}^{\mathrm{NVT}}(r) - 1\right] \mathrm{d}r \tag{2.16}$$

under the assumption that $g_{\alpha\beta}^{\mathrm{NVT}}(r) = 1$ for all values $r \geq r_c$.

2.3.2 Thermodynamic and structural properties of the solution

The free energy of transferring ions of indistinguishable type α in presence of solvent molecules β from infinite to close (binding) distances between components α and β can be written as

$$\Delta F_{\mathrm{tr}}^* = -k_B T \rho_\alpha (G_{\alpha\alpha} - G_{\alpha\beta}), \tag{2.17}$$

which can be inserted into Eqn. (A.5) in accordance with

$$a_{\alpha\alpha} = \frac{1}{1 - (\Delta F_{\mathrm{tr}}^* / k_B T)}. \tag{2.18}$$

in order to highlight the close connection between the derivative of the chemical activity and the transfer free energy [172]. In consequence, a preferential binding between the ions due to electrostatic attraction is reflected by $\Delta F_{\mathrm{tr}}^* < 0$, whereas a preferential exclusion is represented by $\Delta F_{\mathrm{tr}}^* > 0$. The analysis of the accumulation behavior between the ion species also can be studied by the calculation of the local/bulk partition coefficient [39, 141, 119, 172], which

reads for the local environment around lithium ions in a ternary solution (components $+$,$-$ and β = ADN) with distinguishable ions

$$K_{+}^{p}(r) = \frac{(\langle n_{-}(r)\rangle / \langle n_{\beta}(r)\rangle)}{(n_{-}^{\mathrm{tot}}/n_{\beta}^{\mathrm{tot}})}, \tag{2.19}$$

where $\langle n_x(r)\rangle$ denotes the average number of coordinating ADN molecules ($x = \beta$) or anions ($x = -$) within a distance r around the lithium ions, and n_x^{tot} the total number of solvent molecules or anions in the simulation box. In accordance, the coordination number of molecules or ions β around species α reads

$$n_{\beta}(R) = 4\pi\rho_{\beta}\int_{0}^{R} r^2 g_{\alpha\beta}(r)\,\mathrm{d}r \tag{2.20}$$

as an integrated radial distribution function. Hence, the local/bulk partition coefficient can be also interpreted as ratio between radial distribution functions with regard to $K_{+}^{p}(r) = g_{+-}(r)/g_{+\beta}(r)$. At short distances of usually $r \leq 0.5$ nm, depending on the size of the species, a preferential binding mechanism between ions results in $K_{+}^{p}(r) > 1$, such that significantly more anions over ADN molecules are located around the lithium ions when compared to bulk solution.

2.4 Simulation details

2.4.1 Atomistic molecular dynamics simulations

All atom atomistic MD simulations were performed with the GROMACS 4.6.5 software package [139]. Enforced by deviations between experimental results and calculated values in regards of the dielectric constant and the mass density, standard OPLS/AA based force fields for adiponitrile [82] were reparameterized by refining the partial charges in terms of quantum chemical calculations with the ORCA 3.0.3 software package [125]. The ADN structure was optimized at the level of density functional theory (DFT) using the B3LYP functional [98] in combination with the def2-TZVPP [201] basis set for all atoms. The calculations utilize the atom-pairwise dispersion correction with the Becke-Johnson damping scheme. [60, 59]. The conductor-like screening model (COSMO) [87] was used for all calculations with a dielectric constant of $\varepsilon_r = 30$ in order to consider an implicit ADN environment [1]. Partial atomic charges were then obtained by using the CHELPG method [27] with regard to the geometry-optimized structure. All partial charges in the OPLS/AA force field for ADN were changed accordingly, and corresponding atomistic MD simulations at 300 K of pure ADN

without ions (comparable simulation protocol as described in the remainder of this section) revealed a sufficient agreement for the mass density with $\rho_{\mathrm{M}} = 950$ g/L and dielectric constant $\varepsilon_r = 25$ obtained by Eqn. (4.3) with experimental values $\varepsilon_r = 30$ and $\rho_{\mathrm{M}} = 951$ g/L. For all other components of the electrolyte, we used a combination between the OPLS/AA force field [82] for lithium ions and the corresponding OPLS/AA compatible CL&P force field parameters for the tetrafluoroborate (in the following abbreviated as BF_4) and TFSI anions, the coressponding parameters are described in Ref.[107]. Deviations between experimental and simulation results for structural and thermodynamical properties are in the range between 1% and 2%, which is sufficient for our purposes[105].
Electrostatic interactions for all systems were calculated by the Particle Mesh Ewald method [41] with a Verlet cutoff scheme in combination with a short-range cutoff radius of 1 nm. The same cutoff scheme was also used for the calculation of the Lennard-Jones interactions in combination with energy-pressure dispersion corrections. The Fourier grid spacing was 0.16 nm and all bonds were constrained by the LINCS algorithm [69]. The time step in all simulations was 2 fs. We performed all atomistic MD simulations for typical salt concentrations [206, 207] ranging from $c_s = 0.15$ mol/L -1.61 mol/L for LiTFSI and $c_s = 0.14$ mol/L -0.74 mol/L for $LiBF_4$, depending on the individual solubility of the salts in ADN. In more detail, our experimental outcomes at 300 K revealed limiting saturation concentrations around $c_s \approx 0.6$ mol/L for $LiBF_4$ and $c_s \approx 1.5$ mol/L for LiTFSI in ADN, which highlights the better solubility of LiTFSI when compared with $LiBF_4$. All systems were equilibrated for 10 ns in NPT ensemble with an initial cubic box size of $(5.72 \times 5.72 \times 5.72)$ nm^3 including 996 ADN molecules at 300 K and 1 bar pressure by using the Nose-Hoover thermostat and the Parrinello-Rahman barostat [52, 133]. The number of $LiBF_4$ and LiTFSI ion pairs was adjusted to the aforementioned concentrations by insertion of $15, 30, 65$ and 100 ion pairs in the simulation box. We performed 200 ns NPT production runs for each lithium salt concentration.

2.5 Results

2.5.1 Structural and thermodynamic properties of ions

Adiponitrile has nucleophilic nitrile group. The two triple bond between terminal nitrogen and carbon atoms, consisting of one $\sigma-$ and two π-bonds can be regarded as nucleophilic locations for lithium ion coordination. ADN has a electrochemical stability window $\Delta_{\mathrm{ESW}} >$ 7.3 V which highlights the potential use of ADN as electrolyte solvent in high voltage LIBs [58].

Here we show the values for the derivative of the chemical activity $a_{\alpha\alpha}$ (Eqn. (A.5)) with regard to the indistinguishable ion approach for $LiBF_4$ and LiTFSI at various concentrations are shown in Fig. 2.3. In terms of the condition $\lim_{c_s \to 0} a_{\alpha\alpha} = 1$ in accordance with

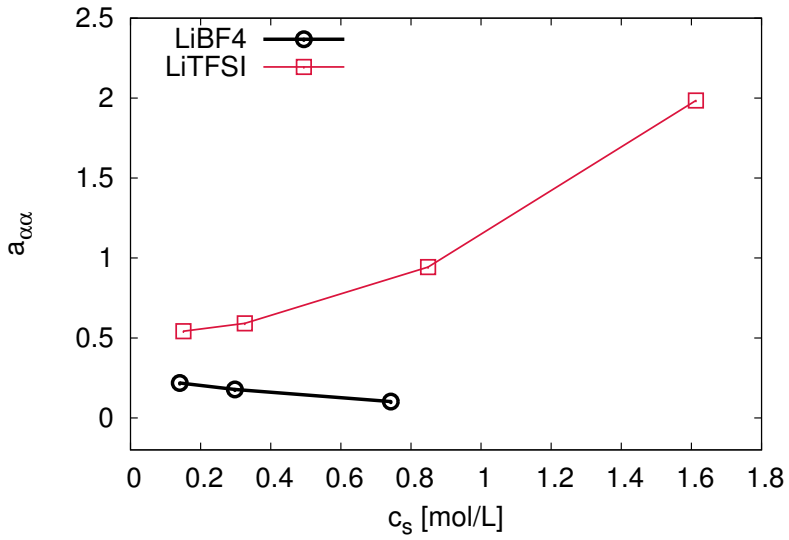

Fig. 2.3 Values for the derivative of the chemical activity $a_{\alpha\alpha}$ for LiTFSI (red line with squares) and $LiBF_4$ (black line with circles) at various salt concentrations c_s. The solid lines are guides for the eyes.

Eqn. (A.5), it becomes obvious that even at low salt concentrations of $c_s \leq 0.14$ mol/L, a significant deviation from ideal conditions can be observed. Moreover, LiTFSI and $LiBF_4$ reveal a completely distinct behavior at higher salt concentrations. Whereas $LiBF_4$ shows a decrease of $a_{\alpha\alpha}$ with increasing salt concentration, an opposite trend can be observed for LiTFSI. The low values for the derivative of the chemical activity for $LiBF_4$ point at pronounced ion correlation effects, such that the ion-ion KB integrals are significantly larger than the corresponding KB integrals for ADN and ions in terms of $G_{\alpha\alpha} \gg G_{\alpha\beta}$. Furthermore, values of $a_{\alpha\alpha} \approx 0$ for $c_s \geq 0.7$ mol/L for $LiBF_4$ indicate the onset of the saturation limit, where higher concentrations of salts leads to strong phase seperation, which is in good agreement with previous experimental results. As it was discussed previously [16, 79], values of $a_{\alpha\alpha} \leq 0$ violate stability conditions and thus point at phase separation behavior for the individual components of mixtures. In contrast to $LiBF_4$, the values for the derivatives of the chemical activity increase for LiTFSI with higher salt concentration. In more detail, ion-ion aggregates thus dominate over ion-ADN contacts for $c_s < 1$ mol/L due to $a_{\alpha\alpha} < 1$, whereas the corresponding behavior changes for higher concentrations in terms of $G_{\alpha\alpha} \approx G_{\alpha\beta}$ and thus $a_{\alpha\alpha} \approx 1$. At high LiTFSI concentration, even values of $a_{\alpha\alpha} > 1$ with $G_{\alpha\alpha} < G_{\alpha\beta}$ can

be observed.
The tendency of ion aggregate formation is also verified with regard to the results for the transfer free energies in terms of the indistinguishable ion approach as shown in Fig. 2.4. The corresponding findings reveal a strong tendency of ion aggregate formation for $LiBF_4$

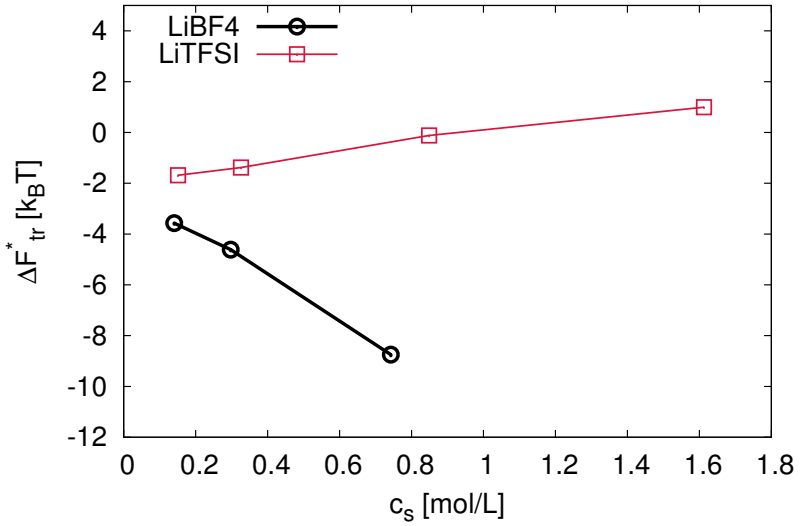

Fig. 2.4 Transfer free energies ΔF^*_{tr} for ions of LiTFSI (red line with squares) and $LiBF_4$ (black line with circles) at various salt concentrations c_s. The solid lines are guides for the eyes and the transfer free energies are calculated by the indistinguishable ion approach, as it is in more detail outlined in the main text.

($\Delta F^*_{\mathrm{tr}} \leq -3.9\,k_BT$ for all salt concentrations) whereas the values of the transfer free energies for LiTFSI reveal only marginally stable ion complexes with $\Delta F^*_{\mathrm{tr}} \geq -1\,k_BT$. In consequence, ions of $LiBF_4$ are bound on time scales $\tau \approx 0.05\,\mathrm{ns} - 8$ ns in accordance with the relation [22]

$$\tau = \tau_0 \exp(\Delta F^*_{\mathrm{tr}}/k_BT) \tag{2.21}$$

with $\tau_0 = \hbar/k_BT \approx 1$ ps, where $\hbar$ denotes the Planck constant. In contrast, the corresponding shorter time scale of several picoseconds for ion complexes of LiTFSI highlights a pronounced dynamic instability in terms of fast ion contact formation and breakage processes, and are thus comparable to corresponding values for low concentrated alkali halide salts in aqueous solution [190].

Further, the anion coordination numbers $n_-(r)$ around lithium ions for both salts are shown in Fig. 2.5.

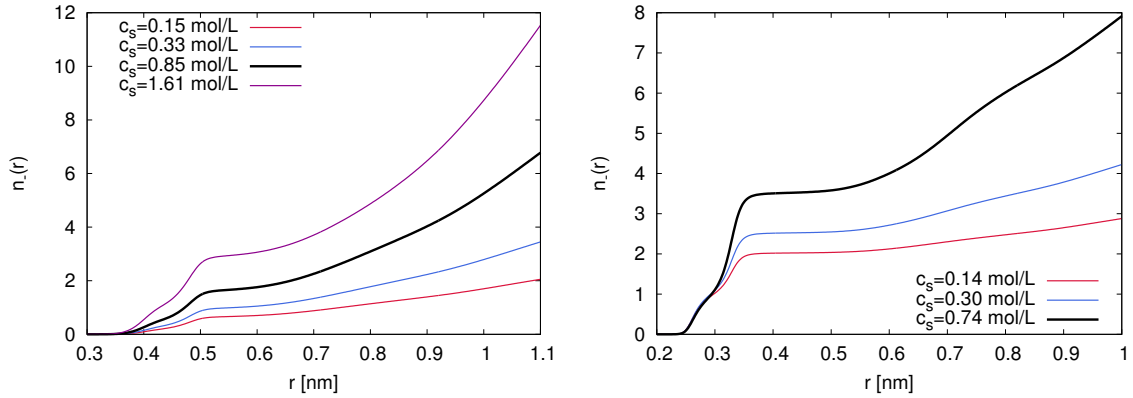

Fig. 2.5 Left: Center-of-mass coordination number $n_{-}(r)$ of TFSI anions around lithium ions for different salt concentrations as denoted by the color code in the legend. Right: Center-of-mass coordination number $n_{-}(r)$ of BF_4^- anions around lithium ions for different salt concentrations as denoted by the color code in the legend.

As can be seen for LiTFSI, an increase of the salt concentration implies a moderate increase of the anion first shell coordination number to a maximum value of $n_{-}(r) \approx 3$ at $r = 0.5$ nm for the highest salt concentration. Moreover, even the values of $n_{-}(r)$ at shorter distances $r \leq 0.5$ nm increase with higher salt concentrations, which highlights a higher occurrence probability of monodentate-coordinated lithium ions by TFSI anions with increasing salt concentration. These findings reveal that the amount of contacts between ions increases moderately for higher salt concentrations.

In contrast, the values for $LiBF_4$ (right of Fig. 2.5) reveal significantly higher values for the anion coordination number when compared with LiTFSI. Thus, even a moderate salt concentration of $c_s = 0.74$ mol/L promotes an anion first shell coordination number of $n_{-}(r_{1st}) \approx 3.5$ at $r_{1st} = 0.35$ nm, whereas the corresponding values of LiTFSI for comparable concentrations are below unity. Moreover, a monotonous increase of $n_{-}(r)$ at distances $r <$ 0.32 nm becomes obvious, which is independent of the salt concentration. These outcomes highlight the dominant and stable presence of ion contacts even at low salt concentrations. In consequence, the corresponding values for the anion coordination number reveal a higher BF_4^- coordination number around lithium ions, which also occurs at shorter length scales when compared to TFSI, and thus provides a rationale for the higher energetic stability in terms of lower transfer free energies.

With regard to these results, the question arises why the salts differ so fundamentally in their aggregation behavior? In order to provide an answer to the aforementioned question, we calculated the radial distribution functions (center-of-mass) for ADN molecules around TFSI and BF_4^- anions as shown in the left and right of Fig. 2.6. A significant difference

between both anions can be observed concerning the maximum height of the first solvation shell peak value. In detail, TFSI anions show nearly constant values for different salt concentrations, whereas BF_4^- ions reveal a significant decrease of the peak height with increasing salt concentrations. These results clearly imply a desolvation of BF_4^- with increasing salt concentration, which can be attributed to the pronounced formation of ion contacts by replacing ADN molecules with lithium ions.

Hence, although the ADN peak heights at shorter distances are slightly higher for BF_4^-, it can be assumed that the ADN coordination numbers around BF_4^- ions are indeed lower when compared to TFSI. This assumption can be rationalized by the larger size of TFSI anions and the corresponding higher values for the solvent accessible surface area (SASA) [75] ($\Sigma \approx 1.8$ nm^2 (BF_4^-) and $\Sigma \approx 3.6$ nm^2 (TFSI) for water molecules with a probe radius of 0.14 nm), as also indicated by the larger distance of the first minimum for ADN coordination shells ($r_{1st} \approx 0.81$ nm) when compared to BF_4^- ($r_{1st} \approx 0.68$ nm). With regard to the molecular structure, the slightly broader first ADN coordination shell for TFSI anions can be attributed to the more ellipsoidal shape of TFSI when compared to the more spherical shape of BF_4^- anions. Hence, the distribution of the center-of-mass distances between the TFSI anions and the ADN molecules shows a higher variation when compared to BF_4^-.
In consequence, and as can be seen by the values in Tab. 2.1, the corresponding ADN first shell coordination numbers $n_{ADN}(r_{1st})$ around TFSI are significantly higher when compared with BF_4^-. Thus, one can assume, that the larger number of coordinating ADN molecules contributes significantly to the enthalpic part of the solvation free energy for the anions, which is hence more favorable for TFSI when compared to BF_4^-. With regard to the differences between the maximum and minimum values of ADN coordination numbers for different salt concentrations between $c_s = 0.1\,\text{mol/L} - 0.8\,\text{mol/L}$ in terms of $\Delta n_{ADN}(r_{1st}) \approx 0.3$ (TFSI) and $\Delta n_{BF4}(r_{1st}) \approx 1.1$ (BF_4^-), a relative decrease R of 3% (TFSI) and 15% (BF_4^-) with respect to the lowest salt concentration demonstrates the crucial impact in accordance with a partial desolvation behavior for BF_4^- anions. Moreover, if we compare the corresponding coordination numbers in the first ADN shell around the ions between both salts for roughly comparable lithium salt concentrations, we obtain a net difference of $\Delta n_{ADN}(r_{1st}) \approx 4.0$ for $c_s \approx 0.15$ mol/L, $\Delta n_{ADN}(r_{1st}) \approx 4.2$ for $c_s \approx 0.3$ mol/L, and $\Delta n_{ADN}(r_{1st}) \approx 4.8$ for $c_s \approx 0.8$ mol/L. In consequence, larger TFSI anions are better solvated due to a larger number of first solvent shell ADN molecules when compared with BF_4^-, which is in good agreement with our previous conclusions on the weaker ion pairing tendency for LiTFSI. Hence, the missing enthalpic gain by forming ion contacts is partly compensated by the good ADN coordination behavior of TFSI anions, and thus promotes the higher occurrence of free ion species when compared with $LiBF_4$.

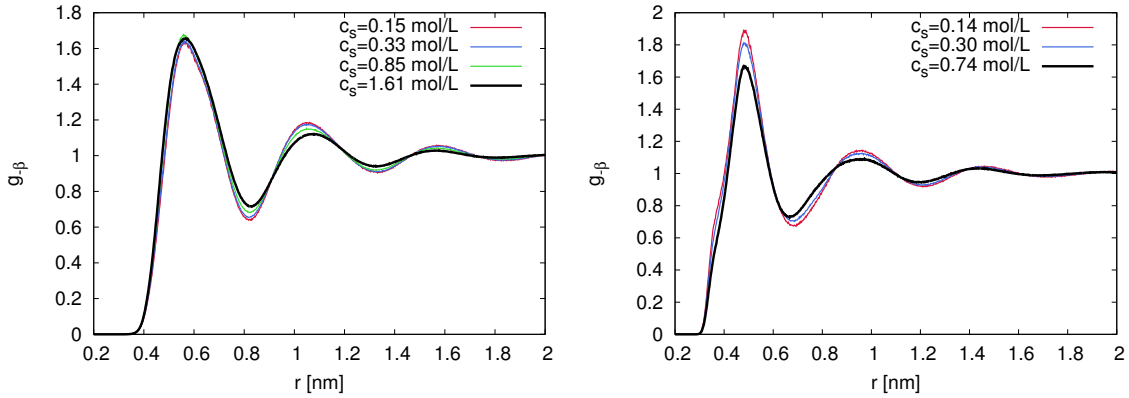

Fig. 2.6 Left: Center-of-mass radial distribution function for ADN molecules around TFSI anions for different salt concentrations as denoted in the legend. Right: Center-of-mass radial distribution function for ADN molecules around BF_4^- anions for different salt concentrations as denoted in the legend.

Table 2.1 Coordination numbers $n_{\mathrm{ADN}}(r_{1\mathrm{st}})$ for ADN molecules around BF_4^- and TFSI anions at first minimum position in the radial distribution functions with $r_{1\mathrm{st}} \approx 0.81$ nm for LiTFSI and $r_{1\mathrm{st}} \approx 0.68$ nm for $LiBF_4$. The relative decrease of the coordination number R is calculated with respect to the value for the lowest salt concentration.

c_s [mol/L]	Anion	$n_{\mathrm{ADN}}(r_{1\mathrm{st}})$	R
0.15	TFSI	11.14	0%
0.33	TFSI	11.05	1%
0.85	TFSI	10.82	3%
1.61	TFSI	9.87	11%
0.14	BF4	7.10	0%
0.30	BF4	6.87	3%
0.74	BF4	6.05	15%

As one would have expected, differences in the desolvation behavior of lithium ions by ion complex formation are rather negligible for this effect. The corresponding values for the first ADN shell coordination numbers show a comparable decrease in the lithium ion desolvation behavior for both salts with increasing salt concentrations. We observe a significantly weaker desolvation effect for lithium ions, which is represented by a decrease of the first shell coordination number from $n^{\mathrm{Li}}_{\mathrm{ADN}}(r_{1\mathrm{st}}) = 4$ to 3.4 ADN molecules for the lowest and highest $LiBF_4$ salt concentration, and a corresponding variation from $n^{\mathrm{Li}}_{\mathrm{ADN}}(r_{1\mathrm{st}}) = 4.9$ to 3.8 ADN molecules for the lowest and highest LiTFSI concentration. Noteworthy, for a LiTFSI concentration of $c_s = 0.85$ mol/L, which is comparable to the highest $LiBF_4$ concentration, the corresponding ADN coordination number reads $n^{\mathrm{Li}}_{\mathrm{ADN}}(r_{1\mathrm{st}}) = 4.4$. The larger number of ADN molecules around lithium ions from LiTFSI can be attributed to the

lower ion correlation tendency when compared with $LiBF_4$. The relative decrease of the ADN coordination number around lithium ions reads $R^{Li} = 15\%$ for $LiBF_4$ with $c_s = 0.74$ mol/L, and $R^{Li} = 10\%$ for LiTFSI with $c_s = 0.85$ mol/L. Hence, even for the lithium ions, one can observe slight differences in the desolvation behavior between the salts, although they are less pronounced when compared to the anion desolvation behavior.
In order to shed more light on the structure of the ion complexes and the corresponding solvation behavior by ADN molecules, we calculated the local/bulk partition coefficients including lithium ions, anions and ADN molecules in accordance with Eqn. (4.1). The results are shown in Fig. 2.7. In agreement with our previous findings, also the individual values

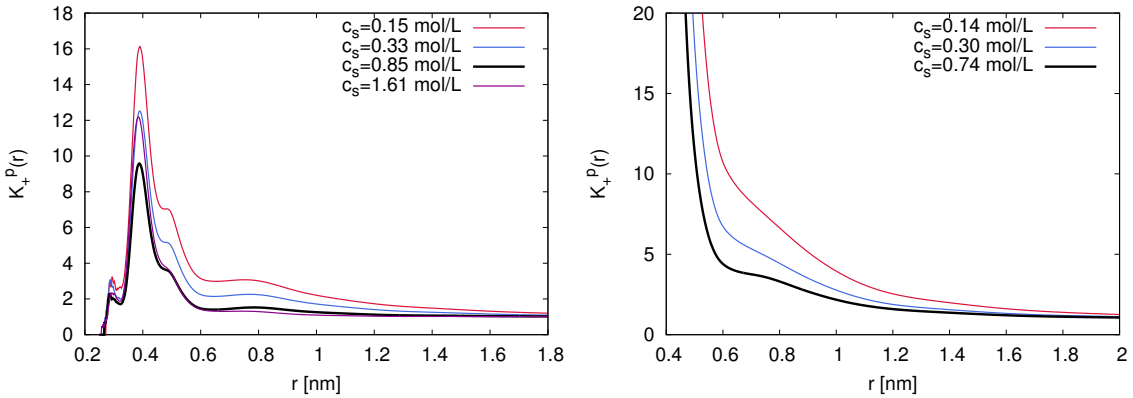

Fig. 2.7 Left: Local/bulk partition coefficients $K_+^p(r)$ at different distances r around lithium ions for different concentrations of LiTFSI (nitrogen as reference atom) as indicated by different colors. Right: Local/bulk partition coefficients $K_+^p(r)$ at different distances r around lithium ions for different concentrations of $LiBF_4$ (fluoride as reference atom) as indicated by different colors.

for the local/bulk partition coefficients reveal significant differences between both salts, which again can be attributed to the corresponding solvation and ion correlation behavior. Hence, LiTFSI (left of Fig. 2.7) shows a pronounced peak at $r \approx 0.4$ nm, which can be attributed to partially solvated ion aggregates in terms of $[Li^+ \cdot TFSI_x^-] \cdot ADN_y$ complexes with $y/x < 1$. The occurrence of non-vanishing values for $K_+^p(r)$ at $r \approx 0.3$ nm can be assigned to short distance contacts between nitrogen atoms of TFSI and lithium ions [101], in combination with coordinating nitrile groups of ADN. Moreover, the decreasing peak height at $r \approx 0.4$ nm for increasing concentrations of LiTFSI reveals decreasing values of anion-solvent fractions around lithium ions. At concentrations of $c_s = (0.85 - 1.61)$ mol/L, this trend is reversed, such that the TFSI coordination number increases stronger than the ADN coordination number. In combination with Fig. 2.5, the formation of LiTFSI ion aggregates thus becomes visible. Comparable findings for significantly higher LiTFSI concentrations were also reported recently for aqueous solutions [24].

In contrast to LiTFSI, the absence of a well-defined peak for $LiBF_4$ as an indication of partially solvated ion complexes becomes obvious (Right of Fig. 4.6). Here, a steeply increasing behavior of $K_+^p(r)$ for $r \leq 0.5$ nm can be observed. It can be concluded that due to the high values of the local/bulk partition coefficient at short distances, the formation of 'dry' ion complexes according to $[Li^+ \cdot BF4_x^-] \cdot ADN_y$ with $y/x \ll 1$ dominates the ion association behavior. In addition, the dominance of dry complexes even increases as the higher values of $K_+^p(r)$ for higher salt concentrations at short distances reveal. With regard to these findings, it can be concluded that LiTFSI-based electrolytes are dominated by less strongly bound and partially solvated ion aggregates when compared to $LiBF_4$, such that the values for the derivative of the chemical activity are only weakly affected by non-ideal effects. Nevertheless, the corresponding estimated relaxation time scales for Li^+ and TFSI anions as described in the previous and the following section reveal a high stability of the contacts. In contrast, $LiBF_4$ forms 'dry' contact ion aggregates, which are strongly bound and thus significantly affect the values for the derivative of the chemical activity in terms of non-ideal effects. These findings are further supported by our experimental results concerning the lower solubility of $LiBF_4$ when compared with LiTFSI. Hence, our results reveal that the anion size with regard to the values of the SASA and hence the surface charge density play an important role in order to rationalize the ion correlation behavior.

2.5.2 Dynamic properties of the electrolyte solution

The corresponding values for the effective (correlated) and ideal (uncorrelated) ionic conductivity in combination with experimental results are shown in Fig. 2.8, the experimental ionic conductivity was obtained from this Ref. 123 . In general, a good agreement between the experimental and simulation results for both salts and all concentrations can be observed, which highlights the validity of our refined force field approach. As it was already discussed, the ideal Nernst-Einstein ionic conductivity (Eqn. (2.1)) accounts only for the self-diffusion coefficients D_+ and D_- of the lithium and anion species, whereas all correlations between the ions are neglected. Noteworthy, the experimental values and the effective ionic conductivities are significantly lower for both conducting salts, which highlights the presence of pronounced ion correlation effects. In more detail, the maximum effective Einstein-Helfand ionic conductivity for both lithium conducting salts was observed at salt concentrations $c_s = 0.5\,\text{mol/L} - 1$ mol/L with values of $\sigma \approx 1$ mS/cm ($LiBF_4$) and $\sigma \approx 3$ mS/cm ($LiBF_4$). Although these values are smaller when compared with standard alkyl carbonates ($\sigma \approx 6 - 12$ mS/cm) [32], they are nevertheless still acceptable in combination with high voltage electrodes. Furthermore, a comparable ideal ionic conductivity can be observed for both lithium salts. Thus, one

can assume that the underlying viscosities and diffusion coefficients are mostly comparable for both conducting salts.

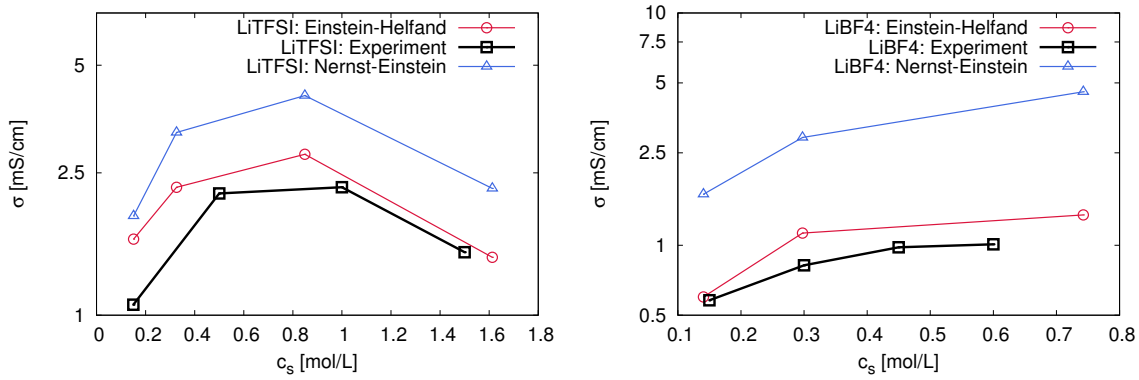

Fig. 2.8 Ideal Nernst-Einstein (blue lines with triangles) and effective Einstein-Helfand ionic conductivities (red lines with circles) for varying concentrations of LiTFSI (left panel) and $LiBF_4$ (right panel) in ADN. Experimental results are shown as squares with black lines. The solid lines are guides for the eyes.

2.6 Summary and conclusion

We performed atomistic MD simulations and quantum chemical calculations in order to elucidate the dynamic and structural properties of $LiBF_4$ and LiTFSI as conducting salts in ADN-based electrolytes. ADN can be regarded as a beneficial solvent for lithium ions with a pronounced electrochemical stability, as it was already reported in Refs. 51, 32. Further results of atomistic MD simulations highlighted that the properties of the anions impose a significant influence on the ion correlation behavior and on the dynamic properties of the electrolyte solution. In more detail, the simulation outcomes revealed pronounced differences between the derivatives of the chemical activities and the ion solvation behavior. Based on our findings, it can be concluded that LiTFSI is better solvated in ADN when compared to $LiBF_4$. In consequence, the tendency of ion complex formation for LiTFSI is significantly lowered when compared to $LiBF_4$. Cormparable findings were also reported for acetonitrile based electrolytes [165, 164, 163].

The underlying differences in the anion-solvation behavior can be mainly attributed to the distinct sizes of the anions. A schematic representation of the ADN-anion coordination behavior is shown in Fig. 2.9. Our results revealed, that the ADN coordination number around TFSI anions differs by $4-5$ ADN molecules when compared to BF_4^-. With regard to roughly identical solvation properties of lithium ions in presence of distinct anions, it can

be assumed that these differences can be solely attributed to the different sizes of the BF_4^- and TFSI anions. In more detail, the larger SASA of TFSI when compared to BF_4^- anions

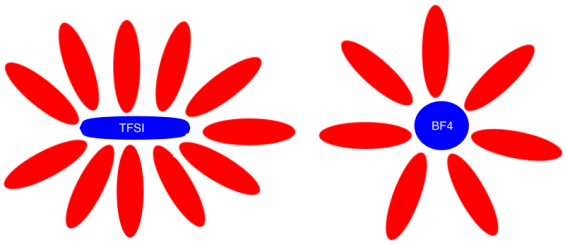

Fig. 2.9 Schematic representation of anion solvation by ADN molecules. The ellipsoidal TFSI anion and the spherical tetrafluoroborate anion are colored in blue, whereas ADN molecules are colored in red.

provides a higher ADN coordination number in the first solvent shell, which compensates the missing electrostatic interaction between TFSI and lithium ions in absence of ion complex formation when compared to BF_4^-, and thus promotes a higher occurrence of free ion species. With regard to further differences, we also observed pronounced deviations between both lithium salts in terms of the ionic conductivity. We are able to rationalize these outcomes by the fact that the higher affinity between BF_4^- anions and lithum cations decreases the effective ionic conductivity remarkably.

In summary, our results highlight the pronounced influence of specific anion effects on dynamic processes and structural properties of organic solvent-based electrolyte formulations. Previous considerations already brought forward the donor and acceptor number concept in order to distinguish between cation and anion solvents [62, 140, 112]. Recent simulation studies highlighted the qualitative agreement of this molecular concept with the observed ion complexation behavior [175, 92, 124]. Moreover, our and previous related findings for acetonitrile [165, 164, 163] are also in qualitative agreement with the *law of matching water affinities* (LMWA) [37, 150, 112], if applied to organic solvents. The LMWA states, that ions with comparable water affinity and influence on the water properties form stable contact pairs in aqueous solutions. Thus, smaller anions with high surface charge densities likely form stable contact pairs with small cations, whereas an opposite effect can be observed for ion species which differ in size. In fact, the binding properties of LiTFSI and $LiBF_4$ in ADN showed comparable effects, which means that the solvation properties of the ions play a decisive role in order to rationalize their binding behavior. However, more salts and further solvents have to be studied in order to underpin the general validity of the LMWA for organic solvents.

We further elucidate specific ion effects in organic solvents in the next chapter with a model polyelectrolyte.

2.7 Acknowledgement

Most part of this chapter was reproduced from Ref [123] with permissions from the Royal Society of Chemistry, Physical Chemistry Chemical Physics.

Chapter 3

Specific ion effects for polyelectrolytes in aqueous and non-aqueous media

3.1 Introduction

Despite their ubiquitous occurrence, the mechanisms underlying specific ion effects in aqueous or non-aqueous solution are even nowadays poorly understood [104, 93, 83, 116]. Noteworthy, a lot of work was spent on specific ion effects and their influence of protein precipitation in aqueous solution, for which the corresponding ion ranking scheme is called Hofmeister or lyotropic series [104]. Although the term 'series' implies an universal behavior, further research already revealed the presence of reverse Hofmeister series effects besides other modifications in terms of varying system properties [104, 93, 83]. In addition to monoatomic ions in alkali halide salts, specific ion and size-related effects were also observed for molecular ions, which are often components of ionic liquids [212, 213, 102, 150, 172, 47, 132]. The observed differences between the results of these studies concerning concentration-dependent effects, varying solutes, or different salt compositions impede a thorough theoretical understanding and initiated further research, which also includes the study of specific ion effects in non-aqueous media [117, 118].

Despite the overwhelming dominance of aqueous solutions for most biological processes, novel non-aqueous solutions became important for lithium ion and post lithium ion batteries [206]. Hence, more insight concerning the ion behavior in non-aqueous media is needed for a proper understanding and optimization of these novel electrolyte solutions. An excellent overview on specific ion effects in non-aqueous solutions was recently published [116].
Specific ion effects were also observed in atomistic molecular dynamics (MD) simulations in terms of ion pairing mechanisms [56, 54, 190], and for the counterion condensation behavior

around highly charged polyelectrolytes in aqueous solution [71, 12]. There, it was found that the individual alkali metal cations differ in their condensation strength, which was explained by their underlying solvation behavior in terms of a modified Poisson-Boltzmann approach [71]. A standard electrostatic mean-field theory to estimate the number of condensed counterions is represented by the Manning-Oosawa (MO) counterion condensation theory [108, 109, 131]. The central quantity in this approach is the so-called Manning parameter ξ, which includes the Bjerrum length, the charge, and the line charge density of the polyelectrolyte. In accordance with the theory, counterion condensation sets in for values $\xi \geq 1$, a condition which is met for polyelectrolytes with high line charge density, multivalent ions, and solvents with large Bjerrum lengths.
Various coarse grained MD simulations have confirmed the validity of the MO approach [122, 46, 25], for which the explicit molecular nature of the solvent is replaced by a dielectric continuum approach in agreement with the original formulation of the theory. However, more detailed atomistic computer simulations already showed pronounced deviations in terms of salt decrement effects or specific solvation mechanisms [106, 3, 72, 134, 147, 126, 94, 50]. More refined mean-field descriptions were thus developed in order to cover the presence of flexible polyelectrolytes and ion specific effects [154, 155, 93, 104]. However, a satisfying description, specifically with regard to the molecular nature of the solvent, is still yet to be developed.
In this chapter, a report on counterion-specific condensation behavior around highly charged model polyelectrolytes immersed in water, methanol and N-,N-dimethylacetamide (DMAc) is made. Molecular snapshots of methanol and DMAc are shown in Fig. 3.1.

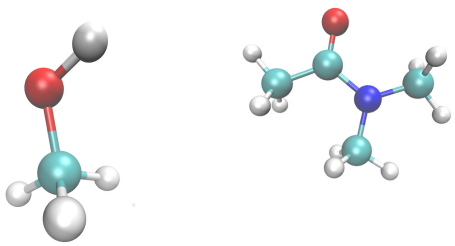

Fig. 3.1 Molecular snapshots of methanol (left side) and DMAc (right side). Carbon atoms are colored as green spheres, nitrogen atoms as blue spheres, hydrogen atoms as white spheres, and all oxygen atoms are colored in red.

3.1.1 Counterion condensation theory

The MO counterion condensation theory [108, 109, 131] is an electrostatic mean-field theory, which allows us to estimate the fraction of condensed counterions around an infinite rod-like polyelectrolyte with constant and homogeneously distributed line charge density. In its simplest form, the theory neglects ion-solvent and ion-ion interactions, and further assumes the absence of excess salt, such that the solution only includes the polyelectrolyte, the solvent and the counterions in order to achieve electroneutrality. The central quantity in this framework is the so-called Manning parameter

$$\xi = q\lambda_B b \tag{3.1}$$

with the Bjerrum length

$$\lambda_B = \frac{e^2}{4\pi\varepsilon_0\varepsilon_r k_B T}, \tag{3.2}$$

including the relative dielectric constant of the solution ε_r, the vacuum permittivity ε_0, the elementary charge e, the charge of monovalent counterions q, and thermal energy $k_B T$, in combination with the line charge density b of the polyelectrolyte. In accordance with the theory, counterion condensation sets in for values $\xi \geq 1$, a condition which is met for polyelectrolytes with high values of b, solvents with large λ_B, or the presence of multivalent ions.
With regard to the use of mean field approximations [109], a simple estimate for the fraction of condensed counterions around the rod can be derived

$$\theta = 1 - \left(\frac{1}{\xi}\right) \tag{3.3}$$

which is in good agreement with more sophisticated approaches like the Poisson-Boltzmann cell model theory [46, 45].

3.1.2 Fraction of condensed counterions and coordination numbers

As can be seen, the fraction of condensed counterions θ (Eqn. (3.3)) reveals a constant value for well-defined solvent and ion parameters. In reality, counterions are not glued to the rod, but follow a distribution which can be evaluated from the corresponding coordination numbers $\mathrm{CN}(r)$ of the ions around the polyelectrolyte. Due to radial symmetry in terms of a rigid and linear polyelectrolyte, the ion coordination number with the counterion number

density ρ_c can be calculated by

$$\mathrm{CN}(r) = 2\pi l_{\mathrm{rod}}\,\rho_c \int_0^r R\, g_{\mathrm{pc}}(R)\,\mathrm{d}R \tag{3.4}$$

with l_{rod} being the length of the rod-like polymer, which also corresponds to the box vector length in z-direction, and with the radial distribution function $g_{\mathrm{pc}}(R)$ between the polyelectrolyte (p) and the counterions (c). The distance-dependent fraction of counterions located within the cylindrical shell up to radius r is then given by

$$Q(r) = \frac{\mathrm{CN}(r)}{\rho_c V}, \tag{3.5}$$

with system volume V. In order to define a constant value of Q in terms of Eqn. (3.3), one has to introduce a fixed distance r_{M} as separatrix to distinguish between condensed and free counterions. A reasonable value is given by $r_{\mathrm{M}} = \lambda_B$ [92, 111, 170], which means that counterions are considered as condensed, when their electrostatic energy is stronger than the thermal energy. With regard to this argument, we define the fraction of condensed counterions as $Q^{\mathrm{M}} = Q(\lambda_B)$.
Furthermore, the spherical coordination number of molecules or ions of species β around molecules or ions of species α is given by

$$\mathrm{CN_s}(r) = 4\pi\rho_\beta \int_0^r R^2\, g_{\alpha\beta}(R)\,\mathrm{d}R, \tag{3.6}$$

which allows us to estimate the coordination number of solvent molecules around the ions.

3.1.3 Calculation of the dielectric constant

As can be seen in Eqn. (3.2), the value of the dielectric constant ε_r of the solution heavily affects the Bjerrum length, and thus the counterion distribution behavior, as well as the distance for the separatrix between condensed and free counterions. In order to obtain a reliable value of ε_r for the solvents considered in the simulations, we use the fluctuation formula as introduced in this equation Eqn. (4.3)[43, 127]. The so-obtained dielectric constants from our simulations for pure solvents without additional components are shown in Tab. 3.1. The corresponding results reveal an acceptable agreement with experimental outcomes [68, 167] at 298.15 K. With regard to the dielectric constant in combination with the system temperature $T = 300$ K, and polyelectrolyte parameters $q = \pm 1e$ and $b = \pm 2.48\, e/\mathrm{nm}$ (more details can be found in the next section), the resulting values for the Manning constant are $\xi > 1$ for all solvents. Exact values for ξ and θ can be also found in Tab. 3.1. Therefore,

Table 3.1 Dielectric constant ε_r from the simulations (Eqn. (4.3)) and dielectric constants $\varepsilon_r^{\text{exp}}$ from experiments [68, 167] at 298.15 K, resulting Bjerrum lengths λ_B, Manning parameters ξ, and fractions of condensed counterions θ (Eqn. (3.3)) for the solvents in the simulations. The values for the acceptor (AN) and donor numbers (DN) are presented in Ref. 140 and were derived by standardized experimental procedures. The SPC/E model [18] is used for water, whereas methanol (MeOH) and N,N-dimethylacetamide (DMAc) are modeled as KB force fields published in Refs. 200, 84. The errorbars for the dielectric constant are of the order of the first digit.

Solvent	ε_r	$\varepsilon_r^{\text{exp}}$	λ_B [nm]	ξ	θ	DN	AN
Water	71	78	0.78	1.93	0.48	18.0	54.8
MeOH	35	33	1.58	3.92	0.74	19.0	41.5
DMAc	42	38	1.30	3.22	0.69	27.8	13.6

we expect to see counterion condensation in all considered systems. Although it is known that the dielectric constant of the solution changes in presence of charged species [120], the counterion concentration in all systems is around $c = 0.12$ mol/L, which implies that ion-induced variations of ε_r can be safely ignored due to minor contributions [92].

3.2 Simulation Details

MD simulations of highly charged model polyanions and polycations and their corresponding counterions in water, methanol and DMAc at 300 K using the GROMACS 4.6.5 software package were performed [139]. In more detail, the distribution of alkali metal (Li^+, Na^+, K^+, Rb^+ and Cs^+) and halide ions (F^-, Cl^-, Br^- and I^-) as modeled by a Kirkwood-Buff (KB) based force field [57] was studied in aqueous solution by using the SPC/E water model [18]. Moreover, we also used a KB force field for methanol [200] and a KB force field for DMAc [84] in order to achieve full consistency for all force field combinations in the solution. In general, KB force fields are parameterized to reproduce thermodynamic properties like activities, enthalpy of mixing, densities and compressibilities to be in good agreement with experimental findings. Although polarization effects are missing, KB force fields provide a reasonable choice to study specific ion effects [57, 53]. In terms of definitions, the value of r_0 for each ion corresponds to the closest contact distance between the polyelectrolyte and the specific ion. Furthermore, the value of r_s denotes the closest contact distance between ions and solvent molecules. The partial charges with regard to the most important molecular groups for water, methanol and DMAc are shown in Tabs. A.2, 3.3 and 3.4. As can be seen, the oxygen atom in all molecules reveals the most negative charge, except for the

Table 3.2 Partial charges of atoms for SPC/E water as taken from Ref. 18.

Atom	$q[e]$
O	-0.84
H	0.42

Table 3.3 Partial charges of molecular groups for methanol as taken from the KB force field presented in Ref. 200.

Molecular group	$q[e]$
CH_3	0.30
O	-0.82
H	0.52

Table 3.4 Partial charges of molecular groups for DMAc as taken from the KB force field presented in Ref 84.

Molecular group	$q[e]$
(C)CH_3	0.00
C	0.62
O	-0.62
N	-0.70
(N)CH_3	0.35

nitrogen atom in DMAc, whereas the partial charge of methyl groups is rather low. In more detail, the absence of proton donors in DMAc classifies this solvent as aprotic, whereas water and methanol are considered as protic solvents [140], whose properties are dominated by hydrogen bonds between the molecules. Due to the high and moderate values for the dielectric constants (Tab. B.1), all solvents can be also regarded as polar media [140].
In combination with the electrolyte solution, we constructed a simple linear and rigid polyelectrolyte with 30 'CH2' beads as defined in the GROMOS force field [153]. The polyelectrolyte can be interpreted as a rod of infinite length by using the periodicity of the simulation box with a fixed cubic side length of $L_z = L_y = L_x = 6.06$ nm in agreement with the approach presented in Ref. 72. We assigned a charge of $q = \pm 1e$ to each second monomer while the other monomers remain uncharged, which gives a line charge density of $b = \pm 2.48$ e/nm. The sign of the charge depends on the considered ion species in order to achieve electroneutrality. An exemplary snapshot of the system for aqueous Li^+ and I^- solutions is shown in Fig. 3.2.
Pure solvents without ions were simulated after equilibration (5 ns) for 100 ns with 2 fs

timestep in NpT ensemble at 300 K and 1 bar pressure with the Parinello Rahman barostat [133], in combination with the Nose-Hoover thermostat [129]. All pure solvent simulations were performed in a cubic box with initial side length of $L_z = L_y = L_x = 4$ nm. These simulations were used to calculate the dielectric constant of water (SPC/E), DMAc, and methanol (Tab. B.1) and to generate well equilibrated solvent configurations. The polyion was

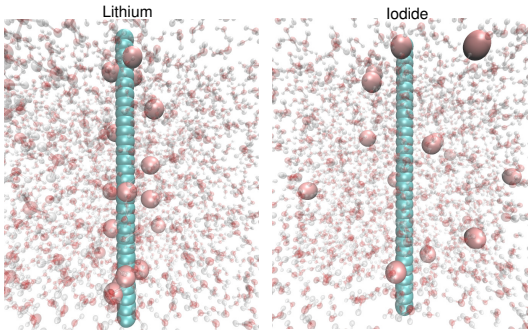

Fig. 3.2 Snapshots of the simulation box with typical configurations for lithium (left) and iodide (right) ions (light red spheres) in the presence of water and the model polyanion (left) and the model polycation (right), respectively (both represented by light blue spheres).

immersed into the pre-equilibrated solvent configuration, and we randomly inserted $N_c = 15$ counterions in the box to achieve electroneutrality, which yields a counterion concentration of $c = 0.12$ mol/L for all solutions. Finally, the positions of the polyion monomers were fixed in order to prevent sampling artifacts from metastable conformations. After energy minimization, an equilibration run of 5 ns length was performed, which was followed by a 100 ns production run in the NVT ensemble for each system, where the temperature of 300 K has been kept constant by the Nose-Hoover thermostat [129]. Electrostatic interactions were calculated by the Particle Mesh Ewald method[41] with a Verlet pair list cutoff scheme and a short-range cutoff of 1 nm. The same cutoff scheme was also used for the calculation of the Lennard-Jones (LJ) interactions in combination with dispersion corrections. The Fourier grid spacing was 0.16nm.

3.3 Results

3.3.1 Counterion distribution

The distance-dependent fractions of condensed counterions $Q(\ln(r/r_0))$ (Eqn. (3.5)) around the polycations and polyanions in water, methanol and DMAc are shown in Fig. 3.3. As can be seen at first glance, the values for $Q(\ln(r/r_0))$ differ crucially between the ions and

between the solvents. In general, cations in methanol and water show a higher binding affinity at shorter distances when compared with anions, while this finding is reversed for DMAc. Moreover, smoothly increasing functions $Q(\ln(r/r_0))$ can be observed for anions in water,

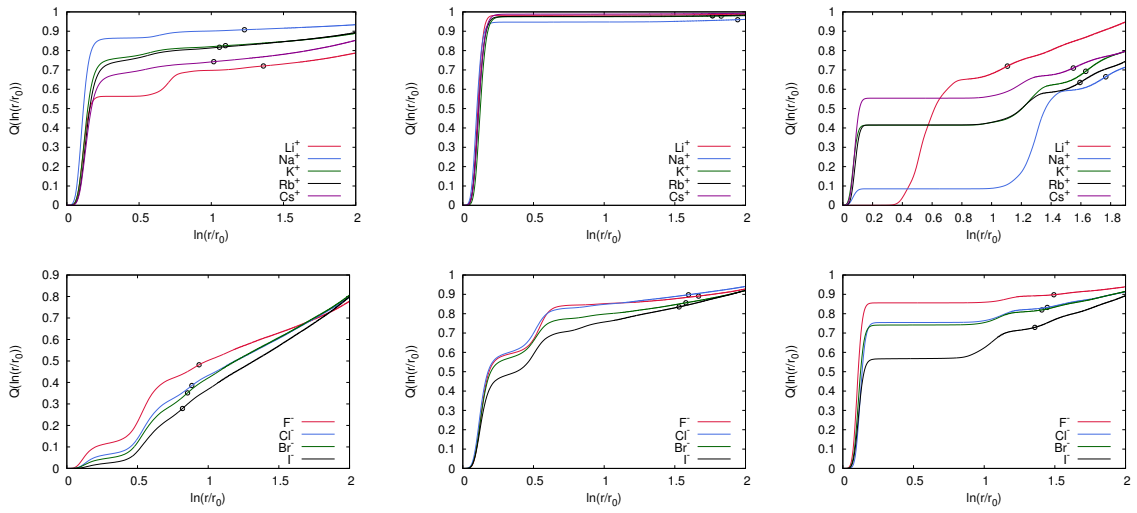

(a) Water (b) Methanol (c) DMAc

Fig. 3.3 Fraction $Q(\ln(r/r_0)$ of condensed cations (top) and anions (bottom) around the oppositely charged and rod-like model polyelectrolyte in a) water (left side), b) methanol (middle) and c) DMAc (right side). The value of r_0 for each ion corresponds to the closest contact distance between the polyelectrolyte and the specific ion. The circles at the lines denote the corresponding values of $\ln(\lambda_B/r_0)$, which are used for the evaluation of the fraction of condensed counterion Q^{M} in Fig. 3.4.

whereas a completely different behavior in terms of a sharp and a step-wise increase becomes obvious for some ions in DMAc and methanol. For aqueous systems, the first coordination shell around the polyelectrolyte is formed by cations, whereas water molecules form the first coordination shell around the polyelectrolyte in presence of anions. For methanol, the first coordination shell is formed by cations in contrast to mixed methanol-ion shells in presence of anions. Due to the larger size of the solvent molecules, the first coordination shells in DMAc are formed by cations or anions, respectively, whereas DMAc molecules are located at larger distances. Interestingly, only for Li^+ and Na^+, the first coordination shell around the polyelectrolyte is formed by DMAc molecules, which explains the deviating results for these ions in Fig. 3.3. We will come back to this point in more detail in the remainder of this chapter. In consequence, the corresponding simulation outcomes reveal a rich plethora of specific ion effects as reflected by the observed varying counterion distributions.

With regard to a more detailed study of the ion ranking in terms of the condensation behavior, we evaluated the fraction of condensed counterions Q^{M} as described in section 3.1.2. The

corresponding values in combination with the simple MO prediction for θ (Eqn. (3.3)) are shown in Fig. 3.4. It becomes evident that the values of θ deviate significantly from Q^{M} for

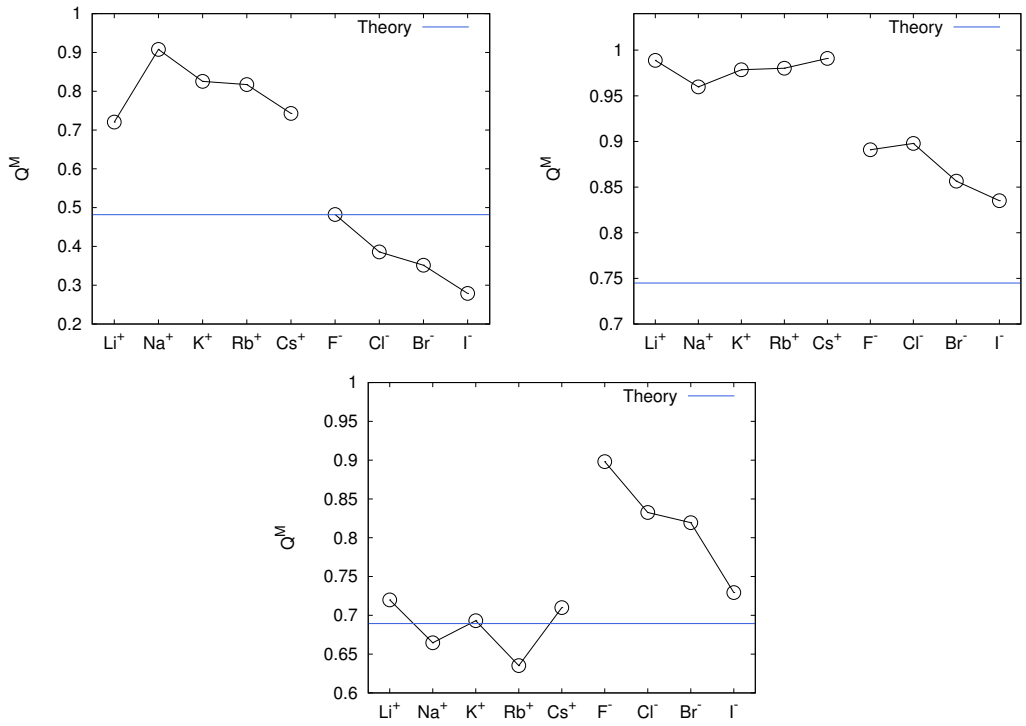

Fig. 3.4 Fraction of condensed counterions Q^M at the Bjerrum length in water (top), in methanol (middle) and in DMAc (bottom). The blue lines denote the values of θ in accordance with standard MO counterion condensation theory (Eqn. (3.3)).

most ions in all solvents. With regard to the variation of Q^{M} among cations and anions, it can be seen that anion-specific effects are more pronounced when compared with cations. These findings are valid for all solvents and thus in agreement with previous experimental results [118]. Moreover, an ion size-related decrease of Q^{M} can be observed for anions Cl^-, Br^- and I^- in all media. This outcome would also explain the observed specific ion effects for I^- and Cl^- on the osmotic coefficient for polyelectrolyte-counterion systems in Refs. 21, 5, 4. In contrast, the values for F^- are slightly lower in methanol when compared with Cl^-, but follow the trend in water and DMAc. In agreement with the anions, all cations except Li^+ show a size-dependent decrease of Q^{M} in water, while comparable values of Q^{M} can be observed for all cations in methanol, and no clear trend becomes visible for DMAc.

If we define the maximum and minimum values of the fraction of condensed counterions for cations or anions within a specific solvent with $\Delta^{\pm}Q^{\mathrm{M}} = Q^{\mathrm{M}}(\mathrm{max}) - Q^{\mathrm{M}}(\mathrm{min})$, it can be concluded that water shows the broadest range of cation-specific effects ($\Delta^{+}Q^{\mathrm{M}} \approx 0.2$),

followed by DMAc ($\Delta^{+}Q^{\mathrm{M}} \approx 0.1$) and methanol ($\Delta^{+}Q^{\mathrm{M}} \approx 0.02$). A comparable ranking can be found for anions in accordance with $\Delta^{-}Q^{\mathrm{M}} \approx 0.2$ for water, $\Delta^{-}Q^{\mathrm{M}} \approx 0.18$ for DMAc, and $\Delta^{-}Q^{\mathrm{M}} \approx 0.06$ for methanol. Although it has to be noted that these values strongly depend on the properties of the solute or the polyelectrolyte [117, 118], they provide a first glimpse of the occurrence of specific ion effects in different solvents. In summary, the presence of specific ion effects is mostly pronounced for water, followed by DMAc, whereas only small variations can be observed in methanol, which is in good agreement with recent experimental results on elution times in solvatochromatography experiments [117, 118].
In terms of standard MO counterion condensation theory (section 3.1.1), one would not expect such a rich plethora of specific ion effects. The corresponding findings imply that molecular properties of the solvent are more important when compared with electrostatic binding energies between the counterions and the polyelectrolyte. As can be seen in Fig. 3.4, all results deviate significantly from mean-field electrostatic theories, which implies that the dielectric constant and thus the Manning constant contributes only minor to the observed condensation behavior. Even more important, we observe pronounced differences between cation and anion distributions for identical solvents. For instance, cation condensation is more pronounced in methanol and water, which stands in sharp contrast to the outcomes for DMAc. Thus, it can be assumed that the solubility of anions is higher in methanol and water when compared with DMAc, such that all anions are located at larger distances around the polyelectrolyte in order to increase the total ion solvent accessible surface area. In contrast to water and methanol, a higher solubility of cations in DMAc according to the findings for Q^{M} in Fig. 3.4 can be also assumed. In consequence, besides the strength of electrostatic interactions, also ion-solvent mechanisms play a pivotal role in order to rationalize the observed counterion condensation behavior in terms of specific ion effects. The corresponding implications will be discussed in the next sections.

3.3.2 Ion solvation behavior

As an explanation for the occurrence of specific ion effects, we studied the solvation behavior of the individual ions in the considered solvents. A detailed inspection is presented in Fig. 3.5 and Fig. 3.6, where the spherical coordination numbers $\mathrm{CN_s}(r/r_s)$ (Eqn. (3.6)) of solvent molecules around the ions are shown. The value of r_s denotes the closest contact distance between ions and solvent molecules. As can be seen in Fig. 3.5, lithium ions reveal a pronounced and rigid first solvent shell in all solvents as demonstrated by constant values of $\mathrm{CN_s}(r/r_s)$ after a rapid increase at short distances $r/r_s \approx 1.5$. This finding can be associated with the small size of the ion, which implies a well-pronounced coordination behavior in terms of strong next-nearest neighbor interactions for the solvent molecules, as

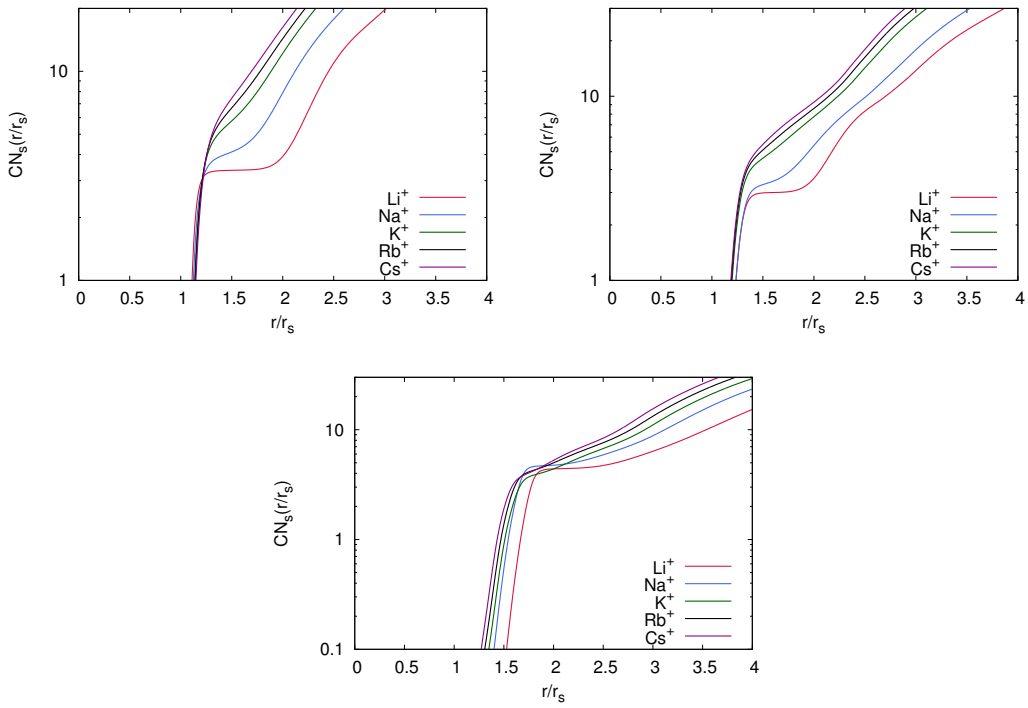

Fig. 3.5 Coordination numbers $\mathrm{CN_s}(r/r_s)$ (Eqn. (3.6)) of solvent molecules around the cations in water (top), methanol (middle) and DMAc (bottom). The distance r_s denotes the closest contact distance between ions and solvent molecules.

it was also discussed in Refs. 92, 101. In more detail, the corresponding values in the first coordination shell around lithium are around $\mathrm{CN_s}(r) = 3-4$ in methanol and water, whereas significantly higher values of $\mathrm{CN_s}(r) = 4-5$ at larger distances $r/r_s \approx 2$ can be observed for DMAc. Hence, the larger size of the DMAc molecules promotes a favorable solvent accumulation at larger distances, such that more DMAc molecules can arrange around the lithium ions. Comparable conclusions can be also drawn for sodium ions, which also show a step-wise increase at $r/r_s = 1.6-2.0$ in their DMAc coordination behavior. Interestingly, strong variations at short distances for $r/r_s \leq 1.6$ can be observed for all cations in DMAc, whereas the coordination numbers coincide for $r/r_s \approx 1.9$. Thus, the total number of DMAc molecules around the cations within two coordination shells are comparable.

In contrast, larger cations like K^+, Cs^+ and Rb^+ and all anions (Fig. 3.6) dissolved in all solvents do not show such a well-defined coordination behavior at short distances. After a comparable increase for $r/r_s \leq 1.5$, the associated coordination numbers of the solvents are significantly larger when compared with Li^+ and Na^+, which can be related to the larger size of the considered ions. In contrast to Li^+, the smallest anion F^- does not reveal such a

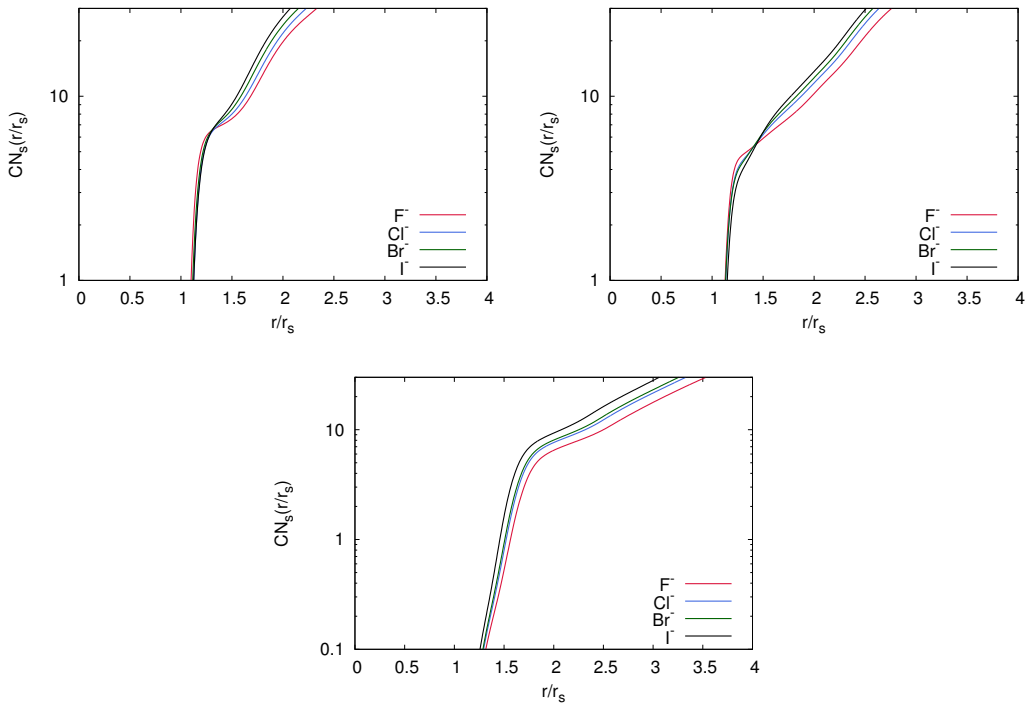

Fig. 3.6 Coordination number $\mathrm{CN_s}(r/r_s)$ (Eqn. (3.6) of solvent molecules around the anions for water (top), methanol (middle) and DMAc (bottom). The distance r_s denotes the closest contact distance between ions and solvent molecules.

well-defined coordination shell at short distances. Thus, one can conclude that the molecular orientation of DMAc around the anions differs when compared with cations, which has crucial consequences on the observed ion-specific coordination behavior. We will come back to this point in the following sections.

In order to study the influence of the molecular size on the solvation behavior and the occurrence of specific ion effects, we evaluated the excess volume of solvent molecules around the individual ion species. The excess volume

$$V^{\mathrm{xs}} = 4\pi \int_0^\infty r^2 [g_{\alpha\beta}(r) - 1]\,\mathrm{d}r, \tag{3.7}$$

is closely related with Kirkwood-Buff integrals [85, 16, 172] and provides an estimate for the deviation from an ideal gas state. In combination with the solvent total number density ρ_s, the excess number of solvent molecules

$$N^{\mathrm{xs}} = \rho_s V^{\mathrm{xs}} \tag{3.8}$$

around the individual ion sites can be computed straightforwardly [172]. Due to finite distances in computer simulations and the corresponding consequences for Eqn. (3.7), one usually introduces a cut-off length r_c, such that $V^{\mathrm{xs}}(r) \approx V^{\mathrm{xs}}$ or $N^{\mathrm{xs}}(r) \approx N^{\mathrm{xs}}$ approach constant values for all distances $r \geq r_c$. For water and methanol, the obtained cutoff-length are $r_c = 2.5$ nm, while the cutoff length in DMAc reads $r_c = 2.8$ nm.
The corresponding values for the excess numbers of solvent molecules are shown in Fig. 3.7. As can be seen, for most ions in water and methanol, the corresponding values are slightly

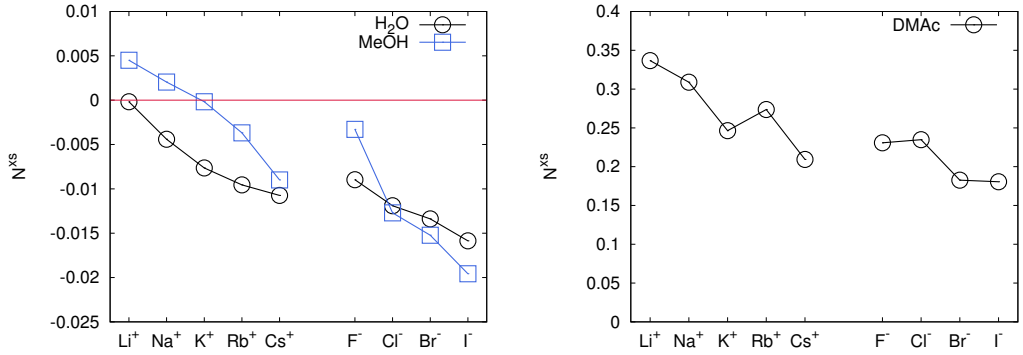

Fig. 3.7 Top: Excess numbers (Eqn. (3.8)) of water (H_2O) and methanol (MeOH) molecules around the individual ion species. The red line denotes $N^{\mathrm{xs}} = 0$ as a help for the eye. Bottom: Excess numbers (Eqn. (3.7)) of DMAc molecules around the individual ion species. All standard deviations are within symbol size.

negative, implying a comparable accumulation behavior when compared with the ideal gas state. The only exceptions are Li^+ and Na^+ in methanol, whereas all ions show a decreasing value with increasing ion size. This can rationalized by the excluded volume of the ions, which thus provides more negative values of V^{xs} for larger ions when compared with smaller ions. This conclusion is also in agreement with the values for the anions, which are larger and thus show more pronounced excluded-volume effects when compared with cations. However, a different behavior in comparison to methanol and water can be observed for DMAc. Here, all values are positive and significantly larger when compared with the other solvents. This outcome can be mostly attributed to the large size of the DMAc molecules and the corresponding larger distance of the solvation shells in combination with the increased local DMAc density around the ions (Fig. 3.5 and Fig. 3.6).
However, all results imply that the excess numbers of solvent molecules are not directly related to the observed counterion distributions in Fig. 3.3, and the fraction of condensed counterions in Fig. 3.4. Hence, local solvation properties at short length scales, as well as specific molecular details of the solvent dominate the counterion distribution, whereas the size of the molecules and the values of the dielectric constant are of minor importance. In

order to study the interactions between the ions and the solvent molecules, we also evaluated the potential binding energies between both components, which will be discussed in more detail in the next section.

3.3.3 Enthalpic contributions to specific ion effects

A recent publication [117] speculated that the occurrence of specific ion effects can be mostly attributed to different energetic contributions between the solvent molecules and the ions. Although we use atomistic MD simulations, which crucially rely on parameterization processes in terms of KB based force fields, the inspection of energetic contributions gives a first hint concerning the underlying behavior. Nevertheless, it is clear that classical atomistic force fields are limited by the introduction of phenomenological potential energy functions (for instance Lennard-Jones 12-6 potentials or missing electronic polarization effects) when compared to sophisticated quantum chemical calculations [63]. However, in order to study dispersion and ion-multipole interactions separately, we rely on the force-field based approach as a rough estimate.

In order to study the individual enthalpic contributions, which also provide insights into the underlying favorable or unfavorable ion solvation behavior, we evaluated the Lennard-Jones short-range (LJ (SR)) and the Coulomb short-range (Coulomb (SR)) energies between the ions and the solvent molecules. Due to the fact that the solvent molecules are net uncharged, the Coulomb energies can be attributed to ion-dipole or generally multipole interactions, as reflected by different partial charges of the atoms in the solvent molecules. Furthermore, in agreement with previous findings for charged species [111], we assume that the free solvation energy $\Delta F = \Delta U - T\Delta S$ is dominated by enthalpic interactions ΔU, such that all entropic contributions are rather negligible in terms of $|\Delta U| \gg |T\Delta S|$, which means that the solvation free energy reads $\Delta F \approx \Delta U$ within reasonable approximations. The results concerning the total interaction energy between ions and solvent molecules are shown in Fig. 3.8. It is striking that most of the total interaction energy between the ions and the solvent molecules can be attributed to ion-dipole or multipole electrostatic interactions in terms of favorable Coulomb energies. In consequence, short-range LJ interactions are rather negligible, although slight differences between the ions in combination with distinct solvents are also apparent. As can be seen, the total interaction energies differ strongly between the solvents and among the individual ion species. For instance, we observe a well-pronounced ranking scheme in water with regard to the ion size. Hence, the smallest cation (Li^+) and the smallest anion (F^-) show the most negative total binding energies. In addition, it has to be pointed out that the interactions between anions and water are more favorable when compared with cations. Comparable conclusions can be also drawn for methanol (middle

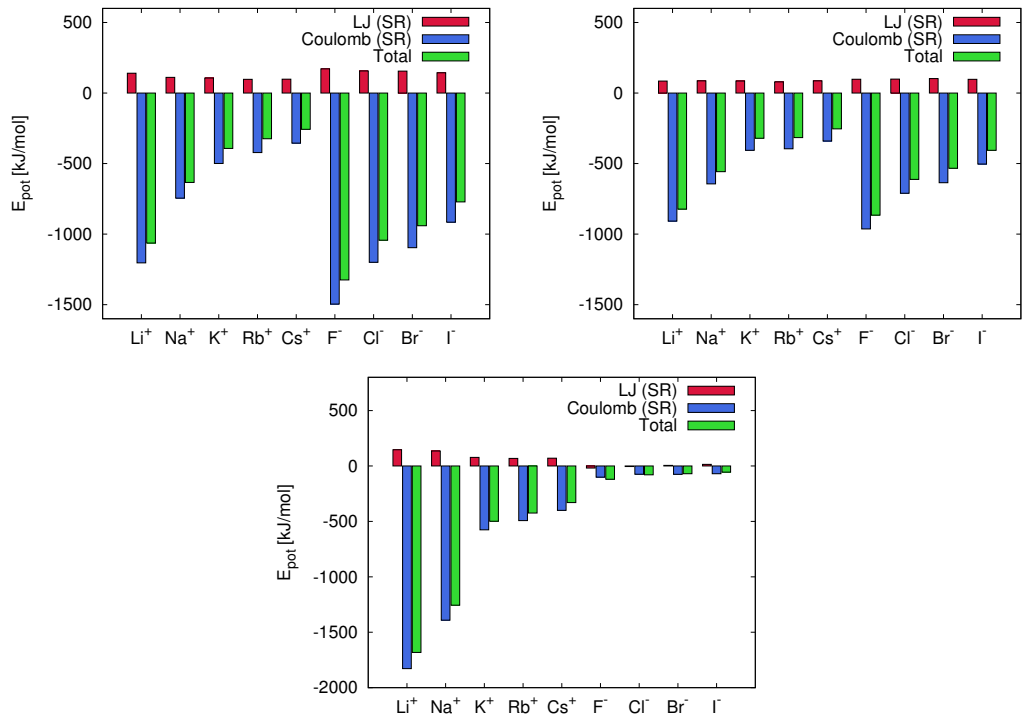

Fig. 3.8 Lennard-Jones short-range (LJ (SR)) and Coulomb short-range (Coulomb (SR)) energies between ions and water molecules (top), ions and methanol molecules (middle) and ions and DMAc molecules (bottom).

inset of Fig. 3.8). In more detail, it has to be noted that the corresponding net values for Coulomb potential energies are higher when compared with water, but the ranking scheme of the ions is indeed identical. A different behavior can be observed for DMAc (bottom inset of Fig. 3.8). Here, the total interaction energies strongly differ from the results obtained for water and methanol. As can be seen, the strongest interactions can be observed for cations, which rationalizes the reversed condensation behavior in DMAc in Fig. 3.4. Interestingly, the small cations (Li^+ and Na^+) show the most negative values concerning the interaction energies when compared with methanol and water, whereas all anions reveal negligible values in DMAc. In consequence, the interaction energies between DMAc and anions are significantly smaller when compared with the cations.

Furthermore, it was speculated [117] that ion interactions with solute species crucially influence the strength of specific ion effects. In order to verify this assumption, we calculated the corresponding LJ and Coulomb interaction energies between the ions and the polyanion or polycation, respectively. The results are depicted in Fig. 3.9. As expected, stronger condensed species show more negative electrostatic binding energies with the polyion. The

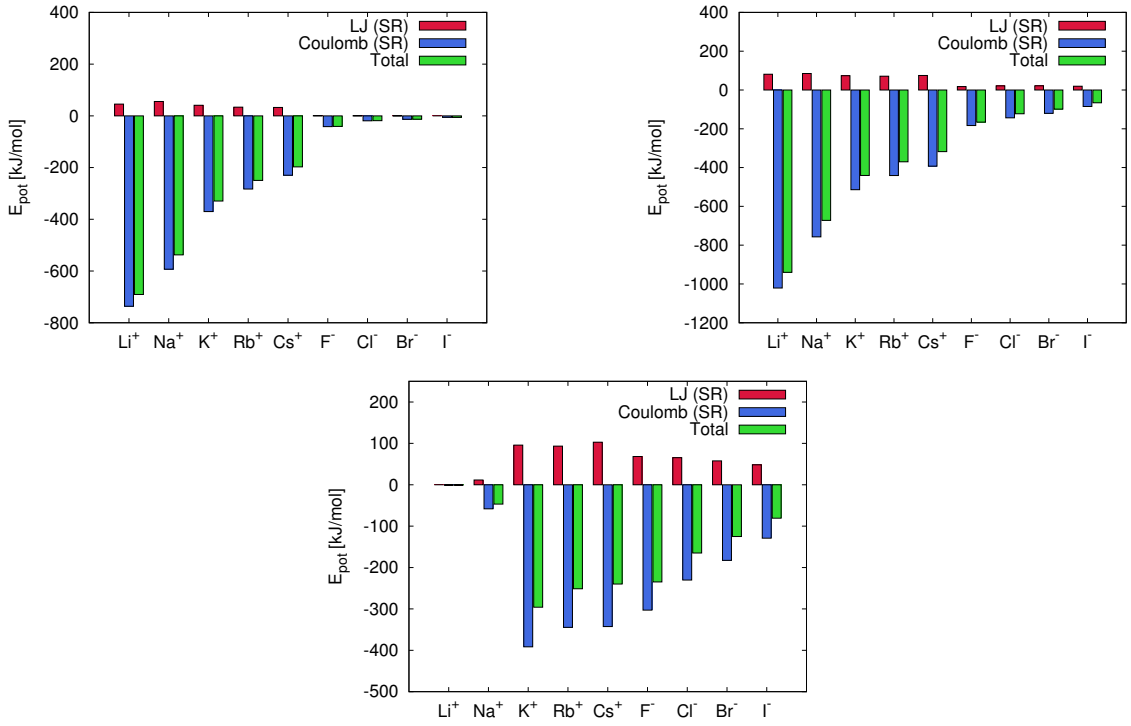

Fig. 3.9 Lennard-Jones short-range (LJ (SR)) and Coulomb short-range (Coulomb (SR)) interaction between ions and the polycation or polycation, respectively, in water (top), in methanol (middle) and in DMAc (bottom).

corresponding data reveal distinct ion-size effects, which can be attributed to a stronger accumulation behavior around the polyelectrolyte for smaller ions at short distances in terms of more favorable Coulomb interactions. The deviations for Li^+ and Na^+ can be attributed to the pronounced solvation of these ions in DMAc, which becomes also visible with regard to the large distances between the ions and the polyanion as shown in Fig. 3.3. In consequence, the electrostatic interactions between these ions and the polyanion are rather negligible.
In summary, our findings reveal that specific ion effects are dominated by ion-solvent and ion-solute interactions, which modify the strength of these effects when compared to bulk solution behavior. Hence, based on our findings, we are able to underpin recent assumptions concerning experimental results [117]. In fact, it has to be mentioned that LJ interactions play a minor role for the occurrence of specific ion effects in the considered force fields. As a last point, the individual ion-ion interaction energies are largely comparable, which allows us to neglect them for our discussion of specific ion effects.

3.3.4 Ion solvation and counterion distributions in connection with the donor and acceptor number concept

In agreement with a previous publication [170], a reasonable concept in order to take solvation properties into consideration is the introduction of donor (DN) and acceptor (AN) numbers [62, 140]. In more detail, the donor and acceptor numbers provide estimates for the ability of the considered solvent to dissolve cations or anions, respectively. The corresponding DN and AN values for all solvents as derived by standardized experimental procedures [62] are shown in Table 3.1. A high value of DN expresses a pronounced cation solvation behavior and vice versa, a high value of AN implies a pronounced solvation of the anions. With regard to our discussion, it was also argued, that ion pair formation is minimized in solvents with high AN and DN values [170, 62].

In consequence, methanol and water are high AN solvents, while they are only moderate DN solvents. Hence, the solvation of anions is favored in methanol and water (AN $>$ DN), such that anions are located at larger distances around the polyelectrolyte in order to increase the total solvent accessible surface area. In contrast, the values for DMAc imply AN $<$ DN, which highlights a better solubility of cations in DMAc, which is in also agreement with the findings for Q^{M} in Fig. 3.4. Specifically in presence of water, the resulting high AN value leads to a favorable solvation of the polyanion and the corresponding anionic counterions in presence of the polycation. Comparable conclusions can be also drawn for methanol. In contrast, DMAc shows a higher preference to dissolve the polycation and smaller cations, which is specifically evident for the coordination numbers around the polyelectrolyte in presence of Li^+ and Na^+. Thus, the AN and DN numbers can be brought into agreement with the interaction energies between ions and solvent molecules. The more favorable Coulomb energy of the anions in water and methanol (Fig. 3.8) when compared with the cations is thus in qualitative agreement with the high AN values (cf. Table 3.1). In contrast, the high DN value of DMAc is in agreement with the strong interactions between solvent molecules and cations as also depicted in Fig. 3.8. In consequence, the considered force fields allow us a reliable representation of experimental AN and DN values in terms of ion-solvent interaction energies. Furthermore, the AN and DN values in combination with the interaction energies provide a rationale for the observed differences between cation and anion condensation behavior in distinct solvents. Although the DN and AN concept strongly relies on empirical values [62, 140], it provides a simple estimate to understand general deviations from standard electrostatic mean field theories. Our findings reveal that the interaction energies between the ions and the solvent molecules reflect the experimentally measured AN and DN values, and thus provide a reasonable approach to rationalize the condensation behavior in terms of specific ion effects.

3.4 Summary

We performed atomistic MD simulations to investigate specific ion effects in aqueous and non-aqueous media. As reference systems, we introduced highly charged and rigid rod-like polyanion and polycation models in water, methanol and DMAc. Specific ion effects were studied with regard to the corresponding counterion distributions of alkali metal cations and halide anions around the polyelectrolytes. The simulation outcomes revealed distinct effects concerning the individual ion distribution behavior in different solvents. Furthermore, we computed the fraction of condensed counterions and compared the values to the outcomes of MO counterion condensation theory. Noteworthy, the validity of counterion condensation theores was often verified with good accuracy in terms of implicit solvent approaches using a restricted primitive model [46]. The results of our simulations demonstrated significant deviations to these theories, which can be mainly attributed to the influence of solvent-ion interactions, as usually neglected in mean-field approaches. In order to overcome these limitations, recent approaches [71, 12] thus introduced phenomenological hydration potentials in order to consider counterion-specific condensation behavior in aqueous solutions.
Interestingly, our findings concerning the cation and anion condensation behavior is also in agreement with the empirical donor and acceptor number concept. The introduction of acceptor and donor numbers provides a rationale to understand the solubility of salts in different solvents. Hence, it can be concluded that the force fields indeed reproduce experimental behavior [117, 118], and that the observed differences between the ion species can be mostly attributed to the underlying solvation properties in combination with electrostatic interactions. A more detailed analysis of the enthalpic contributions to the ion solvation energy highlighted the importance of ion-dipole and multipole interactions in combination with ion-size effects. With regard to our findings, we conclude that specific ion effects in different solvents thus depend on the size of the ions and the dipolar properties of the solvent molecules besides further aproptic or protic characteristics. The size of the solvent molecules is of minor importance, and becomes only important for small ion species like Li^+ and Na^+. We observed specific ion effects in pure solvents, but it is also important to understand ion solvation behavior in solvent mixtures, where ion solvation behavior can influence conductivity and ion pairing mechanisms. This is explained in detail in next chapters.

3.5 Acknowledgement

Most part of this chapter was reproduced from [91] with permissions from the Royal Society of Chemistry, Soft Matter.

Chapter 4

Preferential solvation and ion association properties in aqueous dimethyl-sulfoxide

4.1 Introduction

It was discussed that ion pairing effects have to be minimized in energy storage devices like polymer electrolyte membrane fuel cells to increase the efficiency and to achieve a higher ionic conductivity [88]. Over the last decades, specific attention was spent to the formation of ion pairs [113]. One can distinguish between contact and solvent-separated ion pairs [35, 54, 113, 190], while the mechanisms leading to the formation of these aggregates are still under debate [113, 54, 64]. Previous results reveal that the solvent is strongly involved in the formation of ion pairs, the occurrence of specific ion effects [111, 93, 104, 83] and the ion condensation behavior around macromolecules [210, 78, 106, 70, 194, 3, 71, 135, 204]. Further results revealed the importance of the solvent chemical activity for the occurrence of binding and ion pairing effects [113, 142, 143]. Vice versa, it was also found that the properties of the solvent are significantly modified under the influence of ions [36, 37, 111]. In terms of non-aqueous solutions, a recent study also analyzed the influence of polar and apolar solvents on the counterion condensation behavior around polyelectrolytes [175]. Indeed, it was found that the dielectric constant of the solvent imposes only a small influence on the condensation behavior [108] whereas the specific molecular details of the solvent are of main importance.

Hence, one can assume that also binary mixtures would have a drastic influence on the ion pairing effect. Closely related, an often discussed concept is preferential solvation [140]. One can distinguish between homoselective solvation, where both ion species are dissolved by the same co-solvent and heteroselective solvation where the solvation shells around the

ion species differ. A typical example for homoselective solvation is the dissolution of $CaCl_2$ in water-methanol mixtures [149], where both ion species are preferentially solvated by water molecules. In contrast, silver nitrate in acetonitrile-water mixtures reveals a heteroselective solvation such that the silver ions are solvated by acetonitrile whereas the nitrate ions are surrounded by water molecules in the first solvent shell [110]. In fact, one can assume that heteroselective solvation of ion species fosters low ion association constants which is beneficial for technological applications. Thus, solvents with different donor numbers [62, 140] can be used to establish heteroselective solvation of the ion species. In more detail, solvents with a high donor number usually accumulate around cations whereas solvents with a low donor number surround the anions. The rationale of the donor number concept was recently revealed by experiments and simulations [89, 175]. The results of these studies indicate that DMSO has a strong influence on polyelectrolytes and provides lower ion association constants compared to an aqueous solution. Thus, it can be speculated that a binary mixture of DMSO and water might result in a beneficial heteroselective solvation of the ion species. In this chapter, we study the ion pairing behavior between lithium ions and a sulfonated diphenylene sulfone [175] in presence of binary DMSO-water mixtures. In fact, we considered low concentrations of DMSO such that water can be interpreted as the solvent and DMSO as a co-solute. Comparable attempts for deep eutectic electrolytes also revealed promising results in presence of low concentrations of urea and sulfoneamides [181, 136]. Moreover, we study the solvation of a single ion pair to avoid the influence of long range electrostatic interactions and possible correlation effects between ion pairs. Our results indicate the appearance of pronounced ion pairing effects with increasing mole fractions of DMSO. The study of the pure solution without solutes reveals a significant non-ideal behavior, which is not reflected by the solvation shells around the ions. Thus, we found a homoselective solvation of both ion species which results in high association constants for increasing DMSO mole fractions and low ionic conductivities. Further results of the dielectric spectra verify a subtle mixing effect between DMSO and water which is in agreement to other structural and dynamic properties.

4.2 Theoretical Background

The presence of a preferential solvation mechanism can be detected by the calculation of the local/bulk partition coefficient [141, 39, 119] according to

$$K_\alpha(r) = \frac{(\langle n_\alpha(r)\rangle / \langle n_\beta(r)\rangle)}{(n_\alpha^{tot}/n_\beta^{tot})}, \tag{4.1}$$

where $\langle n_x(r)\rangle$ denotes the average number of solvent ($x = \alpha$) or co-solvent molecules ($x = \beta$) within a distance r to the solute and n_x^{tot} the total number of solvent or co-solvent molecules in the simulation box. A preferential solvation mechanism of the solvent molecules α results in $K_\alpha(r) > 1$ whereas preferential exclusion can be detected in accordance to $K_\alpha(r) < 1$ at short distances $r \leq 1$ nm.

The occurrence of ion pairs can be studied by the normalized cumulative number distribution function or distance-dependent association constant [175]

$$\theta(r) = \frac{4\pi}{N_c}\rho_c \int_0^\infty r^2 g_{ic}(r) dr \tag{4.2}$$

with the number N_c and the number density ρ_c of counterions and the radial distribution functions $g_{ic}(r)$ between ions and counterions. The association constant $\theta(l_B)$ can be estimated at the Bjerrum length $l_B = e^2/4\pi\varepsilon_r k_B T$ with the thermal energy $k_B T$, the elementary charge e and the dielectric constant ε_r.

The dielectric constant of the solution without ions can be calculated by

$$\varepsilon_r = 1 + \frac{4\pi}{3}\frac{\langle \Delta\vec{M}_{tot}^2 \rangle}{V k_B T}, \tag{4.3}$$

where $\langle \Delta\vec{M}_{tot}^2 \rangle$ denotes the fluctuations of the squared net total dipole moment of the solvent and co-solvent molecules in the simulation box with volume V[127]. In presence of charged species, Eqn. 4.3 is not applicable and one has to use an expression for the autocorrelation function of the total current or the individual currents in the system [152]. The frequency-dependent total conductivity can be calculated by

$$\sigma(\omega) = \frac{1}{3Vk_B T}\langle \vec{j}_T(t)\vec{j}_T(t_0)\rangle_\omega \tag{4.4}$$

with the total current $\vec{j}_T$ for angular frequencies $\omega = 2\pi\nu$. The brackets $\langle\cdot\rangle_\omega$ denote the averaged autocorrelation function transformed into Fourierspace reading

$$\langle\vec{j}_T(t)\vec{j}_T(t_0)\rangle_\omega = \int_{t_0}^{\infty}\langle\vec{j}_T(t)\vec{j}_T(t_0)\rangle e^{i\omega t}dt\,, \tag{4.5}$$

which can be inserted into

$$\varepsilon(\omega) = 1 + \frac{4\pi i\sigma(\omega)}{\omega} \tag{4.6}$$

to yield the static dielectric perimittivity $\varepsilon_r = \varepsilon(0)$ after evaluating the real part in the limit $\lim_{\omega\to 0}\Re(\varepsilon(\omega)) = \varepsilon_r$. The real part of the dielectric spectra ("permittivity") is denoted by $\varepsilon'(\omega)$ while the negative imaginary part ("loss") is represented by $\varepsilon''(\omega)$, so that $\varepsilon(\omega) := \varepsilon'(\omega) - \varepsilon''(\omega)$. In fact, one can also calculate the individual contributions of the different molecular constituents by taking into account the distinct currents $\vec{j}_x$ with $x \in \{\alpha,\beta,i,c\}$ in addition to cross-correlations. In addition, the ionic conductivity $\sigma := \sigma(\omega = 0)$ can be calculated via

$$\lim_{t\to\infty}\langle\Delta\vec{M}_j^2(t)\rangle = 2\langle\vec{M}_j^2(t_0)\rangle + 6Vk_BT\sigma t\,, \tag{4.7}$$

which can be interpreted as the mean squared displacement of the collective translational dipole moment in the simulation box. The corresponding conductivity can be obtained by the slope of the linear regression. It was shown in Ref. [152] that this so-called Einstein-Helfand conductivity gives a more reliable description of the true ionic conductivity than methods which are purely based on diffusion coefficients. We refer the reader to Refs. 152, 161 for more details.

4.3 Simulation Details

The ion pair is formed by two lithium ions (Li^+) and a single sulfonated diphenyle sulfone (SDS^{2-}). A snapshot of the molecular geometry is depicted in Fig. 4.1. Recent numerical and experimental results revealed interesting findings for polyelectrolytes with sulfonated diphenyl sulfones as monomeric building blocks [175, 204]. For example, it was shown that an ortho-form and meta-forms of the dimer result in different association constants [204]. Thus, we decided to study this system in more detail with regard to the aim that preferential solvation might facilitate even lower ion association constants. All-atom molecular dynamics simulations were performed with the GROMACS 4.5.5 software package [139]. The topologies and force fields of the dimer and the DMSO molecule were modeled as Generalized Amber Force Fields (GAFF)[198, 197] using ACPYPE [40]. The water model was TIP3P [81]. It was shown in Refs. 196, 29 that the dynamic and static properties of a

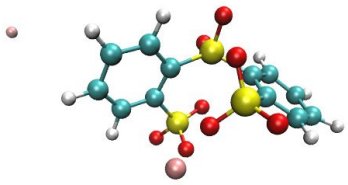

Fig. 4.1 Snapshot of the sulfonated diphenyle sulfone (SDS^{2-}) and two lithium ions (Li^{+}).

broad variety of solvents, and specifically DMSO (dimethyl sulfoxide), are well reproduced by GAFF. Two sets of DMSO-water solvent mixtures simulations were performed. One set of simulations in presence of the dimer and two lithium ions and the other set for the study of pure DMSO-water mixtures. For pure DMSO-water mixtures, we simulated mole fractions of $x_{\mathrm{DMSO}} = 0.1 - 0.9$ and also all ion simulations were carried out in mixtures with mole fractions of $x_{\mathrm{DMSO}} = 0.1 - 0.9$. Preferential solvation and association properties of ion pairs are studied for mole fractions of $x_{\mathrm{DMSO}} = 0.1 - 0.5$. Therefore, we are able to interpret the influence of DMSO as a co-solute which is in accordance to urea and sulfonamides in recent simulations of deep eutectic electrolytes [181, 136].
Electrostatic interactions for all systems were calculated by the Particle Mesh Ewald method [41] and all bonds were constrained by the LINCS algorithm [69]. The time step in all simulatons was 2 fs. All systems were equilibrated for 5 ns at 300 K and 1 bar pressure in an NpT ensemble by using the Nose-Hoover thermostat and the Parrinello-Rahman barostat [52, 133]. The initial box size was $(4 \times 4 \times 4\times)$ nm^3. All pure solvent mixture simulations were simulated for 20 ns whereas the systems with a single dimer and two lithium ions were simulated for 50 ns in a NpT ensemble at 300 K and 1 bar.

4.4 Results

4.4.1 DMSO/water mixture without ions

We first studied the properties of a binary DMSO-water mixture without ions. In fact, the properties of DMSO-water solutions were already studied in a series of publications [42, 188, 107, 23, 193, 209] in which non-ideal behavior for an increasing DMSO mole fraction was found. As a starting point, we study the dynamic properties of both components. The results for the diffusion coefficients are presented in Fig. 4.2. For pure water and pure DMSO, we found diffusion coefficients of $D_{cm} = (0.79 \pm 0.01) \times 10^{-5}$ cm^2/s (DMSO) and $D_{cm} = (5.91 \pm 0.01) \times 10^{-5}$ cm^2/s (water) which are in reasonable agreement with

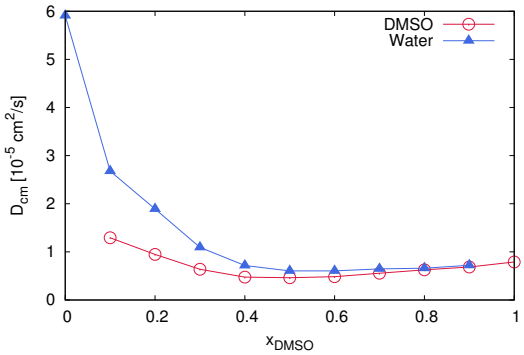

Fig. 4.2 Diffusion coefficient for DMSO (blue triangles) and water (red circles) in a DMSO-water mixture for different mole fractions x_{DMSO}.

previous experimental findings and simulation results [74, 114]. A minimum diffusion constant for both constituents can be found in the mixture for DMSO mole fractions between $x_{\mathrm{DMSO}} = 0.4 - 0.6$. Thus, the diffusion constant of water dramatically decreases roughly about one order of magnitude whereas the effects on DMSO are less significant. It has already been discussed [107, 209] that the minimum diffusion coefficients reveal a non-ideal behavior of the mixture which can be easily detected in terms of a nonlinear variation of the diffusivity. It has also been discussed that the occurrence of these effects can be mainly attributed to the formation of DMSO-water clusters in the aqueous solutions as DMSO has a tendency to form multiple hydrogen bonds with hydrogen atoms of water molecules [107]. Nevertheless, one of the most important indicators for a non-ideal solution behavior is given by the chemical activity and its derivatives. We calculated the derivative of the chemical activity a_{ss} with $s = \alpha, \beta$ in accordance to Eqn. (A.5) for both components. As depicted in Fig. 4.3, water reveals a nearly ideal behavior for all mole fractions due to values $a_{ss} \approx 1$. A value of $a_{ss} = 1$ indicates an ideal behavior as it was discussed for Eqn. A.5 due to the equivalence of the water-water and water-DMSO Kirkwood-Buff integrals. In contrast, DMSO shows a highly non-ideal behavior with the largest value $a_{ss} \approx 13.5$ at $x_{\mathrm{DMSO}} = 0.5$. The large value of a_{ss} indicates that the Kirkwood-Buff integral for DMSO-DMSO radial distribution functions, which can be interpreted as an excess volume, is smaller compared with the DMSO-water integral. Therefore, one can assume that the excess volume of the DMSO-DMSO accumulation is smaller than the excess volume for the DMSO-water aggregates. Moreover, also the excess particle number for DMSO-water pairs after multiplying with the corresponding bulk number density [137] in accordance to

$$N_{\alpha}^{xs} = \rho_{\alpha} G_{\beta\alpha} \tag{4.8}$$

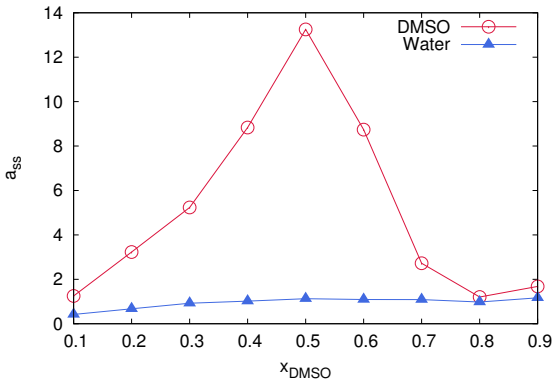

Fig. 4.3 Derivative of the chemical activity a_{ss} for DMSO (red circles) and water (blue triangles) in a DMSO-water mixture for different mole fractions x_{DMSO} for DMSO.

is larger for DMSO-water than for the DMSO-DMSO accumulation behavior. Hence, compared to an ideal solution, it can be concluded that DMSO interacts more with water compared to itself, which supports the assumption of local DMSO-water clusters [107].
In addition, we also calculated the dielectric constant ε_r for different mole fractions x_{DMSO} by evaluating Eqn. 4.6 in the limit of $\omega \to 0$. The results are depicted in Fig. 4.4. The black line corresponds to an ideal solution with $\varepsilon_r^{\mathrm{id}} = \varepsilon_r^{\mathrm{H_2O}}(1 - x_{\mathrm{DMSO}}) + \varepsilon_r^{\mathrm{DMSO}} x_{\mathrm{DMSO}}$ with the dielectric constants $\varepsilon_r^{\mathrm{H_2O}} = 95.32$ and $\varepsilon_r^{\mathrm{DMSO}} = 55.54$ for the pure solvents. The results for pure TIP3P water are in good agreement with previous simulations [73] whereas the results for DMSO are in reasonable coincidence with further simulation findings and experimental results [175]. Based on our findings, it can be concluded that a direct pairing between water and DMSO molecules due to $\varepsilon_r(x_{\mathrm{DMSO}}) < \varepsilon_r^{\mathrm{id}}(x_{\mathrm{DMSO}})$ is evident such that the resulting total dipole moment is significantly smaller than in an ideal solution in agreement to the values for the derivative of the chemical activity.

4.4.2 Properties of ion pairs in aqueous DMSO solutions

With regard to the interpretation of DMSO as a co-solute in presence of the ions, we are restricted to study Li^+/SDS^{2-} pairs for DMSO fractions $x_{\mathrm{DMSO}} \leq 0.5$ as it was discussed in the introduction. We first study the radial distribution functions (RDFs) for DMSO and water molecules around lithium ions and SDS^{2-}. The results can be found in Fig. 4.5. It becomes evident that the first solvent shell around lithum ions at $r \approx 0.2$ nm is purely composed of water molecules. With increasing mole fractions of DMSO, this effect is even more pronounced with regard to slightly higher values for the first peak in the RDFs. In contrast, the second solvent shell at $r \approx 3$ nm is formed by DMSO molecules where the peak value

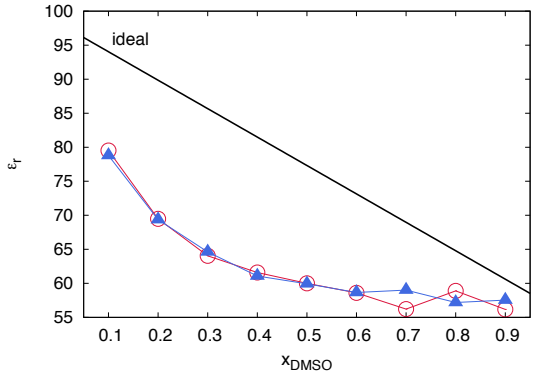

Fig. 4.4 Dielectric constant ε_r of the solution for different mole fractions x_{DMSO}. The black line represents the values for an ideal solution whereas the red circles denote the results for the pure solution and the blue triangles the results for the DMSO-water solution in presence of the ion pair as calculared by Eqn. 4.6.

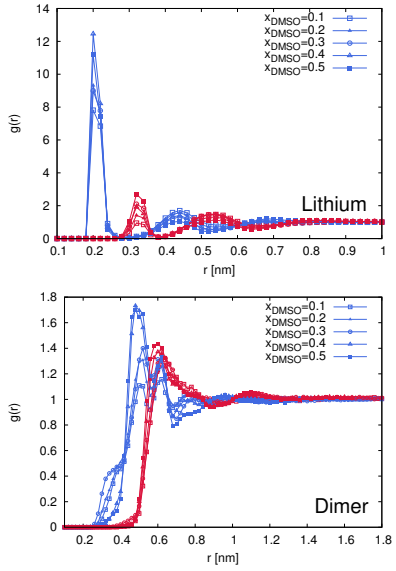

Fig. 4.5 Radial distribution functions at different mole fractions x_{DMSO} for the center-of-masses of DMSO and water molecules around lithium ions (top) and SDS^{2-} (bottom). The different mole fractions are denoted by the symbols described in the legend. Blue lines correspond to the RDFs between water and the ions whereas all red lines represent the results for the RDFs of DMSO molecules around the ions.

decreases for higher DMSO mole fractions. Hence, one can observe five distinct water and DMSO solvent shells for distances $r \leq 0.9$ nm. The formation of distinct local solvent shells was also found for spherical solute particles in ionic liquids [101, 99]. This finding can be mostly rationalized in terms of entropic effects due to the smaller size of the water molecules compared to DMSO in accordance to the properties of ionic liquids [101, 99]. However, the first solvent shell is always occupied by water molecules which contradicts the higher donor number for DMSO compared to water [175]. Therefore, it can be clearly seen that size effects dominate the preferential solvation of lithium ions in contrast to specific chemical details as it was discussed in a previous publication for one-component solvents [175].
A comparable behavior can be found for the dimer SDS^{2-}. The first solvent shell including several subpeaks at distances $r \approx 0.2 - 0.75$ nm is formed by water molecules. A mixed solvent shell composed of DMSO and water molecules can be found at $r \approx 0.65$ nm. Moreover, one can clearly see that higher mole fractions of DMSO lead to a depletion of water molecules around SDS^{2-} at distances $r \leq 0.4$ nm. In fact, for larger values of x_{DMSO}, the water molecules strongly assemble at distances $r \approx 0.4$ nm which results in a significant inrease of the first peak value for $x_{\mathrm{DMSO}} \geq 0.3$.
The results for the local/bulk partition coefficient in accordance to Eqn. (4.1) are shown in Fig. 4.6. We first discuss the properties of the local/bulk partition coefficient for DMSO (bottom of Fig. 4.6). It can be clearly seen that the local / bulk partition DMSO coefficient around SDS^{2-} is given by $K_\beta(r) < 1$ for all distances. Thus, it becomes evident that DMSO is preferentially excluded from SDS^{2-}. This finding is also validated by the strong preferential solvation of SDS^{2-} by water molecules (bottom right side of Fig. 4.6). All local/bulk partitioning coefficients reveal $K_\alpha(r) > 1$ at short distances which even increases for higher mole fractions of DMSO. Thus, a preferential solvation of SDS^{2-} by water molecules is validated.
In contrast to SDS^{2-}, lithium ions show a more subtle solvation behavior (top part of Fig 4.6). In accordance to the radial distribution functions shown in Fig. 4.5, it can be clearly seen that the first solvent shell at short distances is fully occupied by water molecules due to negligible values of $K_\beta(r) \approx 0$ at $r \leq 0.2$ nm. In more detail, a preferential solvation of SDS^{2-} by DMSO as indicated by $K_\beta(r) \geq 1$ can be only found for $r \geq 0.6$ and DMSO mole fractions $x_{\mathrm{DMSO}} \geq 0.4$. In contrast, a large value of the local/bulk partition coefficient can be observed for water molecules around lithium ions (right upper part of Fig. 4.6). Thus, based on these findings, we conclude that the first solvent shells around lithium ions and SDS^{2-} are formed by water molecules. Both constituents are therefore more likely to be surrounded by water molecules which verifies a homoselective solvation mechanism. Indeed, these results reveal the failure of the donor and acceptor number concept for DMSO/water mixtures whereas it

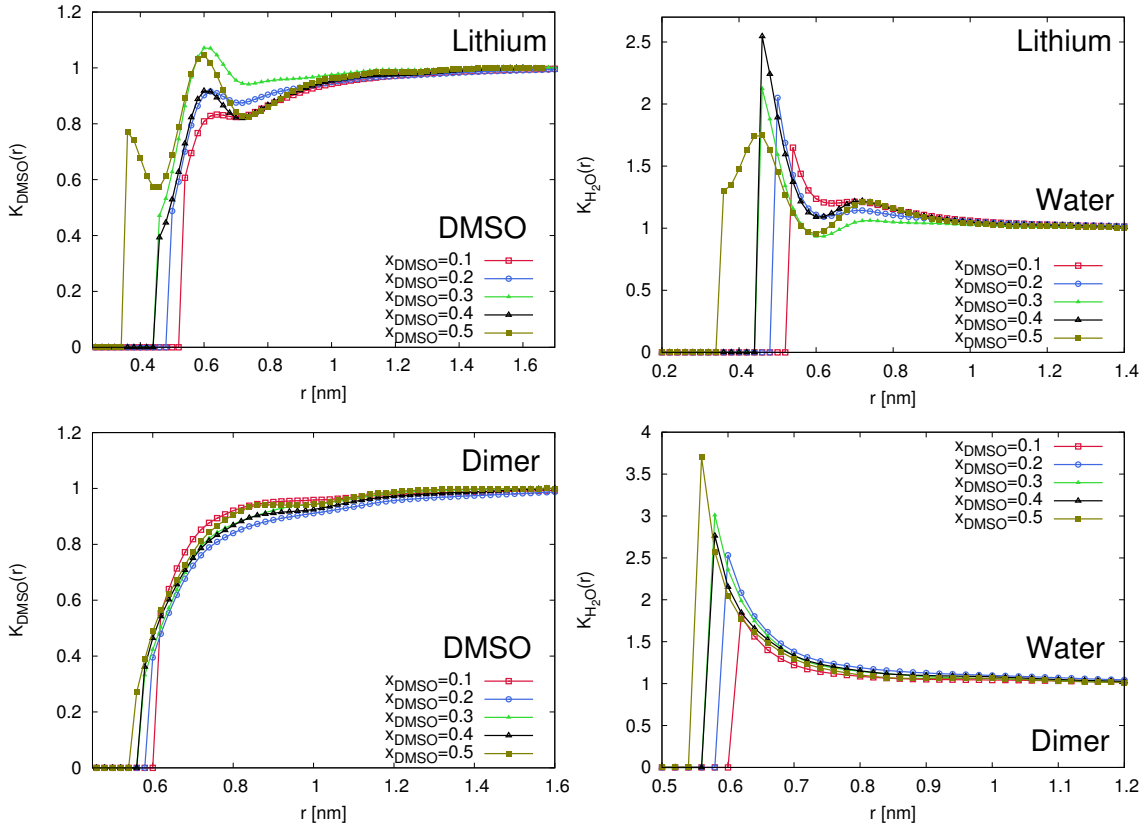

Fig. 4.6 Local/bulk partition coefficient for DMSO (left side) and water (right side) around lithium ions (top) and the SDS^{2-} dimer (bottom) for different DMSO mole fractions x_{DMSO}.

was validated for pure solutions in Ref. 175. Hence, although the donor numbers between water and DMSO differ, both ionic components are more preferentially solvated by water molecules.

4.4.3 Ion pairing and ionic conductivity

Finally, we also studied the formation of ions pairs. Several theories were proposed to describe the degree of ion pairing in aqueous systems (for an overview we refer the reader to Refs. 113, 190). In fact, we found a highly non-trivial binding behavior where a systematic distinction in terms of theoretical attempts is more challenging than expected. The corresponding results are presented in Fig. 4.7. One can clearly see that the association constant θ_c, which represents the fraction of ion pairs, grows non-linearly with the mole fraction of DMSO. We distinguished between bound pairs and free ions by the calculation of the Bjerrum length $l_B \propto 1/\varepsilon_r$ where we inserted the corresponding values for the mixtures of the dielectric constant. Hence, if lithium ions are within a distance of the Bjerrum length to the charged -SO_3^- group, we consider them as condensed. However, the results for the radial distribution function between the dimer and the lithium ions indicated that only direct contact pairs [113] at distances $d \approx 0.2$ nm are evident. We compared the results for the association constant to standard theories like the Eigen-Fuoss approach and the Manning-Oosawa counterion condensation theory [113]. Due to the limited amount of data points, a satisfying agreement with these theories was absent. This can be explained by non-ideal effects as well as the limited set of data points. More detailed studies in the future will help to shed light at this mechanism. Nevertheless, it becomes evident that significant ion pair formation occurs for higher mole fractions of DMSO which reveals the absence of the preferential solvation concept. These findings are supported by recent molecular dynamics simulations [175] where it was also found that specific chemical details of the solvent strongly influence the condensation behavior. Hence, it can be speculated that the non-ideal properties of the solvent are also reflected by the association constant.

Moreover, also the ionic conductivity σ in accordance to Eqn. 4.7 shows a non-linear decrease for increasing DMSO fractions. The results are presented in Fig. 4.8. It can be clearly seen that large association constants are accomplished by low ionic conductivities. Due to the fact that we caclulated the Einstein-Helfand conductivity (Eqn. 4.7), it can be assumed that these findings are in good agreement with the real conductivity. Hence, a significant fraction of ion pairs decreases the ionic conductivity. These findings indicate that the non-ideal properties of DMSO-water mixtures prevent a usage as solvents for ionic systems. Thus, the ionic conductivity decreases by roughly one order.

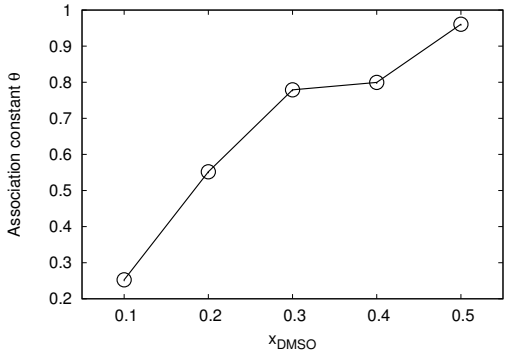

Fig. 4.7 Association constant found in the simulation by the fraction of condensed counterions θ_c for different mole fractions x_{DMSO}. All counterions within the actual Bjerrum length were considered as condensed in the simulations.

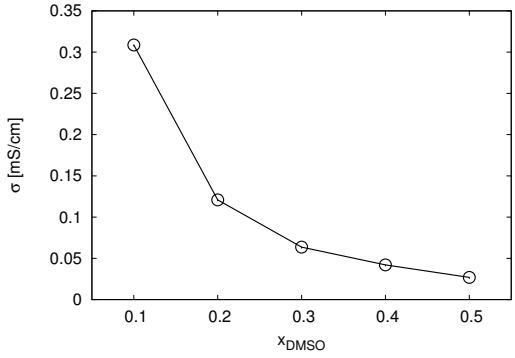

Fig. 4.8 Ionic conductivity σ for combined lithium ion and dimer contributions for different DMSO mole fractions x_{DMSO}. The solid line is only a guide for the eye.

4.5 Summary and Conclusion

We studied the properties of dimeric ion pairs in binary solvent mixtures of DMSO and water by molecular dynamics simulations. Our results for the derivative of the chemical activity indicate a strong non-ideal behavior of the pure solution for mole fractions $x_{\mathrm{DMSO}} \geq 0.4$. The absence of a preferential solvation for the ions is evident. In fact, the first solvation shell around both constituents is formed by water molecules. Moreover, we observed a preferential exclusion of DMSO by the evaluation of the local/bulk partition coefficients around the ions. Hence, with regard to the functionality of DMSO molecules in the mixture and on their action on the constituents, it can be speculated that the co-solvent of DMSO can be brought into agreement with protein protectants, also called kosmotropic osmolytes, such as trimethylamine-N-oxide (TMAO), ectoine or hydroxyectoine [171]. Specifically for these molecules, a preferential exclusion around charged and uncharged molecules can be found. Thus, the concept of additive preferential solvation is perturbed by the properties of solvents and co-solvents as recently demonstrated for high molar concentrations of urea and intermediate values for ionic liquids and their subtle binding behavior [119]. In summary, our study indicates that preferential solvation of different solutes with regard to varying values for the donor and acceptor numbers fails. Competing effects like preferential exclusion in aqueous solution win. In fact, it is not clear if preferential solvation fails only in aqueous binary mixtures whereas other organic solvents show more subtle properties. Thus in our next chapter, we try to formulate a theoretical model to understand the ion pairing behaviour in ideal and partially non ideal solvent mixtures using KB theory.

4.6 Acknowledgement

Most part of this chapter was reproduced from Ref [92] with permissions from the Royal Society of Chemistry, Physical Chemistry Chemical Physics.

Chapter 5

Influence of co-solutes on chemical equilibrium

5.1 Introduction

Aqueous electrolyte solutions of simple salts reveal a plethora of specific ion effects and ion pairing mechanisms [113, 189]. One can distinguish between contact, solvent-shared and solvent-separated ion pairs, whereas the theoretical description of ion pair formation is challenging and even nowadays under debate [35, 54, 113, 190]. In order to complement theoretical predictions, computer simulations allow us to achieve deeper insights into the underlying behavior [189]. Hence, it was found that ions differ in their binding behavior and can be further distinguished by their chaotropic and kosmotropic properties [37]. As it was often discussed [104, 211], smaller ions like fluoride reveal kosmotropic properties, meaning that they are water structure makers whereas larger ions like iodide are chaotropes, which highlights their water-structure breaking effects. Based on these concepts, the law of matching water affinities was developed [37], which states that kosmotropic and chaotropic cations and anions form the most stable ion pairs. In fact, although specifically the presence of chaotropic properties remains highly debated, it is evident with regard to experimental results, that the individual hydration properties of the ions play a decisive role in their pairing behavior.

As it was recently pointed out [113, 189], the fundamental mechanism leading to ion pair formation is yet to be found. Computer simulations revealed that contact ion pairs (CPs) are marginally stable configurations with life times of several picoseconds. Dynamic transitions to solvent-shared (1SP) and solvent-separated (2SP) ion pairs take place, which significantly differ from contact ion pairs due to the presence of hydration shells between the ions. Hence,

solvent-separated and solvent-shared ion pairs can be detected at larger ion distances by the corresponding local minimima in the potential of mean force curves between the ions. Hence, the distance between the ions increases with the order CP $>$ 1SP $>$ 2SP, which also expresses their energetic stability. This can be briefly rationalized by the fact that the net electrostatic binding energy between the ions decreases for increasing distances. Due to the fact that Coulomb forces are long-ranged, it is usually assumed that ion pair formation occurs up to distances of 0.7 nm for aqueous solutions, which agrees with the Bjerrum length in pure water [37]. With regard to the definition and the formation of ion pairs, it becomes clear that the properties of the solvent play a decisive role [116]. Thus, it is clear that an ion pair dissociates only in highly polar solvents with high dielectric constants in order to minimize the electrostatic binding energy. However, the fundamental role of solvation shells on ion pair formation is still under debate. Previous results demonstrated that the solvent itself as well as the solvent chemical activity [113, 142, 143] strongly influence many effects, *e. g.* the formation of ion pairs [113, 190], the occurrence of specific ion effects [111, 93, 104, 83] and the ion condensation behavior around macromolecules [210, 78, 106, 70, 194, 3, 71, 135, 204]. Furthermore, in recent years, more effort was spent on the role of different solvents and the occurrence of specific ion effects as been evident for ions in water [116].

The rising interest in non-aqueous solutions can be mostly rationalized by the rapid growth of electrochemical applications. Often used non-aqueous electrolytes are carbonates and ionic liquids (ILs) which reveal a broad electrochemical window and a reasonably high dielectric constant among other beneficial properties [8]. Unfortunately, the properties of the ions in these solutions are still under debate and were only sparsely investigated for non-IL solutions. A promising new route was established by using co-solutes or additives as a third component in the solution. In accordance with previous findings, one can assume that tunable mixtures provide a controllable influence on the ion pairing mechanism. IAn often discussed concept for binary solutions in order to minimize the number of ion pairs is preferential solvation [140]. One can distinguish between homoselective solvation, where both ion species are dissolved by the same compound of the solution, and heteroselective solvation where the solvation shells around the ions differ. A typical example for homoselective solvation is the dissolution of $CaCl_2$ in water-methanol mixtures [149], where both ion species are preferentially solvated by water molecules. In contrast, silver nitrate in acetonitrile-water mixtures reveals a heteroselective solvation [110].

A well established empirical framework to understand preferential solvation was proposed by the donor number concept [62, 140]. Herewith, the ability of the solvent to dissolve cations can be quantified. In more detail, solvents with a high donor number usually accumulate around cations, whereas solvents with a high acceptor number prefer the solvation

of anions. Notably, the implications of the donor number concept for polyelectrolytes in water, DMSO and chloroform were recently demonstrated by experiments and simulations [89, 175]. The results of these studies indicated that DMSO with a high donor number fosters the occurrence of free alkali ions, and thus provides a lower association constant compared to water. Therefore, it can be assumed that the usage of binary mixtures for increasing ion dissociation behavior can be regarded as a possible option to improve the ion transport efficiency in electrochemical devices. In contrast to these findings, recent simulations by us [92] revealed that the presence of DMSO significantly increases the amount of ion pairs in aqueous solution. Hence, a complex interplay between solutes, solvents and co-solutes occurs which is often hard to predict. A theoretical framework to study higher component solutions was introduced by Kirkwood and Buff in 1951 [85].

5.2 Theoretical Background

5.2.1 Chemical reaction: Ion pair dissociation-association equilibrium

For the development of our theory, we consider a simple ion pair dissociation-association reaction in aqueous solution and in chemical equilibrium according to

$$(\mathrm{X^+Y^-})_{\mathrm{aq}} <=> \mathrm{X^+_{aq}} + \mathrm{Y^-_{aq}}$$

with the associated contact ion pair $(\mathrm{X^+Y^-})_{\mathrm{aq}}$ and the fully dissociated ion species $\mathrm{X^+_{aq}}$ and $\mathrm{Y^-_{aq}}$. Although we assume an aqueous reaction medium, it has to be noted, that also any other one-component solvent is sufficient for our purposes. The corresponding equilibrium reaction constant reads

$$K = \prod_j a_i^{\nu_j} = \frac{a_{\mathrm{X^+_{aq}}} \cdot a_{\mathrm{Y^-_{aq}}}}{a_{(\mathrm{X^+Y^-})_{\mathrm{aq}}}} \tag{5.1}$$

with the stoichiometric coefficients ν_j and the chemical activities a_j for each species. With the definition of the chemical potential [7]

$$\mu_j = \mu_j^0 + RT \ln a_j \tag{5.2}$$

with the molar gas constant R, the temperature T and the standard chemical potential μ_j^0, the difference in the chemical potentials for an equilibrium reaction can be written as $\Delta\mu = \sum_j \nu_i \mu_j$. In chemical equilibrium, it follows $\Delta\mu = 0$ and Eqn. (5.2) can be inserted into Eqn. (5.1) to yield

$$\Delta\mu^0 = -RT \ln K \tag{5.3}$$

with $\Delta\mu^0 = \sum_j \nu_j \mu_j^0$. Thus, it can be concluded that any influence of co-solutes on the chemical equilibrium has its origin in a modification of the chemical potential difference.

5.2.2 The influence of co-solutes on the chemical equilibrium

In order to develop an expression for the influence of co-solutes on the chemical equilibrium, we introduce the concepts of transfer free energies and *m*-values, which were shown to be helpful for the understanding of protein denaturation and stabilization experiments in presence of co-solutes [30, 137, 172]. Via the analysis of experimental data, the so called *m*-value [30, 137] can be determined, which is defined by

$$\Delta\mu_{\mathrm{cs}} = \Delta\mu^0 - mRTc_3 \tag{5.4}$$

with the concentration of co-solute species c_3 and the *m*-value, where $\Delta\mu_{\mathrm{cs}}$ denotes the modified chemical potential difference in presence of co-solutes. Thus, negative values for m indicate a shift of the chemical equilibrium towards the associated state with $\Delta\mu_{\mathrm{cs}} > \Delta\mu^0$, whereas positive values for m imply the preference of the dissociated state with $\Delta\mu_{\mathrm{cs}} < \Delta\mu^0$. Thus, Eqn. (5.1) can be reformulated in order to read

$$K_{\mathrm{cs}} = \exp(-\Delta\mu_{\mathrm{cs}}/RT) = \exp(-\Delta\mu^0/RT)\cdot\exp(mc_3) = K\cdot K_{\mathrm{app}} \tag{5.5}$$

with

$$K_{\mathrm{app}} = \exp(mc_3) \tag{5.6}$$

where K_{app} denotes the apparent chemical equilibrium constant due to the presence of co-solutes. In combination with Eqn. (5.3), one can thus write

$$\Delta\mu_{cs} = -RT\ln K - RT\ln K_{\mathrm{app}} \tag{5.7}$$

The question now arises how co-solutes induce a shift of the chemical equilibrium? A consistent description based on thermodynamic and statistical mechanics arguments is provided by the Kirkwood-Buff (KB) theory, which was originally developed as a molecular theory of solutions and solution mixtures [86]. In the following, we will present a heuristic derivation of the KB theory, whereas more rigorous formulations can be found in Refs. [86, 66, 128, 34, 16, 176, 177, 166, 156, 142, 144, 179, 145, 180, 170, 13, 138]. More specifically, we focus on the corresponding analysis of the binding behavior between ions ('$j = 2$') and co-solute species ('$j = 3$') in presence of water molecules or more generally solvent molecules ('$j = 1$'). It has to be noted, that we always obey the restriction that the mole fraction of

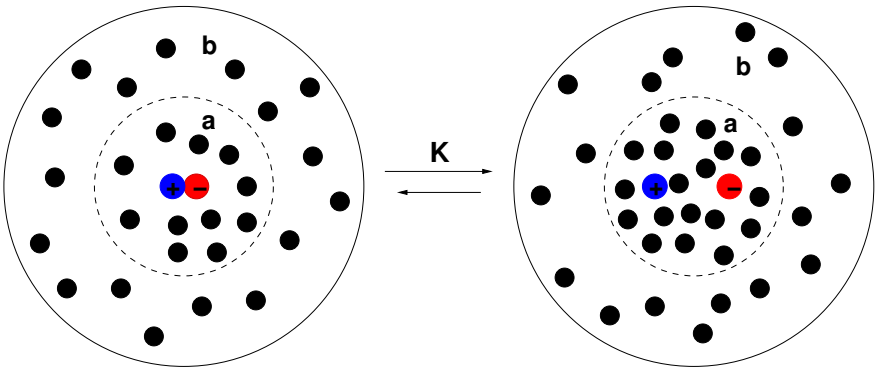

Fig. 5.1 Schematic illustration of ion dissociation in presence of co-solutes (black spheres). The cation (blue sphere) and the anion (red sphere) are located in the local region (a) and form a contact ion pair on the left side. The more pronounced binding of co-solutes to the dissociated ions favors a dissociation of the ion pair (right side). The chemical potential in the bulk region (b) remains constant.

co-solute species is $x_i \ll 1$. According to standard approaches for ions [95–97, 176, 137], we assume that X^+ and Y^- are indistinguishable. Furthermore, we assume a constant temperature T and a vanishing ion concentration in the limit of infinite dilution. The total system including all species can be divided into two subsystems [66]: system (a) with volume V_α including co-solute species, water molecules and the ions and system (b) with volume V_β containing only co-solute and water molecules. A schematic presentation of the system is shown in Fig. 5.1. The volume relation reads $V_\beta \gg V_\alpha$, which also means that the ions do not perturb the co-solute and solvent distribution in the larger system. With regard to thermodynamic and chemical equilibrium, one can define two Gibbs-Duhem relations [66, 128, 137]

$$-N_1' d\mu_1 - N_2' d\mu_2 - N_3' d\mu_3 + (V_\alpha - N_2' \bar{V}_2)(d\pi + dp) = 0 \tag{5.8}$$

and

$$-N_1 d\mu_1 - N_3 d\mu_3 + V_\beta dp = 0 \tag{5.9}$$

with the osmotic pressure π and the total pressure p, the partial molar volume of the ions $\bar{V}_2$ and the number of molecules N_j' and N_j with $j = 1,2,3$ as mentioned above in systems (a) and (b), respectively. For constant pressure $dp = 0$, the second equation can be used to yield a definition for μ_1, which can be inserted into Eqn. (5.8). With van't Hoff's law $\pi = RT(N_2'/V_\alpha)$ [7] for $N_2'/V_\alpha \to 0$ and the approximation $(V_\alpha - N_2'\bar{V}_2) \approx V_\alpha$, the resulting chemical potential after division by $N_2' = 1$, in terms of an associated contact ion pair, reads $d\mu_2^* = d(\mu_2 - RT \ln \rho_2')$ with $\rho_2' = N_2'/V_\alpha$. In the limit of negligible ion concentration, the

chemical potential of the ion pair further reduces to the standard chemical potential with $d\mu_2^* \approx d\mu_2^0$. Differentiation with respect to the chemical potential of the co-solute finally gives

$$\nu_{23} = -\left(\frac{\partial \mu_2^0}{\partial \mu_3}\right)_{p,T,\rho_2 \to 0} = N_{23} - \frac{\rho_3}{\rho_1} N_{21} \tag{5.10}$$

as an expression for the preferential binding coefficient ν_{23} between co-solute molecules and the ions, including the new definition $N_{2j} = N'_j$ and the bulk number density $\rho_j = N_j/V_\beta$. Hence, the value of Eqn. (5.10) can be interpreted as an estimator for the accumulation or exclusion of co-solute molecules in the local region around the ions. A comparable calculation for non vanishing solute or protein concentrations was presented in Ref. 66.
The connection between the preferential binding model and the Kirkwood-Buff (KB) theory can now be established by the corresponding cumulative number of molecules around the ions

$$N_{2j}(r) = 4\pi\rho_j \int_0^r R^2 g_{2j}(R)\, dR \tag{5.11}$$

where the pair radial distribution function between the ions and species j is defined by $g_{2j}(R) = \rho_{2j}(r)/\rho_j$, where $\rho_{2j}(r)$ denotes the local number density. In more detail, Eqn. (5.10) can be also expressed by Kirkwood-Buff integrals according to

$$G_{ij} = 4\pi \int_0^\infty r^2 [g_{ij}(r) - 1]\, dr \tag{5.12}$$

which can be approximated by

$$G_{ij} = \lim_{r_c \to \infty} G_{ij}(r_c) = 4\pi \lim_{r_c \to \infty} \int_0^{r_c} r^2 [g_{ij}(r) - 1]\, dr \tag{5.13}$$

where r_c denotes a finite cutoff distance as defined by the relation $\lim_{r_c \to \infty} g_{ij}(r_c) = 1$, such that $G_{ij}(r_c) \approx G_{ij}$ [34, 177, 138]. The so-derived relation for Eqn. (5.10) in combination with Eqn. (5.13) and Eqn. (5.11) reads

$$\nu_{23} = \rho_3 \lim_{r \to \infty} (G_{23}(r) - G_{21}(r)) = \rho_3 (G_{23} - G_{21}) \tag{5.14}$$

which takes the differences of the excess volumes of co-solute and solvent molecules around the ions into account. [176, 177, 166, 156, 168, 169, 142, 144, 179, 145, 180, 170, 13, 138]. The corresponding KB integrals according to Eqn. (5.14) for ion-solvent and ion-co-solute interactions, respectively, are defined by

$$G_{2j} = G_{j2} = \frac{n_+}{n_\pm} G_{+j} + \frac{n_-}{n_\pm} G_{-j} \tag{5.15}$$

with $G_{2j} = G_{\pm j} = G_{j\pm}$, where n_+ and n_- denote the number of species in the chemical reaction with $n_\pm = n_+ + n_-$.
If we now assume different chemical potentials of the states (associated ion pair state with μ_A^0 and dissociated ions with μ_D^0) in accordance with $\Delta\mu_2 = \mu_D^0 - \mu_A^0$, one can calculate the difference in the preferential binding coefficients between the dissociated and the associated ion state according to

$$\Delta\nu_{23} = -\left(\frac{\partial\Delta\mu_2}{\partial\mu_3}\right)_{p,T,\rho_2'\to 0} = \Delta N_{23} - \frac{\rho_3}{\rho_1}\Delta N_{21} = \rho_3(\Delta G_{23} - \Delta G_{21}) \tag{5.16}$$

where the corresponding differences under the assumption $\bar{V}_2{}^D \approx \bar{V}_2{}^A$ in the number of co-solute and water molecules and the differences in the KB integrals around the dissociated and the associated state are defined by $\Delta N_{2j} = N_{2j}^D - N_{2j}^A$ and $\Delta G_{2j} = G_{2j}^D - G_{2j}^A$, respectively. In combination with Eqn. (5.7), it follows

$$\Delta\nu_{23} = RT\left(\frac{\partial\ln K_{\mathrm{cs}}}{\partial\mu_3}\right)_{p,T,\rho_2\to 0} = \left(\frac{\partial\ln K_{\mathrm{app}}}{\partial\ln a_3}\right)_{p,T,\rho_2\to 0} \tag{5.17}$$

with $(\partial\ln K/\partial\ln a_3)_{p,T,\rho_2\to 0} = 0$. Thus, the binding properties of co-solutes significantly shift the chemical equilibrium towards the dissociated ($\Delta\nu_{23} > 0$) or the associated state ($\Delta\nu_{23} < 0$).

5.2.3 Implications for dissociation-association reactions

According to the proposed association-dissociation reaction and the corresponding chemical reaction constant in Eqn. (5.1), the probability of ion pair formation is given by p_A, whereas the probability of ion pair dissociation is defined by $p_D = 1 - p_A$. If we now assume that the fraction of ion pairs θ_c represents the corresponding p_A, one can rewrite Eqn. (5.1) in terms of a detailed balance condition according to

$$K = \frac{p_D}{p_A} = \frac{1-p_A}{p_A} = \frac{1-\theta_c}{\theta_c} \tag{5.18}$$

which can be inserted into Eqn. (5.7), whereas the value for $K_{\mathrm{app}} = 1$ in absence of co-solutes. With $\mu = (\partial F/\partial N)_{N,V,T}$ where the free energy is denoted by F in the canonical ensemble and Eqn. (5.6), we can rewrite Eqn. (5.7) in order to read

$$\frac{\Delta F_{\mathrm{cs}}}{k_B T} = -\ln K - m\rho_3 \tag{5.19}$$

which allows us to extract the m-value in regards of the actual co-solute bulk number density ρ_3. Hence, if we define the actual association constant in presence of co-solutes as θ_c^{cs} and in absence of co-solutes as θ_c^0 for $\rho_3 = 0$, we can rewrite the above discussed relation as

$$\ln\left(\frac{1-\theta_c^{\mathrm{cs}}}{\theta_c^{\mathrm{cs}}}\right) = \ln\left(\frac{1-\theta_c^0}{\theta_c^0}\right) + m\rho_3 \tag{5.20}$$

which can be used to determine the m-value from simulation and experimental data via a linear regression for constant m-values which do not depend on the actual value of ρ_3. Furthermore, it has to be noted that a comparable linear expression can be formulated for the co-solute mole fraction instead of the co-solute number density.
Furthermore, we can also find an expression for the m-value. Hence, a free energy difference between the dissociated and the associated ion pair in presence of co-solutes according to Eqn. (5.4) can be also expressed by $\Delta\Delta F_{\mathrm{cs}} = \Delta F_{\mathrm{cs}} - \Delta F = -mk_BT\rho_3$ for $\rho_2 \to 0$ and constant temperature T and pressure p giving

$$m = -\frac{1}{k_BT}\left(\frac{\partial\Delta\Delta F_{\mathrm{cs}}}{\partial\rho_3}\right)_{T,p} = \left(\frac{\partial \ln K_{\mathrm{app}}}{\partial\rho_3}\right)_{T,p} \tag{5.21}$$

which can be further transformed into

$$\left(\frac{\partial \ln K_{\mathrm{app}}}{\partial \ln a_3}\right)_{T,p}\left(\frac{\partial \ln a_3}{\partial\rho_3}\right)_{T,p} = \Delta\nu_{23}\left(\frac{\partial \ln a_3}{\partial\rho_3}\right)_{T,p} \tag{5.22}$$

and

$$\left(\frac{\partial \ln a_3}{\partial \ln\rho_3}\right)_{T,p}\left(\frac{\partial \ln\rho_3}{\partial\rho_3}\right)_{T,p} = \frac{a_{33}}{\rho_3} \tag{5.23}$$

in order to derive an expression for the m-value [137] according to

$$m = \left(\frac{\partial \ln K_{\mathrm{app}}}{\partial\rho_3}\right)_{T,p} = \frac{a_{33}\Delta\nu_{23}}{\rho_3} \tag{5.24}$$

with the derivative of the chemical activity [86, 16, 128, 179, 137]

$$a_{33} = \left(\frac{\partial \ln a_3}{\partial \ln\rho_3}\right)_{T,p} = \frac{1}{1+\rho_3(G_{33}-G_{31})} \tag{5.25}$$

where G_{ij} are the corresponding Kirkwood-Buff integrals [86, 16] as discussed in Eqn. (5.12). Hence, by inserting the expression of Eqn. (A.4) into Eqn. (5.20), one can find the linear

relation

$$\ln\left(\frac{1-\theta_c^{\mathrm{cs}}}{\theta_c^{\mathrm{cs}}}\right) = \ln\left(\frac{1-\theta_c^{0}}{\theta_c^{0}}\right) + a_{33}\Delta\nu_{23} \tag{5.26}$$

which can be tested by plotting the actual values for $\Delta\nu_{23}$ vs. $\ln\left(\frac{1-\theta_c^{\mathrm{cs}}}{\theta_c^{\mathrm{cs}}}\right)$. If a_{33} is constant over the entire mole fraction range, one would thus observe a linear relation. Furthermore, with regard to the defintions $K^{\mathrm{cs}} = 1-\theta_c^{\mathrm{cs}}/\theta_c^{\mathrm{cs}}$ and $K^0 = 1-\theta_c^0/\theta_c^0$, Eqn. (5.26) can be equivalently written as

$$K^{\mathrm{cs}} = K^0 \exp(a_{33}\Delta\nu_{23}) \tag{5.27}$$

and the resulting association constant can be calculated via

$$\theta_c^{\mathrm{cs}} = \frac{1}{1+K^0\exp(a_{33}\Delta\nu_{23})} \tag{5.28}$$

which highlights the fact that the association behavior depends non-linearly on the values of a_{33} or $\Delta\nu_{23}$.

5.3 Simulation results

In order to verify our theory, we performed all-atom molecular dynamics simulations of sodium chloride pairs in water/dimethylacetamide mixtures, the detials of the simulations are provided in A.1. A crucial point for the influence of co-solutes on the chemical equilibrium is given by the derivative of the chemical activity a_{33} according to Eqns. (A.5) and (5.26). Thus, we first determined the derivatives of the chemical activity for DMAc in water and vice versa. The corresponding results are shown in Fig. 5.2. As it was pointed out in Ref. 92, the values for the derivatives of the chemical activity in mixtures provide an estimate for the non-ideality of the solution. Thus, the more the values differ from $a_{\alpha\alpha} = 1$, the more non-ideal is the distribution of the species α in the solution. With regard to the results shown in Fig. 5.2, it becomes evident that the water chemical activity derivative reveals values between $a_{\alpha\alpha} = 1-2$. For lower mole fractions, corresponding larger values for $a_{\alpha\alpha}$ can be observed. Nevertheless, the corresponding values reveal a nearly ideal distribution of water molecules in the solution which slightly deviates for lower mole fractions of water. Thus, the water molecules favor a stronger accumulation around DMAc molecules according to $G_{33} - G_{31} < 0$, which deviates from an ideal water distribution. In contrast, DMAc reveals a highly non-ideal distribution for all mole fractions $x_{\mathrm{DMAc}} \geq 0.3$ which can be assigned to the larger molecular size when compared with water molecules. The largest deviation from ideality can be observed at mole fractions $x_{\mathrm{DMAc}} = 0.5$ in good agreement with recent results

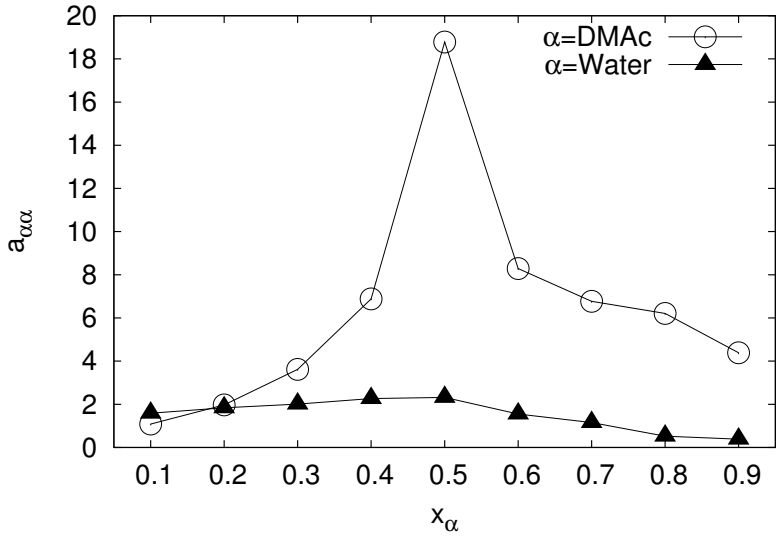

Fig. 5.2 Derivative of the chemical activity $a_{\alpha\alpha}$ for the individual components water (α=Water) and DMAc (α=DMAc) in DMAc/water mixtures with different mole fractions of the constituents.

of water/DMSO mixtures, which were in detail discussed in Ref. 92.

With regard to the influence of co-solutes on the chemical equilibrium, it becomes evident in terms of the results shown in Fig. 5.2, that water as well as DMAc reveals nearly ideal behavior at DMAc mole fractions of $x_{\mathrm{DMAc}} \leq 0.4$. Thus, we focus in our corresponding analysis mostly at these ranges in order to simplify our discussion. It has to be noted that our introduced local/bulk picture is significantly influenced by non-ideal effects in bulk solution. Thus, the non-ideality may be restricted to the local region around the ions and thus we avoid the explicit consideration of non-ideal solution effects in our following discussion. Therefore, we also follow the notation as introduced in the previous section, where DMAc as co-solute is denoted by the index '3' and water molecules with '1'.

In order to clarify the question if the derivative of the chemical activity for DMAc linearly depends on the bulk number density, we plotted the corresponding values for a_{33}/ρ_3 for different mole fractions of DMAc in Fig. 5.3. As can be seen, it becomes clear that a_{33}/ρ_3 is not a constant value for different mole fractions of DMAc. Hence, the chemical activity derivative reveals a non-linear behavior, which significantly increases at higher DMAc mole fractions in good agreement with our previous results. Again, these results reveal that ideal behavior can be mostly found at $x_{\mathrm{DMAc}} \leq 0.4$.

A further crucial point is given by the linear relation between the m-value according to Eqn. (A.4) and the corresponding influence on the chemical equilibrium in terms of

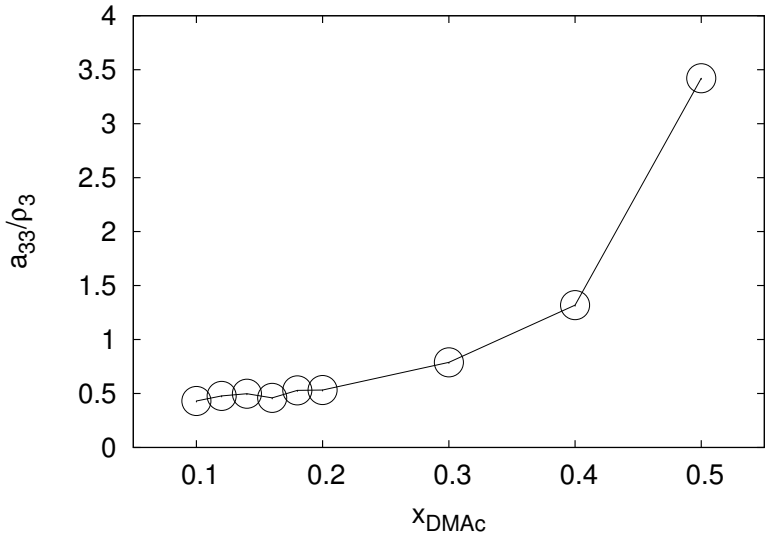

Fig. 5.3 Derivative of the chemical activity of DMAc divided by the bulk number density a_{33}/ρ_3 for different mole fractions of DMAc x_3.

Eqn, (5.20). In order to evaluate the corresponding m-values as obtained by Eqn. (A.4), we need to calculate the differences in the preferential binding coefficient $\Delta\nu_{23}$ for DMAc binding to contact ion pairs and free ions. We thus performed restrained simulations of Na^+Cl^- contact pairs and the corresponding ions which were separated by a distance of 1.2 nm. Hrewith, we fixed the position of the ions in order to avoid sampling problems and calculated the values for $\Delta\nu_{23}$ in accordance with Eqn. (5.16). The so-obtained results for a_{33} in pure solution and the corresponding values for ρ_3 and $\Delta\nu_{23}$ as obtained from the restrained simulations were then inserted in Eqn. (A.4) in order to obtain a value for m for different mole fractions of DMAc. The corresponding results are depicted in Fig. 5.4. It can be seen that the values for m are not constant and increasing with DMAc mole fractions. The corresponding results reveal values between $m = -2.5 to 0$ nm^{-3}, which based on our previously introduced theory corresponds to an increase of the free energy barrier (Eqn. (5.19) and thus a preference of the associated ion state. Moreover, we are able to extract the mean value of m with standard deviation for mole fractions between $x_{\mathrm{DMAc}} = 0.1 - 0.5$ which gives $\bar{m} = (-1.22 \pm 0.44)$ nm^{-3}. Based on these results, one would expect a negative slope of m, which reveals that higher mole fractions of DMAc induce a stronger ion pairing effect. With regard to the numerical values of m as discussed above, one could argue that a linear behavior according to Eqn. (5.19) might be observable.

Finally, we verify the validity of Eqn. (5.26) by plotting the values for $\ln K$ over ρ_3. The corresponding results are presented in Fig. 5.5. It can be clearly seen that in good agree-

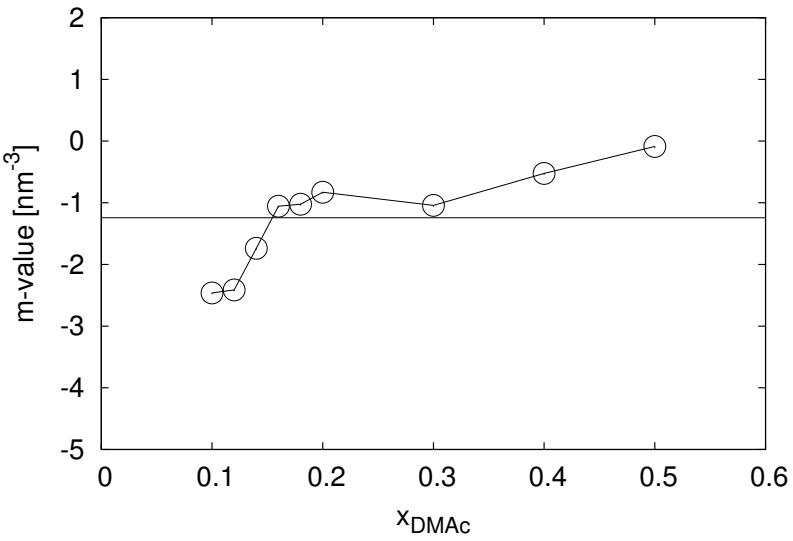

Fig. 5.4 Corresponding values of m in accordance with Eqn. (A.4) for different mole fractions of DMAc. More details on the calculation can be found in the text.

ment with the assumed linear relation as proposed in Eqn. (5.26), the values of $\ln K$ follow a linear decreasing trend with increasing bulk number densities of DMAc. Via a linear regression, we are also able to determine the corresponding value for pure water according to $\ln K^0 = 6.01 \pm 0.58$, which corresponds to an association constant of $\theta_c = 0.002$. Hence, it can be clearly seen that increasing DMAc bulk number density favors ion association. Thus, for nearly ideal values for a_{33}, the validity of Eqn. (5.26) is verified. In agreement the corresponding slope of the linear fit as shown in Fig. 5.5 yields a value of $\tilde{m} = (-1.31 \pm 0.13)$ nm^{-3}, which is in qualitative agreement with the previously obtained value for $\bar{m}$. Slight deviations from the linear behavior occur for higher values of the derivative of the chemical activity, which can be attributed to non-ideal distribution of solvent molecules in bulk solution which significantly modify the local/bulk distribution in our preferential binding model picture.

As a final proof, we compare the derivatives of the chemical activity as obtained by the KB approach without ions and as obtained by Eqn. (5.26). In fact, with regard to Eqn. (5.26), the derivative of the chemical activity can be also expressed by

$$a_{33} = (\ln K - \ln K^0)/\Delta\nu_{23} \tag{5.29}$$

where the values of $\ln K^0$ are known from linear regression of the data shown in Fig. 5.5 and $\Delta\nu_{23}$ can be calculated from the restrained simulations. The corresponding values for a_{33} as obtained from Eqn. (A.6) in comparison the the values as obtained by the KB

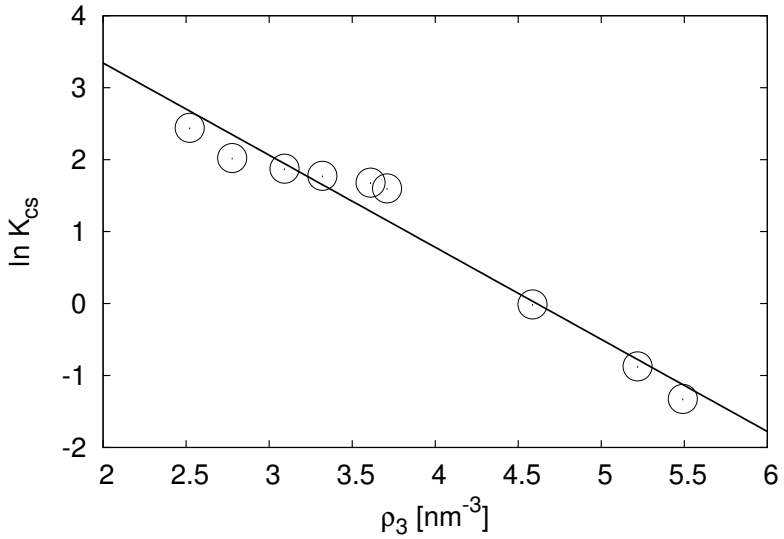

Fig. 5.5 Values for the logarithm of the chemical equilibrium constant for increasing values of the DMAc bulk number density.

approach (Eqn. (A.5)) for DMAc mole fractions $x_{\mathrm{DMAc}} = 0 - 0.4$ are shown in Fig. 5.6. The corresponding results and the high correlation coefficient with $R^2 = 0.98$ reveals a linear relation between both expressions for the derivative of the chemical activity. Hence, it can be clearly stated that the validity of Eqn. (5.26) is verified with all of its corresponding implications. Furthermore, it has to be noted that we were not able to identify a well-defined relation between a_{33} and $\Delta\nu_{23}$, which complicates the theoretical prediction of the influence of co-solutes on the chemical equilibrium.

5.4 Summary and conclusion

We presented a theoretical framework in order to describe co-solute effects on the chemical equilibrium of ion pair association and dissociation. The framework is inspired by the Kirkwood-Buff theory and significantly relies on the introduction of a local and a bulk region around the solute species. The corresponding distribution of solvent and co-solute molecules then defines the shift of the chemical equilibrium with regard to the value of the co-solute preferential binding coefficient. In fact, one can shift the chemical equilibrium either to the associated or the dissociated state, which depends on the chosen solvent and co-solute species in good agreement with previous results on stabilizers and denaturants for proteins [30]. Thus, two crucial parameters define the shift which are the derivative of the chemical activity of the co-solute molecules and the corresponding preferential binding

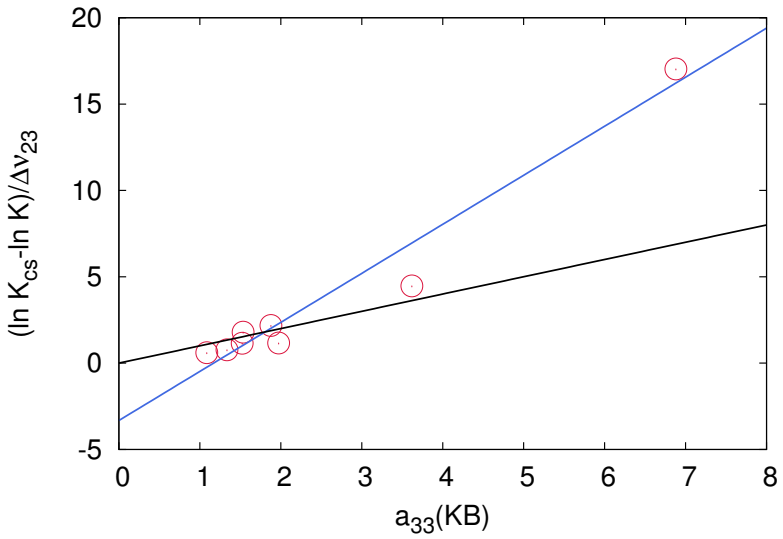

Fig. 5.6 Values for the derivative of the chemical activity as obtained from the KB approach according to Eqn. (A.5) in comparison to the values obtained from Eqn. (A.6) for DMAc mole fractions between $x_{\mathrm{DMAc}} = 0 - 0.4$. The solid line represents a linear fit and the correlation coefficient yields $R^2 = 0.98$.

coefficient. Due to the fact, that one has to compare the distribution of species in bulk and in the local region around the species, it has to be ensured that the global bulk solution reveals a nearly ideal behavior. Thus, our theory is fully applicable for solution mixtures under low concentrations of cosolutes,where the solution mixtures show close to ideal behavior. Further restrictions are also given by the low concentration of solute species in solution. With regard to aqueous solutions, local fluctuations usually decay around 0.7 nm to 1 nm, which indicates a minimum distance of slightly larger than 1 nm between the solute species, which corresponds to concentrations of roughly 0.1 mol/L. Hence, larger deviations from the theory might be also expected for higher solute concentrations.

Unfortunately, the values for the derivative of the co-solute chemical activity are experimentally inaccessible. Nevertheless, it is possible to transform the values for a_{33} in an expression for the derivative of the activity coefficient[172], which can be computed from simulations as well as experiment results. Unfortunately, the value for the preferential binding coefficient to the solute species remains unknown. Thus, one either has to rely on osmometry measurements [166] as discussed for proteins, but mostly the exact value is hard to determine. Due to the reasons, the presented theoretical framework mostly serves as a qualitative picture for the understanding of co-solute induced shifts of the chemical equilibrium. As a rule of thumn, it can be stated that the corresponding ion state is preferred which attracts more co-solute species.

In order to prove the validity of our theory, we also performed all-atom molecular dynamics simulations of sodium and chloride ions in aqueous DMAc mixtures with different DMAc concentrations. The corresponding results revealed the validity of our preferential binding model and also highlight crucial deviations for non-ideal solutions.
In summary, our theory provides a useful framework in order to understand the influence of co-solutes on the chemical equilibrium. The corresponding implications can be used in order to optimize additives in electrolyte solutions with regard to higher ionic conductivities. Furthermore, it can be expected that counterion condensation phenomena around polyelectrolytes might be also influenced by co-solutes. Thus, a plethora a tunable effects can be expected with regard to the presence of solvent and co-solute species in solution.

5.5 Acknowledgement

Most part of this chapter was reprinted(adapted) from Ref [90] with permissions from the American Chemical Society, Journal of Physical Chemistry C.

Chapter 6

Outlook

6.1 Introduction

Chemical species evolve dynamically showing complex mechanisms like ion transport, diffusion and chemical dissociations at molecular level which are very expensive to see experimentally, due to the complexity of these systems, thus computer simulations have become increasingly important in engineering, nanotechnology and life sciences to understand these complex mechanisms. Quantum mechanical (QM) based simulation methods in general are applicable to all chemical systems regardless of the connectivity between atoms but QM methods are computationally very expensive for large systems. Therefore these methods are used to perform single point calculations, energy minimizations, and mainly used to provide theoretical insights at the electronic level. Thus to model large systems, molecular dynamics (MD) is used. A detailed understanding of MD methods from algorithms to applications is explained in Ref 56.

There are two main families of MD methods, which can be distinguished according to the model chosen to represent a physical system. In the 'classical' mechanics approach, it is performed by defining interactions between atoms using force fields (potentials), which are sum of bonded (bonds, angles, dihedrals) and non-bonded (van-der Waals, electrostatics) interactions. These potential functions are empirical and the parameters are obtained from experiments or accurate quantum mechanical calculations. Further, solving classical mechanics is used to obtain position and velocities of the system. The 'quantum' or 'first-principles' MD simulations, which started in the 1980s with the seminal work of Car and Parinello [31], take explicitly into account the quantum nature of interactions. The electron density function for the valence electrons that determine the forces in the system is computed using quantum mechanics, whereas the dynamics of nuclei with their inner electrons is followed classically.

In this thesis, we modeled all complex electrolyte systems using classical forcefields as mentioned in the simulation details in each chapter. Even though this approach allows to model complex systems and is cheap compared to ab-inito MD simulations, these models lack in chemical reactions. This is due to the fact that the model is based out of rigid bonds and further purely depends on the accuracy of the empirical parameters, which is used to define the potentials of these complex systems. On the other hand ab-initio MD gives access to chemical reactions, bond breaking and making process is allowed implicitly in these approaches and are very accurate, since the interactions are treated using quantum mechanical approaches. But are very expensive to treat complex systems.

These factors motivated researchers to bridge the gap between these two approaches to achieve greater speeds by maintaining quantum mechanical accuracies. Several empirical and semi empirical approaches were constructed for the past few decades to model reactive molecular dynamics [2, 185, 28]. Here, the potentials are represented as a function of bond order. Bond order is defined as the effective number of chemical bonds between a pair of atoms. Bond order usually serves as an indicator to bond strength, the higher the bond order, stronger the bond strength. Thus the chemical bonding is described implicitly without expensive QM calculations, hence describing reactive systems with low computational expense. Bond order based formalism was first formulated by Tersoff, which could handle connectivity changes, this was further developed by Brenner (REBO Potentials) for hydrocarbon systems. But the transferability was limited due to small training sets and absence of non-bonded interactions.

Here as an outlook, we are going to introduce machine learning (ML) based potentials, which are very effective to bridge this gap and is currently most effective method to attain ab-initio accuracies and achieve speeds close to standard atomistic models. Machine learning (ML) has impacted on many aspects of modern society. From artificial intelligence, smart homes, social media to an industrial context, for predictive maintenance or in medical diagnosis, ML methods have and still are changing how we interact with computers and our environment. Such methods can then recognize certain features in data sets they've never seen and thus turned out to be an important analysis tool in many subfields of science. Machine learning methods can be roughly subdivided into two main classes of algorithms i-e supervised learning algorithms and unsupervised learning algorithms. Both classes require a training set, a set of reference data from which something has to be learned. In supervised learning the reference data consists of input and output data, a machine learning method in this field is supposed to find out how both data sets correlate. Then it can be used to predict the output for arbitrary input data from what the algorithm has learned. Supervised learning algorithms are further distinguished into classiffication methods and regression methods,

depending on whether the output data is discrete or continuous. By contrast training data in unsupervised learning provides no information about the output. The task for such algorithms is to find unknown patterns or to classify the input data by themselves.

In computational physics and chemistry, machine learning methods were first used for classification tasks (e.g. classifying bonding types, etc.). But more recently supervised learning algorithms were used for finding potential energy surfaces of certain systems. Current machine learning potentials use Neural Networks and Regression models to fit energies from abinito training data sets. ML potentials are constructed on the basis of assumption that the total energy of a system can be described as a sum of local atomic energies. This is arguably valid due to the short sightedness of quantum mechanics, as the energy of an atom is dependent on its local environment[186]. Conventionally ML potentials are fitted from reference electronic structure method and does not contain any physical approximations. One of the most challenging aspects of machine learning is to provide transferable models that can be trained on a small set of references and applied to a larger set with comparable accuracy. In the field of computer vision, some transferability is assumed in the context of transfer learning, i.e., refining pre-trained models for the specific task. Similarly, models for mixed component systems have been systematically fitted on the pure components first and only then refined for the full systems.[65] Recent efforts for prediction of electron densities show that transferability can be achieved by using atom-centered symmetry functions.[38]

To achieve transferability and scalability, it is important that the employed descriptor can suitably accommodate the inclusion of different atomic species without growing proportional to the added chemical diversity. Models trained on large subsets of the vast chemical space offer good performance for various task, from predicting energetics to identifying chemical concepts[157] Hence, current developments focus on generating transferable descriptors that allow reducing the scaling with respect to the number of involved chemical species and thus included fit data[55, 6, 187, 80, 17, 184].

To summarize, descriptors are a representation of structural inputs for the ML algorithm satisfying symmetry invariance. Several descriptors are studied with various systems and their efficiency and accuracy are benchmarked in this reference [214]. Further the whole workflow of building a ML potential is described in a review article [14]. Choice of descriotors influences the accuracies of ML potential and also determines the dimensionality of the coordinate space to be mapped on to the training sets. Here we use smooth overlap of atomic positions (SOAP) [11, 214] for GAP (GAP - Gaussian Approximation Potentials) potentials. These descriptors are found to be more efficient for GAP based ML potentials as described in Ref [214].

This outlook is to investigate under which conditions machine learning models reproduce the underlying energetics, and how much data is needed to reproduce the corresponding physical representation. We investigate results from Gaussian process regression. Here we will use Gaussian based regression models to develop ML potentials for simple noble argon (Ar) liquids.

6.2 Training data

We performed ab initio molecular dynamics simulations (AIMD) based on density functional theory (DFT) for two different bulk noble liquids, Ar108, Kr108 at 120 K. The simulations employed the rVV10 density functional that explicitly accounts for long-range correlation, i.e., dispersion, effects. These AIMD simulations used Kohn-Sham density functional theory (KS-DFT), and were carried out with the program CP2K [192, 76]. The exchange-correlation energy was approximated using a van der-Waals density functional [195, 146]. The Kohn-Sham one-particle wavefunctions were expanded into an atom-centered double zeta basis set optimized for dense liquids [191]. The electron density was expanded in an auxiliary plane-wave basis set with a kinetic energy cutoff of 600 Ry. Initial configurations were obtained from molecular dynamics simulations using a Lennard-Jones (12-6) potential. Newton's equations of motions were integrated using a timestep of 2 fs and the temperature of the system was kept constant at 120 K using a Nosé-Hoover chain thermostat (chain length: 3, time constant: 100 fs) [115]. The final training data was taken as equidistant snapshots from a 60 ps production simulation, after an initial equilibration time of about 25 ps. The data was taken from the late equilibration part of the trajectory and slightly overlapping with its initial production part.

6.3 GAP Parameters

As previously discussed, ML potentials are constructed under the assumption that the total energy of the system can be represented as sum of local atomic energies.

$$E = \sum_{i}^{atoms} \varepsilon(x_i), \tag{6.1}$$

Where x_i is the position of atom i.

All the training data configurations were mapped onto a SOAP descriptor to construct a GAP model. SOAP encodes the atomic entries by using a local expansion of a Guassian smeared atomic density with normal functions based on spherical harmonics and radial basis

function. This is explained in detail in Ref. [10]. In the Gaussian process framework the atomic energy function is given by:

$$\varepsilon(b) = \sum_n \alpha_n G(b, b_n) \tag{6.2}$$

Where G is not a fixed kernel (similarity measure through descriptor) but a continuous function centred on the training data.

The Gaussian process differs from a least square fit by the way the fit coeffients α_n are computed. They are fitted using Gaussian regression as depicted in this equation which represents the covariance matrix.

$$C_{nn'} = \delta^2 G(b, b') + \sigma^2 I \tag{6.3}$$

The interpolation coefficients are given by:

$$\alpha_n \tilde{} \alpha = C^{-1} y, \tag{6.4}$$

Where $y = y_n$ is the set of reference values (training data). This expression gives the atomic energy function in closed form from the training data. Further the GAP hyperparameters are represented in table 6.1. The training accuracy for energy and forces are modeled at

Table 6.1 GAP Parameters

Parameter	Optimized values
δ	0.001 eV
σ_e, σ_f	0.001 eV
Descriptor	SOAP
Cutoff	0.8 nm

1meV/atom as depicted by the σ values. Further, the potentials are fitted using the quippy code from libatoms.org [11].

6.4 Machine learning simulation setup

Molecular dynamics simulations with the machine learning potentials were performed using LAMMPS. We used the quippy pair style as available in LAMMPS [61] to represent the GAP potentials. Newton's equations of motion were integrated using a velocity Verlet algorithm with a timestep of up to 10 fs at 120K with Nose-Hoover thermostat. The cutoff for the construction of the GAP calculation was set to 8 Å, weighting factors were set to the

respective atom's mass in amu divided by 1000, an atomic radius of 2 Å was set for each atom kind, and a factor of 0.95 was used for mapping the radial distance to a third polar angle for the projection onto a 4D sphere.

6.5 Results

Figure 6.1 and 6.2 depicts the correlation plots between the predicted energies and forces with that of the training data for pure argon liquid at 120K. Both plots show a correlation coefficient > 0.99. The root mean square error for energies were achieved less than 0.3meV/atom, which is much better than the desired accuracies for liquid phases.

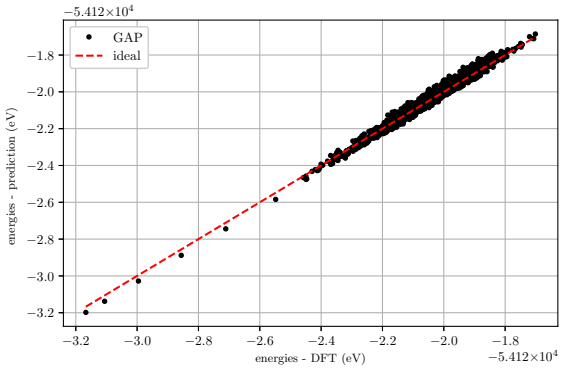

Fig. 6.1 Energy correlations of pure argon liquid

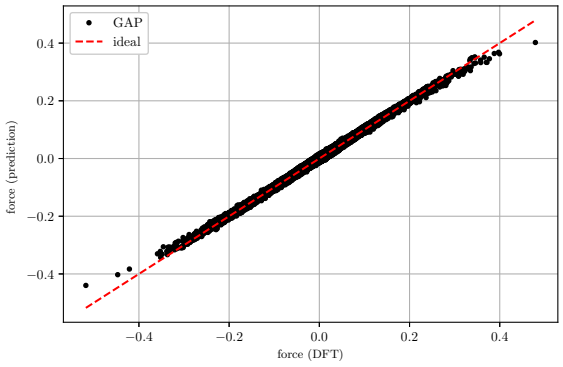

Fig. 6.2 Force correlations of pure argon liquid

As this model predicts highly accurate energies and forces, we now compare the structural quantites like the radial distribution functions (RDFs) from MD simulations to that of the training data, and also the LJ potentials which are predominantly used to model noble liquids in atomistic simulations in Figure 6.3. Here, we can see that the GAP model predicts the

first corrdination peak more accurately compared to the standard LJ potentials for pure argon liquids. The rdf's are generally in very good comparison with the ab initio reference to which they were fitted.

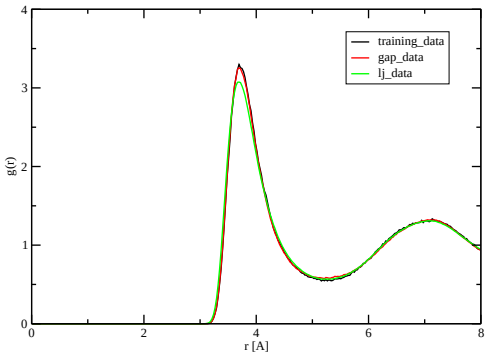

Fig. 6.3 Radial distribution function of a pure argon liquid.

Table 6.2 Diffusion coefficients of argon liquid * $10^{-5} cm^2/s$

Atom	GAP	Abinito data
Ar	1.35	1.29

Also the diffusion coefficients in pure argon at 85 K (see Table 6.2) are in good agreement with the training data. Therefore, it is not possible to identify a model that works better for the investigated systems, which is consistent with literature [14]. Interestingly, we were also able to successfully perform molecular dynamics simulations of the pure component systems with the models obtained from the mixed GAP potential of argon and krypton, and vice versa.

6.6 Summary

Table 6.3 Performance of ML potentials

	computation time	simulated time	relative speeds
DFT	15.93 days	0.3853 ns	1X
GAP	0.7942 days	1 ns	39360X
LJ	0.0024 days	1 ns	437340X

To summarize, we have demonstrated how to obtain meaningful potentials in an economic way for large, and possibly periodic systems from DFT calculations. The fitting appears to be robust with respect to the local energies, if sufficient training data is provided, and even allows some rudimentary transferability between similar systems. The performance of ML potentials are depicted in table 6.3. It can be seen that the GAP based ML potentials are just one order slower compared to LJ potentials and show accuracies close to the abinito reference data. As these potentials do not posses fixed functional form or physical motivations, reactions are allowed to occur in theses systems. Thus, these models can be used to model chemical reactions, dissociation mechanisms, and ionic transport for simple systems that are studied in this thesis. These ML based potentials scale linearly and hence bulk systems can be modeled with ab-initio accuracies. Further investigations in this direction are ongoing. Eventhough simple noble liquids potentials have been constructed with good accuracies, currently it remains to be explored if the methods will also work for more complex systems.

Chapter 7

Conclusion

This thesis provides an overview of prominent features that could be extracted from theoretical and numerical modeling of complex electrolyte systems. This research provides an insight to phenomenona such as specific ion effects, ion condensation , ion pairing mechanisms and influence of solvents and cosolutes on all of these effects. These questions posed in the abstarct are answered in detail with suitable examples and molecular pictures of these systems are provided.

Atomistic MD results of lithium salts in adiponitrile (ADN) solvent revealed the importance of distinct sizes of anions as an important factor for ion association behavior. It is shown that LiTFSI is well solvated in adiponitrile compared to $LiBF_4$ salt, which in turn reveals a pronounced ion complex formation in BF_4 salt compared to TFSI in ADN. This is well supported by large coordination of ADN towards TFSI which enunciates the presence of free ion species in LiTFSI salts compared to $LiBF_4$. This further rationalizes the increased conductivity of LiTFSI. All these findings underline the significance of anion sizes and corresponding anion solvation behavior that influence the ion association behavior. We have shown the importance of specific anion effects in organic solvents like ADN that affect the ion association behavior, which was previously only noted for aqueous solutions.

To further elucidate the importance of specific ion effects in organic solvents, the individual ion distribution behavior (counterion condensation) around model polyelectrolytes in different solvents (DMAc, Methanol and Water) was studied. Distinct ion distributions around the polyelectrolyte was observed for different solvents, denoting the corresponding importance of ion solvation behvior in each solvent. These results highlight the failure of standard mean field models, that show an accurate ion distribution behavior in terms of the implicit solvent approach but fail to reproduce the influence of ion solvation behavior. To overcome these limitations, recent approaches based on the Poisson Boltzmann cell model, introduced phenomenological hydration potentials in order to consider counterion-specific

condensation behavior in aqueous solutions which need to be further improved for all solvents categories with a need for a specific potential ion solvent interaction parameters. The observed counterion condensation behavior is also in agreement with the empirical donor and acceptor number concept. It is shown that the force fields indeed reproduce experimental behavior and that the observed differences between the ion species can be mostly attributed to the underlying solvation properties in combination with electrostatic interactions. Also it was shown that specific ion effects in various solvents depends on the dipolar properties of the solvents and ion-dipole and multipole interactions play a major role in influencing the ion complex formation in the solvent environment.

These systems provided deeper insights into the factors that influence the ion association behavior in pure solvent medium, but state-of-the-art electrolyte systems contain cosolutes, and additional solvents to provide higher conductivites and better ion transport. Thus the influence of these tertiary component on these complex electrolyte systems becomes a prerequisite for designing future applications in battery systems. Most complex mixture systems are non ideal in nature as shown in our test system as well (DMSO-Water mixture), where we use DMSO as cosolvent and the chemical activity of these mixtures indicate a strong non-ideal behavior of the pure solution for mole fractions $x_{\mathrm{DMSO}} \geq 0.4$. The predicted preferential solvation behvior was absent in these systems, and furthermore a preferential exclusion of DMSO was seen by the evaluation of the local/bulk partition coefficients around the ions (Dimeric sulfonic acid based lithium salts). Our results indicate the failure of the preferential solvation model as predicted from empirical concepts like the donor and acceptor number concepts, which however were suitable for pure solvent scenarios. Thus we try to formulate a theoretical model to understand the ion pairing behaviour in ideal and partially non ideal solvent mixtures using KB theory. Finally, a theoretical framework to describe co-solute effects on the chemical equilibrium of ion pair association and dissociation was presented. This is an extension of KB theory to model ion association and dissociation states in presence of cosolutes. Derivative of the chemical activity and the corresponding preferential binding coefficient were identified as crucial parameters to define the shift to the associated or dissociated state. Since one has to compare the distribution of species in bulk and in the local region around the species, it has to be ensured that the global bulk solution reveals a nearly ideal behavior. This theory is fully applicable for ideal and close to ideal solutions. To prove the validity of our theory, we also performed all-atom molecular dynamics simulations of sodium and chloride ions in aqueous DMAc mixtures with different DMAc concentrations. The corresponding results revealed the validity of our preferential binding model and also highlight crucial deviations for non-ideal solutions. In summary, our theory provides a useful framework in order to understand the influence of co-solutes

on the chemical equilibrium of associated and dissociated states. This theory can be used to optimize the choice of cosolutes for increasing ion transport in electrolyte systems.

Thus, we have potentially listed the factors responsible for ion complex formation in pure solvents and solvent mixtures and developed a theoretical model that could help to optmize the choice of cosolutes to increase or decrease ion pairing. Our research using numerical modeling coupled to Kirkwood Buff theory helps in potential identification of solvent environment for these complex ionic moeities, that could find potential applications in battery systems. This also help in designing components that yield better ion transport and higher conductivities.

We performed atomistic MD simulations to model all our systems with suitable forcefields obtained from empirical and quantum mechanical parameters. But with these models one cannot model chemical reactions or ion transport, since these models are rigid and the accuracy is completely dependent on the chosen force field. Eventhough MD simulations provide a qualitative picture of these complex electrolyte systems, there is growing need for methods that can encapsulate ion dissociation and association states, and that determine the underlying ion transport mechanisms in bulk and also in the interface. For this we introduced a machine learning based approach to derive potentials that can model simple systems of noble liquids at ab-initio accuracies. This approach could further be used to model complex systems as those studied in this thesis, which can further give mechanistic insights into ion dissciation in solid electrolyte interfaces and also could model the underlying chemical reactions. Although these systems are yet to be studied, the foundation of the machine learning based potentials are laid out in the outlook of this thesis.

References

[1] Abu-Lebdeh, Y. and Davidson, I. (2009). High-voltage electrolytes based on adiponitrile for li-ion batteries. *J. Electrochem. Soc.*, 156(1):A60–A65.

[2] Adri, v. D. e. a. (2001). Reaxff - a reactive forcefield for hydrocarbons. *JPC A*, 105:9336–9409.

[3] Algaer, E. A. and van der Vegt, N. F. (2011). Hofmeister ion interactions with model amide compounds. *J. Phys. Chem. B*, 115(46):13781–13787.

[4] Antypov, D. and Holm, C. (2006). The osmotic behavior of short stiff polyelectrolytes. *Macromol. Sympos.*, pages 297–306.

[5] Antypov, D. and Holm, C. (2007). Osmotic coefficient calculations for dilute solutions of short stiff-chain polyelectrolytes. *Macromolecules*, 40(3):731–738.

[6] Artrith, N., Urban, A., and Ceder, G. (2017). Efficient and accurate machine-learning interpolation of atomic energies in compositions with many species. *Phys. Rev. B*, 96:014112.

[7] Atkins, P. W. and de Paula, J. (2010). *Physical Chemistry*. Oxford Univ. Press, Oxford (UK).

[8] Balducci, A. (2017). Ionic liquids in lithium-ion batteries. *Top. Curr. Chem.*, 375(2):20.

[9] Ball, P. and Hallsworth, J. E. (2015). Water structure and chaotropicity: their uses, abuses and biological implications. *Phys. Chem. Chem. Phys.*, 17(13):8297–8305.

[10] Bartók, A. P. (2009). *Gaussian Approximation Potential: an interatomic potential derived from first principles Quantum Mechanics*. PhD thesis.

[11] Bartók, A. P., Payne, M. C., Kondor, R., and Csányi, G. (2010). Gaussian Approximation Potentials: The Accuracy of Quantum Mechanics, without the Electrons. *Physical Review Letters*, 104:136403.

[12] Batys, P., Luukkonen, S., and Sammalkorpi, M. (2017). Ability of Poisson–Boltzmann equation to capture molecular dynamics predicted ion distribution around polyelectrolytes. *Phys. Chem. Chem. Phys.*, 19:24583–24593.

[13] Baynes, B. M. and Trout, B. L. (2003). Proteins in mixed solvents: a molecular-level perspective. *J. Phys. Chem. B*, 107(50):14058–14067.

[14] Behler, J. (2016). Perspective: Machine learning potentials for atomistic simulations. *The Journal of Chemical Physics*.

[15] Ben-Naim, A. (2013a). *Statistical thermodynamics for chemists and biochemists*. Springer Science & Business Media.

[16] Ben-Naim, A. (2013b). *Statistical thermodynamics for chemists and biochemists*. Springer Science & Business Media, Berlin, Germany.

[17] Bereau, T., DiStasio, R. A., Tkatchenko, A., and von Lilienfeld, O. A. (2018). Non-covalent interactions across organic and biological subsets of chemical space: Physics-based potentials parametrized from machine learning. *The Journal of Chemical Physics*, 148(24):241706.

[18] Berendsen, H., Grigera, J., and Straatsma, T. (1987). The missing term in effective pair potentials. *J. Phys. Chem.*, 91(24):6269–6271.

[19] Besenhard, J. O., Von Werner, K., and Winter, M. (1999). Fluorine-containing solvents for lithium batteries having increased safety. US Patent 5,916,708.

[20] Blandamer, M. J., Engberts, J. B., Gleeson, P. T., and Reis, J. C. R. (2005). Activity of water in aqueous systems; a frequently neglected property. *Chem. Soc. Rev.*, 34(5):440–458.

[21] Blaul, J., Wittemann, M., Ballauff, M., and Rehahn, M. (2000). The osmotic coefficient of a synthetic rodlike polyelectrolyte in salt-free solution as a test of the poisson-boltzmann cell-model. *J. Phys. Chem. B*, 104:7077–7081.

[22] Bohner, M. U., Zeman, J., Smiatek, J., Arnold, A., and Kästner, J. (2014). Nudged-elastic band used to find reaction coordinates based on the free energy. *J. Chem. Phys.*, 140(7):074109.

[23] Borin, I. A. and Skaf, M. S. (1999). Molecular association between water and dimethyl sulfoxide in solution: a molecular dynamics simulation study. *J. Chem. Phys.*, 110(13):6412–6420.

[24] Borodin, O., Suo, L., Gobet, M., Ren, X., Wang, F., Faraone, A., Peng, J., Olguin, M., Schroeder, M., Ding, M. S., Gobrogge, E., von Wald Cresce, A., Munoz, S., Dura, J. A., Greenbaum, S., Wang, C., and Xu, K. (2017). Liquid structure with nano-heterogeneity promotes cationic transport in concentrated electrolytes. *ACS Nano*, 11:10462–10471.

[25] Boroudjerdi, H., Kim, Y.-W., Naji, A., Netz, R. R., Schlagberger, X., and Serr, A. (2005). Statics and dynamics of strongly charged soft matter. *Phys. Rep.*, 416(3-4):129–199.

[26] Brandt, A., Isken, P., Lex-Balducci, A., and Balducci, A. (2012). Adiponitrile-based electrochemical double layer capacitor. *J. Power Sources*, 204:213–219.

[27] Breneman, C. M. and Wiberg, K. B. (1990). Determining atom-centered monopoles from molecular electrostatic potentials. the need for high sampling density in formamide conformational analysis. *J. Comput. Chem.*, 11(3):361–373.

[28] Brenner, D. W. (1990). Empirical potential for hydrocarbons for use in simulating the chemical vapor deposition of diamond films. *Physical Review B*, 42:9458–9471.

[29] Caleman, C., van Maaren, P. J., Hong, M., Hub, J. S., Costa, L. T., and van der Spoel, D. (2011). Force field benchmark of organic liquids: density, enthalpy of vaporization, heat capacities, surface tension, isothermal compressibility, volumetric expansion coefficient, and dielectric constant. *J. Chem. Theory Comput.*, 8(1):61–74.

[30] Canchi, D. R. and García, A. E. (2013). Cosolvent effects on protein stability. *Ann. Rev. Phys. Chem.*, 64:273–293.

[31] Car, R. and Parrinello, M. (1985). Unified approach for molecular dynamics and density functional theory. *Physical Review Letters*, 55:2471.

[32] Cekic-Laskovic, I., von Aspern, N., Imholt, L., Kaymaksiz, S., Oldiges, K., Rad, B. R., and Winter, M. (2017). Synergistic effect of blended components in nonaqueous electrolytes for lithium ion batteries. *Top. Curr. Chem.*, 375(2):37.

[33] Chandler, D. (1987). *Introduction to Modern Statistical Mechanics*. Oxford University Press.

[34] Chitra, R. and Smith, P. E. (2001). Preferential interactions of cosolvents with hydrophobic solutes. *J. Phys. Chem. B*, 105(46):11513–11522.

[35] Ciccotti, G., Ferrario, M., Hynes, J. T., and Kapral, R. (1989). Constrained molecular dynamics and the mean potential for an ion pair in a polar solvent. *Chem. Phys.*, 129(2):241–251.

[36] Collins, K. D. (1997). Charge density-dependent strength of hydration and biological structure. *Biophys. J.*, 72(1):65.

[37] Collins, K. D. (2004). Ions from the hofmeister series and osmolytes: effects on proteins in solution and in the crystallization process. *Methods*, 34(3):300–311.

[38] Corminboeuf, C., Certiotti, M., meyer, b., Fabrizio, A., Grisafi, A., and Wilkins, D. M. (2018). A transferable machine-learning model of the electron density.

[39] Courtenay, E., Capp, M., Anderson, C., and Record, M. (2000). Vapor pressure osmometry studies of osmolyte-protein interactions: implications for the action of osmoprotectants in vivo and for the interpretation of "osmotic stress" experiments in vitro. *Biochemistry*, 39(15):4455–4471.

[40] da Silva, A. W. S. and Vranken, W. F. (2012). Acpype-antechamber python parser interface. *BMC Res. Notes*, 5(1):367.

[41] Darden, T., York, D., and Pedersen, L. (1993). Particle mesh ewald: An n log (n) method for ewald sums in large systems. *J. Chem. Phys.*, 98(12):10089–10092.

[42] Day, T. J. and Patey, G. (1999). Ion solvation dynamics in water–methanol and water–dimethylsulfoxide mixtures. *J. Chem. Phys.*, 110(22):10937–10944.

[43] de Leeuw, S. W., Perram, J. W., and Smith, E. R. (1980). Simulation of electrostatic systems in periodic boundary conditions. I. lattice sums and dielectric constants. *Proc. Royal Soc. A*, 373(1752):27–56.

[44] Deng, D. (2015). Li-ion batteries: basics, progress, and challenges. *Energy Science & Engineering*, 3(5):385–418.

[45] Deserno, M. and Holm, C. (2001). Cell-model and poisson-boltzmann-theory: A brief introduction. In Holm, C., Kékicheff, P., and Podgornik, R., editors, *Electrostatic Effects in Soft Matter and Biophysics*, volume 46 of *NATO Science Series II - Mathematics, Physics and Chemistry*, pages 27–50. Kluwer Academic Publishers, Dordrecht, Nl.

[46] Deserno, M., Holm, C., and May, S. (2000). Fraction of condensed counterions around a charged rod: Comparison of poisson-boltzmann theory and computer simulations. *Macromolecules*, 33(1):199–206.

[47] Diddens, D., Lesch, V., Heuer, A., and Smiatek, J. (2017). Aqueous ionic liquids and their influence on peptide conformations: denaturation and dehydration mechanisms. *Phys. Chem. Chem. Phys.*, 19(31):20430–20440.

[48] Duncan, H., Salem, N., and Abu-Lebdeh, Y. (2013). Electrolyte formulations based on dinitrile solvents for high voltage li-ion batteries. *J. Electrochem. Soc.*, 160(6):A838–A848.

[49] Ehteshami, N. and Paillard, E. (2017). Ethylene carbonate-free, adiponitrile-based electrolytes compatible with graphite anodes. *ECS Transact.*, 77(1):11–20.

[50] Fahrenberger, F., Hickey, O. A., Smiatek, J., and Holm, C. (2015). Importance of varying permittivity on the conductivity of polyelectrolyte solutions. *Phys. Rev. Lett.*, 115(11):118301.

[51] Farhat, D., Ghamouss, F., Maibach, J., Edström, K., and Lemordant, D. (2017). Adiponitrile–lithium bis (trimethylsulfonyl) imide solutions as alkyl carbonate-free electrolytes for li4ti5o12 (lto)/lini1/3co1/3mn1/3o2 (nmc) li-ion batteries. *ChemPhysChem*, 18(10):1333–1344.

[52] Frenkel, D. and Smit, B. (2001). *Understanding molecular simulation: from algorithms to applications*. Academic press.

[53] Fyta, M. and Netz, R. R. (2012). Ionic force field optimization based on single-ion and ion-pair solvation properties: Going beyond standard mixing rules. *J. Chem. Phys.*, 136(12):124103.

[54] Ganguly, P., Schravendijk, P., Hess, B., and van der Vegt, N. F. (2011). Ion pairing in aqueous electrolyte solutions with biologically relevant anions. *J. Phys. Chem. B*, 115(13):3734–3739.

[55] Gastegger, M., Schwiedrzik, L., Bittermann, M., Berzsenyi, F., and Marquetand, P. (2018). wacsf—weighted atom-centered symmetry functions as descriptors in machine learning potentials. *The Journal of Chemical Physics*, 148(24):241709.

[56] Gavryushov, S. and Linse, P. (2006). Effective interaction potentials for alkali and alkaline earth metal ions in spc/e water and prediction of mean ion activity coefficients. *J. Phys. Chem. B*, 110(22):10878–10887.

[57] Gee, M. B., Cox, N. R., Jiao, Y., Bentenitis, N., Weerasinghe, S., and Smith, P. E. (2011). A kirkwood-buff derived force field for aqueous alkali halides. *J. Chem. Theory Comput.*, 7(5):1369–1380.

[58] Ghamouss, F., Brugere, A., and Jacquemin, J. (2014). Physicochemical investigation of adiponitrile-based electrolytes for electrical double layer capacitor. *J. Phys. Chem. C*, 118(26):14107–14123.

[59] Grimme, S., Antony, J., Ehrlich, S., and Krieg, H. (2010). A consistent and accurate ab initio parametrization of density functional dispersion correction (DFT-D) for the 94 elements H-Pu. *J. Chem. Phys.*, 132:154104.

[60] Grimme, S., Ehrlich, S., and Goerigk, L. (2011). Effect of the damping function in dispersion corrected density functional theory. *J. Comput. Chem.*, 32:1456–1465.

[61] Grindon, C., Harris, S., Evans, T., Novik, K., Coveney, P., and Laughton, C. (2004). Large-scale molecular dynamics simulation of DNA: implementation and validation of the AMBER98 force field in LAMMPS. *ROYAL SOC LONDON*, 362:1373–1386.

[62] Gutmann, V. (1976). Empirical parameters for donor and acceptor properties of solvents. *Electrochim. Acta*, 21(9):661–670.

[63] Hahn, M. B., Uhlig, F., Solomun, T., Smiatek, J., and Sturm, H. (2016). Combined influence of ectoine and salt: spectroscopic and numerical evidence for compensating effects on aqueous solutions. *Phys. Chem. Chem. Phys.*, 18(41):28398–28402.

[64] Hajari, T., Ganguly, P., and van der Vegt, N. F. (2012). Enthalpy–entropy of cation association with the acetate anion in water. *J. Chem. Theory Comput.*, 8(10):3804–3809.

[65] Hajinazar, S., Shao, J., and Kolmogorov, A. N. (2017). Stratified construction of neural network based interatomic models for multicomponent materials. *Phys. Rev. B*, 95:014114.

[66] Hall, D. (1971). Kirkwood-buff theory of solutions. an alternative derivation of part of it and some applications. *Transact. Farad. Soc.*, 67:2516–2524.

[67] Hanna, O., Luski, S., and Aurbach, D. (2017). High-voltage supercapacitors with solutions based on adiponitrile solvent. *J. Electrochem. Soc.*, 164(2):A231–A236.

[68] Haynes, W. M. (2014). *CRC Handbook of Chemistry and Physics*. CRC press.

[69] Hess, B., Bekker, H., Berendsen, H. J. C., and Fraaije, J. G. E. M. (1997). {LINCS}: {A} linear constraint solver for molecular simulations. *J. Comput. Chem.*, 18:1463–1472.

[70] Hess, B. and van der Vegt, N. F. (2009). Cation specific binding with protein surface charges. *Proc. Natl. Acad. Sci.*, 106(32):13296–13300.

[71] Heyda, J. and Dzubiella, J. (2012a). Ion-specific counterion condensation on charged peptides: Poisson–boltzmann vs. atomistic simulations. *Soft Matter*, 8(36):9338–9344.

[72] Heyda, J. and Dzubiella, J. (2012b). Ion-specific counterion condensation on charged peptides: Poisson–boltzmann vs. atomistic simulations. *Soft Matter*, 8(36):9338–9344.

[73] Hochtl, P., Boresch, S., Bitomsky, W., Steinhauser, O., et al. (1998). Rationalization of the dielectric properties of common three-site water models in terms of their force field parameters. *J. Chem. Phys.*, 109(12):4927–4937.

[74] Holz, M., Heil, S. R., and Sacco, A. (2000). Temperature-dependent self-diffusion coefficients of water and six selected molecular liquids for calibration in accurate 1h nmr pfg measurements. *Phys. Chem. Chem. Phys.*, 2(20):4740–4742.

[75] Humphrey, W., Dalke, A., and Schulten, K. (1996). Vmd: visual molecular dynamics. *J. Mol. Graph.*, 14(1):33–38.

[76] Hutter, J., Iannuzzi, M., Schiffmann, F., and VandeVondele, J. (2014). CP2K: atomistic simulations of condensed matter systems. *Wiley Interdisciplinary Reviews: Computational Molecular Science*, 4(1):15–25.

[77] Isken, P., Dippel, C., Schmitz, R., Schmitz, R., Kunze, M., Passerini, S., Winter, M., and Lex-Balducci, A. (2011). High flash point electrolyte for use in lithium-ion batteries. *Electrochim. Act.*, 56(22):7530–7535.

[78] Jagoda-Cwiklik, B., Vácha, R., Lund, M., Srebro, M., and Jungwirth, P. (2007). Ion pairing as a possible clue for discriminating between sodium and potassium in biological and other complex environments. *J. Phys. Chem. B*, 111(51):14077–14079.

[79] Janzen, T., Zhang, S., Mialdun, A., Guevara-Carrion, G., Vrabec, J., He, M., and Shevtsova, V. (2017). Mutual diffusion governed by kinetics and thermodynamics in the partially miscible mixture methanol+ cyclohexane. *Phys. Chem. Chem. Phys.*, 19(47):31856–31873.

[80] Jindal, S. and Bulusu, S. S. (2018). A transferable artificial neural network model for atomic forces in nanoparticles. *ArXiv e-prints*.

[81] Jorgensen, W. L., Chandrasekhar, J., Madura, J. D., Impey, R. W., and Klein, M. L. (1983). Comparison of simple potential functions for simulating liquid water. *J. Chem. Phys.*, 79(2):926–935.

[82] Jorgensen, W. L., Maxwell, D. S., and Tirado-Rives, J. (1996). Development and testing of the opls all-atom force field on conformational energetics and properties of organic liquids. *J. Am. Chem. Soc.*, 118(45):11225–11236.

[83] Jungwirth, P. and Cremer, P. S. (2014). Beyond hofmeister. *Nat. Chem.*, 6(4):261–263.

[84] Kang, M. and Smith, P. E. (2006). A kirkwood-buff derived force field for amides. *J. Comput. Chem.*, 13:1477–1485.

[85] Kirkwood, J. G. and Buff, F. P. (1951a). The statistical mechanical theory of solutions. i. *J. Chem. Phys.*, 19(6):774–777.

[86] Kirkwood, J. G. and Buff, F. P. (1951b). The statistical mechanical theory of solutions. i. *J. Chem. Phys.*, 19(6):774–777.

[87] Klamt, A. and Schüürmann, G. (1993). COSMO: A new approach to dielectric screening in solvents with explicit expressions for the screening energy and its gradient. *J. Chem. Soc, Perkin Trans.*, 5:799–805.

[88] Kreuer, K.-D. (2013). Ion conducting membranes for fuel cells and other electrochemical devices. *Chem. Mat.*, 26(1):361–380.

[89] Kreuer, K.-D., Wohlfarth, A., de Araujo, C. C., Fuchs, A., and Maier, J. (2011). Single alkaline-ion (li+, na+) conductors by ion exchange of proton-conducting ionomers and polyelectrolytes. *ChemPhysChem*, 12(14):2558–2560.

[90] Krishnamoorthy, A. N., Holm, C., and Smiatek, J. (2018a). The influence of co-solutes on the chemical equilibrium - a kirkwood-buff theory for ion pair association-dissociation processes in ternary electrolyte solutions. *J. Phys. Chem. C*, 122:10293–10302.

[91] Krishnamoorthy, A. N., Holm, C., and Smiatek, J. (2018b). Specific ion effects for polyelectrolytes in aqueous and non-aqueous media: the importance of the ion solvation behavior. *Soft Matter*, 14(30):6243–6255.

[92] Krishnamoorthy, A. N., Zeman, J., Holm, C., and Smiatek, J. (2016). Preferential solvation and ion association properties in aqueous dimethyl sulfoxide solutions. *Phys. Chem. Chem. Phys.*, 18(45):31312–31322.

[93] Kunz, W. (2010a). *Specific ion effects*. World Scientific.

[94] Kunz, W. (2010b). *Specific ion effects*. World Scientific.

[95] Kusalik, P. G. and Patey, G. (1987). The thermodynamic properties of electrolyte solutions: Some formal results. *J. Chem. Phys.*, 86(9):5110–5116.

[96] Kusalik, P. G. and Patey, G. (1988a). On the molecular theory of aqueous electrolyte solutions. i. the solution of the rhnc approximation for models at finite concentration. *J. Chem. Phys.*, 88(12):7715–7738.

[97] Kusalik, P. G. and Patey, G. (1988b). On the molecular theory of aqueous electrolyte solutions. ii. structural and thermodynamic properties of different models at infinite dilution. *J. Chem. Phys.*, 89(9):5843–5851.

[98] Lee, C., Yang, W., and Parr, R. G. (1988). Development of the Colle-Salvetti correlation-energy formula into a functional of the electron density. *Phys. Rev. B*, 37:785–789.

[99] Lesch, V., Heuer, A., Holm, C., and Smiatek, J. (2015a). Solvent effects of 1-ethyl-3-methylimidazolium acetate: solvation and dynamic behavior of polar and apolar solutes. *Phys. Chem. Chem. Phys.*, 17(13):8480–8490.

[100] Lesch, V., Heuer, A., Holm, C., and Smiatek, J. (2016a). Properties of apolar solutes in alkyl imidazolium-based ionic liquids: The importance of local interactions. *ChemPhysChem*, 17(3):387–394.

[101] Lesch, V., Heuer, A., Rad, B. R., Winter, M., and Smiatek, J. (2016b). Atomistic insights into deep eutectic electrolytes: the influence of urea on the electrolyte salt litfsi in view of electrochemical applications. *Phys. Chem. Chem. Phys.*, 18(41):28403–28408.

[102] Lesch, V., Heuer, A., Tatsis, V. A., Holm, C., and Smiatek, J. (2015b). Peptides in the presence of aqueous ionic liquids: tunable co-solutes as denaturants or protectants? *Phys. Chem. Chem. Phys.*, 17(39):26049–26053.

[103] Li, S., Zhao, D., Wang, P., Cui, X., and Tang, F. (2016). Electrochemical effect and mechanism of adiponitrile additive for high-voltage electrolyte. *Electrochim. Act.*, 222:668–677.

[104] Lo Nostro, P. and Ninham, B. W. (2012). Hofmeister Phenomena: An Update on Ion Specificity in Biology. *Chem. Rev.*, 112(4):2286–2322.

[105] Lopes, J. N. C. and Pádua, A. A. (2012). Cl&p: A generic and systematic force field for ionic liquids modeling. *Theo. Chem. Acc.*, 131(3):1129.

[106] Lund, M., Vácha, R., and Jungwirth, P. (2008). Specific ion binding to macromolecules: Effects of hydrophobicity and ion pairing. *Langmuir*, 24(7):3387–3391.

[107] Luzar, A. and Chandler, D. (1993). Structure and hydrogen bond dynamics of water–dimethyl sulfoxide mixtures by computer simulations. *J. Chem. Phys.*, 98(10):8160–8173.

[108] Manning, G. (1969). Limiting laws and counterion condensation in polyelectrolyte solutions I. colligative properties. *J. Chem. Phys.*, 51:924–933.

[109] Manning, G. S. and Ray, J. (1998). Counterion condensation revisited. *Journal of Biomolecular Structure and Dynamics*, 16(2):461–476.

[110] Marcus, Y. (1991). Preferential solvation of silver (i), copper (i) and copper (ii) ions in aqueous acetonitrile. *J. Chem. Soc. Dalton Trans.*, (9):2265–2268.

[111] Marcus, Y. (2009). Effect of ions on the structure of water: structure making and breaking. *Chem. Rev.*, 109(3):1346–1370.

[112] Marcus, Y. (2015). *Ions in Solution and their Solvation*. John Wiley & Sons.

[113] Marcus, Y. and Hefter, G. (2006). Ion pairing. *Chem. Rev.*, 106(11):4585–4621.

[114] Mark, P. and Nilsson, L. (2001). Structure and dynamics of the tip3p, spc, and spc/e water models at 298 k. *J. Phys. Chem. A*, 105(43):9954–9960.

[115] Martyna, G. J., Klein, M. L., and Tuckerman, M. (1992). Nosé–hoover chains: The canonical ensemble via continuous dynamics. *Journal of Chemical Physics*, 97(4):2635–2643.

[116] Mazzini, V. and Craig, V. S. (2016). Specific-ion effects in non-aqueous systems. *Curr. Opin. Colloid Int. Sci.*, 23:82–93.

[117] Mazzini, V. and Craig, V. S. (2017). What is the fundamental ion-specific series for anions and cations? ion specificity in standard partial molar volumes of electrolytes and electrostriction in water and non-aqueous solvents. *Chemical science*, 8(10):7052–7065.

[118] Mazzini, V., Liu, G., and Craig, V. S. (2018). Probing the hofmeister series beyond water: Specific-ion effects in non-aqueous solvents. *J. Chem. Phys.*, 148(22):222805.

[119] Micciulla, S., Michalowsky, J., Schroer, M. A., Holm, C., von Klitzing, R., and Smiatek, J. (2016). Concentration dependent effects of urea binding to poly (n-isopropylacrylamide) brushes: a combined experimental and numerical study. *Phys. Chem. Chem. Phys.*, 18(7):5324–5335.

[120] Michalowsky, J., Schäfer, L. V., Holm, C., and Smiatek, J. (2017). A refined polarizable water model for the coarse-grained martini force field with long-range electrostatic interactions. *J. Chem. Phys.*, 146(5):054501.

[121] Nagahama, M., Hasegawa, N., and Okada, S. (2010). High voltage performances of li2nipo4f cathode with dinitrile-based electrolytes. *J. Electrochem. Soc.*, 157(6):A748–A752.

[122] Naji, A. and Netz, R. R. (2006). Scaling and universality in the counterion-condensation transition at charged cylinders. *Physical Review E*, 73(5):056105.

[123] Narayanan Kirshnamoorthy, A., Oldiges, K., Winter, M., Heuer, A., Cekic-Laskovic, I., Holm, C., and Smiatek, J. (2018). Electrolyte solvents for high voltage lithium ion batteries: ion correlation and specific anion effects in adiponitrile. *Physical Chemistry Chemical Physics*, 40(20):25701–25715.

[124] Narayanan Krishnamoorthy, A., Holm, C., and Smiatek, J. (2018). Influence of cosolutes on chemical equilibrium: a kirkwood–buff theory for ion pair association–dissociation processes in ternary electrolyte solutions. *The Journal of Physical Chemistry C*, 122(19):10293–10302.

[125] Neese, F. (2012). The ORCA program system. *WIRes Comput. Mol. Sci.*, 2:73–78.

[126] Netz, R. R. and Horinek, D. (2012). Progress in modeling of ion effects at the vapor/water interface. *Annu. Rev. Phys. Chem.*, 63:401–418.

[127] Neumann, M. (1983). Dipole moment fluctuation formulas in computer simulations of polar systems. *Mol. Phys.*, 50(4):841–858.

[128] Newman, K. E. (1994). Kirkwood–buff solution theory: derivation and applications. *Chem. Soc. Rev.*, 23(1):31–40.

[129] Nosé, S. and Klein, M. L. (1983). Constant pressure molecular dynamics for molecular systems. *Mol. Phys.*, 50(5):1055–1076.

[130] Okur, H. I., Hladílková, J., Rembert, K. B., Cho, Y., Heyda, J., Dzubiella, J., Cremer, P. S., and Jungwirth, P. (2017). Beyond the hofmeister series: ion-specific effects on proteins and their biological functions. *J. Phys. Chem. B*, 121(9):1997–2014.

[131] Oosawa, F. (1971). *Polyelectrolytes*. Marcel Dekker, New York.

[132] Oprzeska-Zingrebe, E. A. and Smiatek, J. (2018). Aqueous ionic liquids in comparison with standard co-solutes: differences and similarities in their interaction with protein and dna structures. *Biophys. Rev.*, page submitted.

[133] Parrinello, M. and Rahman, A. (1981). Polymorphic transitions in single crystals: A new molecular dynamics method. *J. Appl. Phys.*, 52(12):7182–7190.

[134] Paterová, J., Rembert, K. B., Heyda, J., Kurra, Y., Okur, H. I., Liu, W. R., Hilty, C., Cremer, P. S., and Jungwirth, P. (2013a). Reversal of the hofmeister series: specific ion effects on peptides. *J. Phys. Chem. B*, 117(27):8150–8158.

[135] Paterová, J., Rembert, K. B., Heyda, J., Kurra, Y. a., Okur, H. I., Liu, W. R., Hilty, C., Cremer, P. S., and Jungwirth, P. (2013b). Reversal of the hofmeister series: specific ion effects on peptides. *J. Phys. Chem. B*, 117(27):8150–8158.

[136] Pauric, A. D., Halalay, I. C., and Goward, G. R. (2016). Combined nmr and molecular dynamics modeling study of transport properties in sulfonamide based deep eutectic lithium electrolytes: Litfsi based binary systems. *Phys. Chem. Chem. Phys.*, 18(9):6657–6667.

[137] Pierce, V., Kang, M., Aburi, M., Weerasinghe, S., and Smith, P. E. (2008a). Recent applications of kirkwood-buff theory to biological systems. *Cell. Biochem. Biophys.*, 50:1–22.

[138] Pierce, V., Kang, M., Aburi, M., Weerasinghe, S., and Smith, P. E. (2008b). Recent applications of kirkwood-buff theory to biological systems. *Cell. Biochem. Biophys.*, 50:1–22.

[139] Pronk, S., Páll, S., Schulz, R., Larsson, P., Bjelkmar, P., Apostolov, R., Shirts, M. R., Smith, J. C., Kasson, P. M., van der Spoel, D., Hess, B., and Lindahl, E. (2013). Gromacs 4.5: a high-throughput and highly parallel open source molecular simulation toolkit. *Bioinformatics*, 29(7):845–854.

[140] Reichardt, C. and Welton, T. (2011). *Solvents and solvent effects in organic chemistry*. John Wiley & Sons.

[141] Rodríguez-Ropero, F. and van der Vegt, N. F. (2014). Direct osmolyte–macromolecule interactions confer entropic stability to folded states. *J. Phys. Chem. B*, 118(26):7327–7334.

[142] Rösgen, J., Pettitt, B. M., and Bolen, D. W. (2004a). Uncovering the basis for nonideal behavior of biological molecules. *Biochemistry*, 43(45):14472–14484.

[143] Rösgen, J., Pettitt, B. M., and Bolen, D. W. (2004b). Uncovering the basis for nonideal behavior of biological molecules. *Biochemistry*, 43(45):14472–14484.

[144] Rösgen, J., Pettitt, B. M., and Bolen, D. W. (2005). Protein folding, stability, and solvation structure in osmolyte solutions. *Biophys. J.*, 89(5):2988–2997.

[145] Rösgen, J., Pettitt, B. M., and Bolen, D. W. (2007). An analysis of the molecular origin of osmolyte-dependent protein stability. *Protein Sci.*, 16(4):733–743.

[146] Sabatini, R., Gorni, T., and de Gironcoli, S. (2013). Nonlocal van der waals density functional made simple and efficient. *Phys. Rev. B*, 87:041108.

[147] Savelyev, A. and Papoian, G. A. (2006). Electrostatic, steric, and hydration interactions favor na+ condensation around dna compared with k+. *J. Am. Chem. Soc.*, 128(45):14506–14518.

[148] Schmitz, R. W., Murmann, P., Schmitz, R., Müller, R., Krämer, L., Kasnatscheew, J., Isken, P., Niehoff, P., Nowak, S., Röschenthaler, G.-V., et al. (2014). Investigations on novel electrolytes, solvents and sei additives for use in lithium-ion batteries: Systematic electrochemical characterization and detailed analysis by spectroscopic methods. *Progr. Sol. State Chem.*, 42(4):65–84.

[149] Schneider, H. and Strehlow, H. (1962). Über auswählende solvatation von ionen in lösungsmittelgemischen. ii. *Z. Elektrochem.*, 66(4):309–312.

[150] Schröder, C. (2017). Proteins in ionic liquids: Current status of experiments and simulations. *Top. Curr. Chem.*, 375(2):25.

[151] Schröder, C., Haberler, M., and Steinhauser, O. (2008). On the computation and contribution of conductivity in molecular ionic liquids. *J. Chem. Phys.*, 128(13):134501.

[152] Schröder, C. and Steinhauser, O. (2009). On the dielectric conductivity of molecular ionic liquids. *J. Chem. Phys.*, 131(11):114504.

[153] Schuler, L. D., Daura, X., and Van Gunsteren, W. F. (2001). An improved gromos96 force field for aliphatic hydrocarbons in the condensed phase. *Journal of Computational Chemistry*, 22(11):1205–1218.

[154] Schurr, J. M. and Fujimoto, B. S. (2002). Extensions of counterion condensation theory. i. alternative geometries and finite salt concentration. *Biophys. Chem.*, 101:425–445.

[155] Schurr, J. M. and Fujimoto, B. S. (2003). Extensions of counterion condensation theory. 2. cell model and osmotic pressure of dna. *J. Phys. Chem. B*, 107(18):4451–4458.

[156] Schurr, J. M., Rangel, D. P., and Aragon, S. R. (2005). A contribution to the theory of preferential interaction coefficients. *Biophys. J.*, 89(4):2258–2276.

[157] Schütt, K. T., Arbabzadah, F., Chmiela, S., Müller, K. R., and Tkatchenko, A. (2017). Quantum-chemical insights from deep tensor neural networks. *Nature Communications*, 8:13890 EP –. Article.

[158] Schwierz, N., Horinek, D., and Netz, R. R. (2013). Anionic and cationic hofmeister effects on hydrophobic and hydrophilic surfaces. *Langmuir*, 29(8):2602–2614.

[159] Schwierz, N., Horinek, D., and Netz, R. R. (2014). Specific ion binding to carboxylic surface groups and the ph dependence of the hofmeister series. *Langmuir*, 31(1):215–225.

[160] Sears, P. G., Caruso, J. A., and Popov, A. I. (1967). Conductances of some uni-univalent electrolytes in adiponitrile at 25. degree. *J. Phys. Chem.*, 71(4):905–909.

[161] Sega, M., Kantorovich, S., Holm, C., and Arnold, A. (2014). Communication: Kinetic and pairing contributions in the dielectric spectra of electrolyte solutions. *J. Chem. Phys.*, 140(21):211101.

[162] Sega, M., Kantorovich, S. S., Arnold, A., and Holm, C. (2013). On the calculation of the dielectric properties of liquid ionic systems. In Kalmykov, Y. P., editor, *Recent Advances in Broadband Dielectric Spectroscopy*, NATO Science for Peace and Security Series B: Physics and Biophysics, pages 103–122. Springer Netherlands.

[163] Seo, D. M., Borodin, O., Balogh, D., O'Connell, M., Ly, Q., Han, S.-D., Passerini, S., and Henderson, W. A. (2013). Electrolyte solvation and ionic association iii. acetonitrile-lithium salt mixtures–transport properties. *J. Electrochem. Soc.*, 160(8):A1061–A1070.

[164] Seo, D. M., Borodin, O., Han, S.-D., Boyle, P. D., and Henderson, W. A. (2012a). Electrolyte solvation and ionic association ii. acetonitrile-lithium salt mixtures: highly dissociated salts. *J. Electrochem. Soc.*, 159(9):A1489–A1500.

[165] Seo, D. M., Borodin, O., Han, S.-D., Ly, Q., Boyle, P. D., and Henderson, W. A. (2012b). Electrolyte solvation and ionic association. *J. Electrochem. Soc.*, 159(5):A553–A565.

[166] Shimizu, S. and Smith, D. J. (2004). Preferential hydration and the exclusion of cosolvents from protein surfaces. *J. Chem. Phys.*, 121(2):1148–1154.

[167] Shirke, R., Chaudhari, A., More, N., and Patil, P. (2001). Temperature dependent dielectric relaxation study of ethyl acetate—alcohol mixtures using time domain technique. *J. Mol. Liquids*, 94(1):27–36.

[168] Shulgin, I. L. and Ruckenstein, E. (2005). A protein molecule in an aqueous mixed solvent: Fluctuation theory outlook. *J. Chem. Phys.*, 123(5):054909.

[169] Shulgin, I. L. and Ruckenstein, E. (2006). The kirkwood-buff theory of solutions and the local composition of liquid mixtures. *J. Phys. Chem. B*, 110(25):12707–12713.

[170] Smiatek, J. (2014a). Osmolyte effects: Impact on the aqueous solution around charged and neutral spheres. *J. Phys. Chem. B*, 118(3):771–782.

[171] Smiatek, J. (2014b). Osmolyte effects: Impact on the aqueous solution around charged and neutral spheres. *J. Phys. Chem. B*, 118(3):771–782.

[172] Smiatek, J. (2017). Aqueous ionic liquids and their influence on protein conformations: an overview on recent theoretical and experimental insights. *J. Phys. Condens. Matter*, 29:233001.

[173] Smiatek, J., Hansen, N., and Kästner, J. (2016). Free energy calculation methods and rare event sampling techniques for biomolecular simulations. In *Simulating Enzyme Reactivity*, pages 185–214. RSC Publishing Group.

[174] Smiatek, J., Harishchandra, R. K., Galla, H.-J., and Heuer, A. (2013). Low concentrated hydroxiectoine solutions in presence of DPPC lipid bilayers: A computer simulation study. *Biophysical Chemistry*, 180:102–109.

[175] Smiatek, J., Wohlfarth, A., and Holm, C. (2014). The solvation and ion condensation properties for sulfonated polyelectrolytes in different solvents—a computational study. *New J. Phys.*, 16(2):025001.

[176] Smith, P. E. (1999). Computer simulation of cosolvent effects on hydrophobic hydration. *J. Phys. Chem. B*, 103(3):525–534.

[177] Smith, P. E. (2004). Cosolvent interactions with biomolecules:relating computer simulation data to experimental thermodynamic data. *J. Phys. Chem. B*, 108:18716–18724.

[178] Smith, P. E. (2006a). Chemical potential derivatives and preferential interaction parameters in biological systems from kirkwood-buff theory. *Biophys. J.*, 91(3):849–856.

[179] Smith, P. E. (2006b). Chemical potential derivatives and preferential interaction parameters in biological systems from kirkwood-buff theory. *Biophys. J.*, 91(3):849–856.

[180] Smith, P. E., Matteoli, E., and O'Connell, J. P. (2013). *Fluctuation theory of solutions: applications in chemistry, chemical engineering, and biophysics*. CRC Press.

[181] Sun, H., Li, Y., Wu, X., and Li, G. (2013). Theoretical study on the structures and properties of mixtures of urea and choline chloride. *J. Mol. Model.*, 19(6):2433–2441.

[182] Suo, L., Borodin, O., Gao, T., Olguin, M., Ho, J., Fan, X., Luo, C., Wang, C., and Xu, K. (2015). "water-in-salt" electrolyte enables high-voltage aqueous lithium-ion chemistries. *Science*, 350(6263):938–943.

[183] Suo, L., Borodin, O., Wang, Y., Rong, X., Sun, W., Fan, X., Xu, S., Schroeder, M. A., Cresce, A. V., Wang, F., et al. (2017). "water-in-salt" electrolyte makes aqueous sodium-ion battery safe, green, and long-lasting. *Adv. Energy Mat.*, 7(21):1701189.

[184] Tamura, R., Lin, J., and Miyazaki, T. (2018). Machine learning forces trained by gaussian process in liquid states: Transferability to temperature and pressure. *arXiv preprint arXiv:1810.05586*.

[185] Tersoff, J. (1998). *PRB*, 37:6991–7000.

[186] Thompson, A., Swiler, L., Trott, C., Foiles, S., and Tucker, G. (2015). Spectral neighbor analysis method for automated generation of quantum-accurate interatomic potentials. *Journal of Computational Physics*, 285:316 – 330.

[187] Unke, O. T. and Meuwly, M. (2018). A reactive, scalable, and transferable model for molecular energies from a neural network approach based on local information. *The Journal of Chemical Physics*, 148(24):241708.

[188] Vaisman, I. I. and Berkowitz, M. L. (1992). Local structural order and molecular associations in water-dmso mixtures. molecular dynamics study. *J. Am. Chem. Soc.*, 114(20):7889–7896.

[189] Van Der Vegt, N. F., Haldrup, K., Roke, S., Zheng, J., Lund, M., and Bakker, H. J. (2016). Water-mediated ion pairing: Occurrence and relevance. *Chem. Rev.*, 116(13):7626–7641.

[190] van der Vegt, N. F. A., Haldrup, K., Roke, S., Zheng, J., Lund, M., and Bakker, H. J. (2016). Water-mediated ion pairing: Occurrence and relevance. *Chem. Rev.*, 116(13):7626–7641.

[191] VandeVondele, J. and Hutter, J. (2007). Gaussian basis sets for accurate calculations on molecular systems in gas and condensed phases. *The Journal of Chemical Physics*, 127(11):114105.

[192] VandeVondele, J., Krack, M., Mohamed, F., Parrinello, M., Chassaing, T., and Hutter, J. (2005). Quickstep: Fast and accurate density functional calculations using a mixed gaussian and plane waves approach. *Computer Physics Communications*, 167(2):103–128.

[193] Vishnyakov, A., Lyubartsev, A. P., and Laaksonen, A. (2001). Molecular dynamics simulations of dimethyl sulfoxide and dimethyl sulfoxide-water mixture. *J. Phys. Chem. A*, 105(10):1702–1710.

[194] Vlachy, N., Jagoda-Cwiklik, B., Vácha, R., Touraud, D., Jungwirth, P., and Kunz, W. (2009). Hofmeister series and specific interactions of charged headgroups with aqueous ions. *Adv. Coll. Interface Sci.*, 146(1):42–47.

[195] Vydrov, O. A. and Van Voorhis, T. (2010). Nonlocal van der waals density functional: The simpler the better. *The Journal of Chemical Physics*, 133(24):244103.

[196] Wang, J. and Hou, T. (2011). Application of molecular dynamics simulations in molecular property prediction ii: Diffusion coefficient. *J. Comput. Chem.*, 32(16):3505–3519.

[197] Wang, J., Wang, W., Kollman, P. A., and Case, D. A. (2006). Automatic atom type and bond type perception in molecular mechanical calculations. *J. Mol. Graph. Model.*, 25(2):247–260.

[198] Wang, J., Wolf, R. M., Caldwell, J. W., Kollman, P. A., and Case, D. A. (2004). Development and testing of a general amber force field. *J. Comput. Chem.*, 25(9):1157–1174.

[199] Weerasinghe, S. and Smith, P. E. (2003). A kirkwood–buff derived force field for sodium chloride in water. *J. Chem. Phys.*, 119(21):11342–11349.

[200] Weerasinghe, S. and Smith, P. E. (2005). A kirkwood- buff derived force field for methanol and aqueous methanol solutions. *J. Phys. Chem. B*, 109(31):15080–15086.

[201] Weigend, F. and Ahlrichs, R. (2005). Balanced basis sets of split valence, triple zeta valence and quadruple zeta valence quality for H to Rn: Design and assessment of accuracy. *Phys. Chem. Chem. Phys.*, 7:3297–3305.

[202] Weyman, A., Bier, M., Holm, C., and Smiatek, J. (2018). Microphase separation and the formation of ion conductivity channels in poly (ionic liquid) s: A coarse-grained molecular dynamics study. *J. Chem. Phys.*, 148(19):193824.

[203] Winter, M. (2009). The solid electrolyte interphase–the most important and the least understood solid electrolyte in rechargeable li batteries. *Z. Phys. Chem.*, 223(10-11):1395–1406.

[204] Wohlfarth, A., Smiatek, J., Kreuer, K.-D., Takamuku, S., Jannasch, P., and Meier, J. (2015). Proton dissociation of sulfonated polysulfones: Influence of molecular structure and conformation. *Macromolecules*, 48:1134–1143.

[205] Wolynes, P. G. (1980). Dynamics of electrolyte solutions. *Annual Review of Physical Chemistry*, 31:345–376.

[206] Xu, K. (2004). Nonaqueous liquid electrolytes for lithium-based rechargeable batteries. *Chem. Rev.*, 104:4303–4417.

[207] Xu, K. (2014). Electrolytes and interphases in li-ion batteries and beyond. *Chem. Rev.*, 114:11503–11618.

[208] Yamada, Y. and Yamada, A. (2015). Superconcentrated electrolytes for lithium batteries. *J. Electrochem. Soc.*, 162(14):A2406–A2423.

[209] Zhang, N., Li, W., Chen, C., and Zuo, J. (2013). Molecular dynamics simulation of aggregation in dimethyl sulfoxide–water binary mixture. *Comput. Theo. Chem.*, 1017:126–135.

[210] Zhang, Y. and Cremer, P. S. (2006a). Interactions between macromolecules and ions: the hofmeister series. *Curr. Opin. Chem. Biol.*, 10(6):658–663.

[211] Zhang, Y. and Cremer, P. S. (2006b). Interactions between macromolecules and ions: the hofmeister series. *Curr. Opin. Chem. Biol.*, 10(6):658–663.

[212] Zhao, H. (2006). Are ionic liquids kosmotropic or chaotropic? an evaluation of available thermodynamic parameters for quantifying the ion kosmotropicity of ionic liquids. *J. Chem. Technol. Biotechnol.*, 81(6):877–891.

[213] Zhao, H. (2015). Protein stabilization and enzyme activation in ionic liquids: specific ion effects. *J. Chem. Technol. Biotechnol.*, 91:25–50.

[214] Zuo, Y., Chen, C., Li, X., Deng, Z., Chen, Y., Behler, J., Csányi, G., Shapeev, A., Thompson, A., Wood, M. A., and Ong, S. P. (2019). Performance and cost assesment of machine learning interatomic potentials. *Cornell University Press*.

Appendix A

Influence of co-solute on ion assocation-dissociation chemical equilibrium

A.1 Details of the simulated systems

Dimethyl acetamide (DMAc) was modeled using a Kirkwood Buff forcefield for amides [84]. The SPC/E water model was used and Kirkwood Buff alkali halide force fields were employed to model Na^+ and Cl^- ions[57]. All simulations were performed using the Gromacs 4.6.5 software package [139]. The system setup for different DMAc/water mixtures is shown in Tab. B.1. More details on the simulation protocol can be found in the main text.

We performed constrained molecular dynamics (MD) simulation in order to study the influence of co-solutes on associated and dissociated ion states. In more detail, we fixed the positions of a sodium and a chloride ion with a distance of 0.25 nm for the associated state and a distance of 1.3 nm for the dissociated state. These distances were chosen in accordance with the contact ion pair (CP) distance, as can be seen in Fig. A.1, and the maximum Bjerrum length $l_B^{\max} = 1.1$ nm in DMAc and water solutions at different concentrations. For all constrained MD simulations, the box sizes remained identical to the solvent mixture simulations, where only two water molecules were replaced by sodium and chloride ions. For the free ion simulations (MD without constraints on ion pair distances), a comparable setup was used, where ten ion pairs replaced an equivalent number of DMAc and water molecules in the system. The derivatives of the chemical activity coefficients (a_{33}) were obtained from the DMAc/water simulations. The values for the differences in the preferential binding coefficients $\Delta\nu_{23}$ between dissociated and associated ion state are obtained from

x_{DMAc}	DMAc molecules	water molecules	Box volume (nm^3)
0.00	0	2180	$4.01 \times 4.01 \times 4.01$
0.11	150	1262	$3.90 \times 3.90 \times 3.90$
0.12	165	1175	$3.90 \times 3.90 \times 3.90$
0.14	180	1094	$3.88 \times 3.88 \times 3.88$
0.16	195	1006	$3.88 \times 3.88 \times 3.88$
0.18	210	930	$3.87 \times 3.87 \times 3.87$
0.20	220	880	$3.87 \times 3.87 \times 3.87$
0.28	134	350	$3.09 \times 3.09 \times 3.09$
0.38	167	270	$3.17 \times 3.17 \times 3.17$
0.48	192	210	$3.25 \times 3.25 \times 3.25$
0.61	232	150	$3.38 \times 3.38 \times 3.38$
0.67	244	120	$3.43 \times 3.43 \times 3.43$
0.77	270	80	$3.49 \times 3.49 \times 3.49$
0.88	302	40	$3.60 \times 3.60 \times 3.60$
1.00	512	0	$4.25 \times 4.25 \times 4.25$

Table A.1 System setup for DMAc-water mixture simulations.

the constrained MD simulations. The association constant θ_c, as obtained from the free ion simulations (MD without constraints), is calculated with regard to a distance criterion of $r = 1.1$ nm.

A.2 Radial distribution functions for sodium and chloride ions

As can be seen in Fig. A.1, the center-of-mass radial distribution function $g_{\text{Na-Cl}}(r)$ for sodium and chloride ions at different mole fractions x_{DMAc} (*cf.* section A.1: MD without constraints) highlights the presence of a contact ion pair (CP) at distances $r \leq 0.28$ nm, and a solvent shared ion pair (1SP) between 0.38 nm $< r <$ 0.55 nm. The solvent separated ion pair (2SP) is only weakly visible at 0.6 nm $< r <$ 0.8 nm, and thus not clearly defined. In terms of the associated peak heights and the corresponding potentials of mean force (PMF)

$$\Delta_{\text{PMF}} = -k_B T \ln\left(\frac{g_{\text{Na-Cl}}(r)}{g_{\text{Na-Cl}}(r=\infty)}\right), \tag{A.1}$$

it becomes evident that the PMF of ion association is dominated by contact ion pairs, whereas the contribution of solvent shared ion pairs to the PMF is weakly pronounced, and the PMF value of 2SP is negligible.

In addition, it can be seen that the corresponding CP and 1SP peak heights increase with increasing mole fractions of DMAc (corresponding to larger net PMF values), which is a clear signature of co-solute assisted ion pair association with regard to a constant ion concentration.

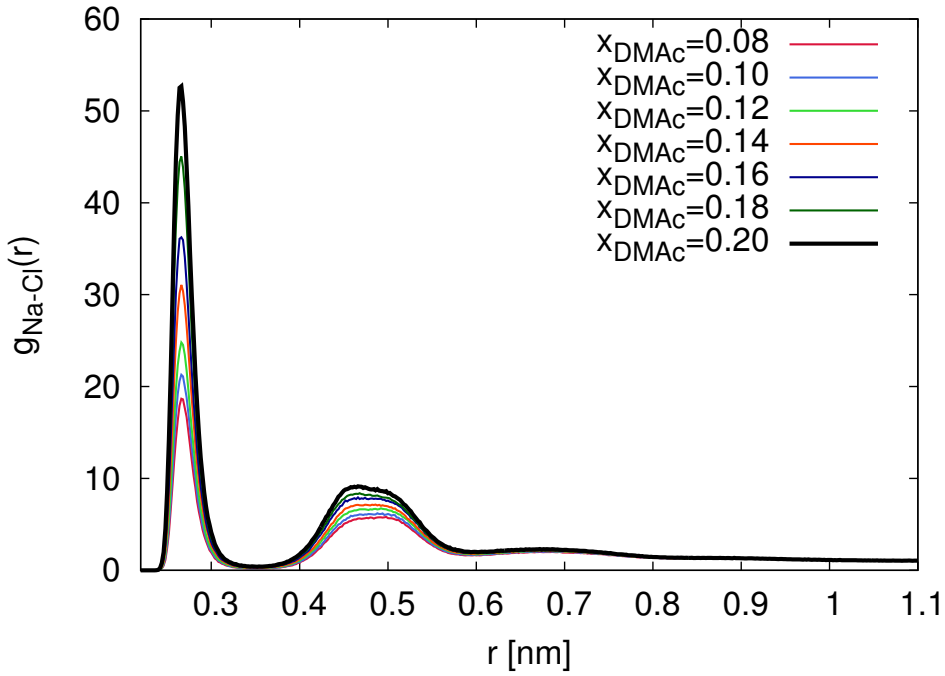

Fig. A.1 Radial distribution function for sodium and chloride ions in solutions with varying mole fractions of DMAc x_{DMAc} (MD without constraints) as denoted in the legend.

A.3 Distance-dependent ion association constant in pure water without constraints on ion positions

In order to compare our value for the ion association constant in pure water $\ln K^0 = 6.01 \pm 0.58$, as determined by linear regression analysis (we refer to the main article for further details), we evaluated the corresponding distance-dependent values

$$\ln K^0_{\mathrm{sim}}(r) = \ln\left(\frac{1-\theta^0_c(r)}{\theta^0_c(r)}\right) \tag{A.2}$$

with

$$\theta^0_c(r) = \frac{4\pi}{N_c}\rho_c \int_0^r r'^2 g_{\text{Na-Cl}}(r')\,\mathrm{d}r' \tag{A.3}$$

for sodium-chloride ions in pure water ($x_{\mathrm{DMAc}} = 0$ and MD without constraints). The results are shown in Fig. A.2. As can be seen, the values for $\ln K^0_{\mathrm{sim}}(r)$ are decreasing sharply for

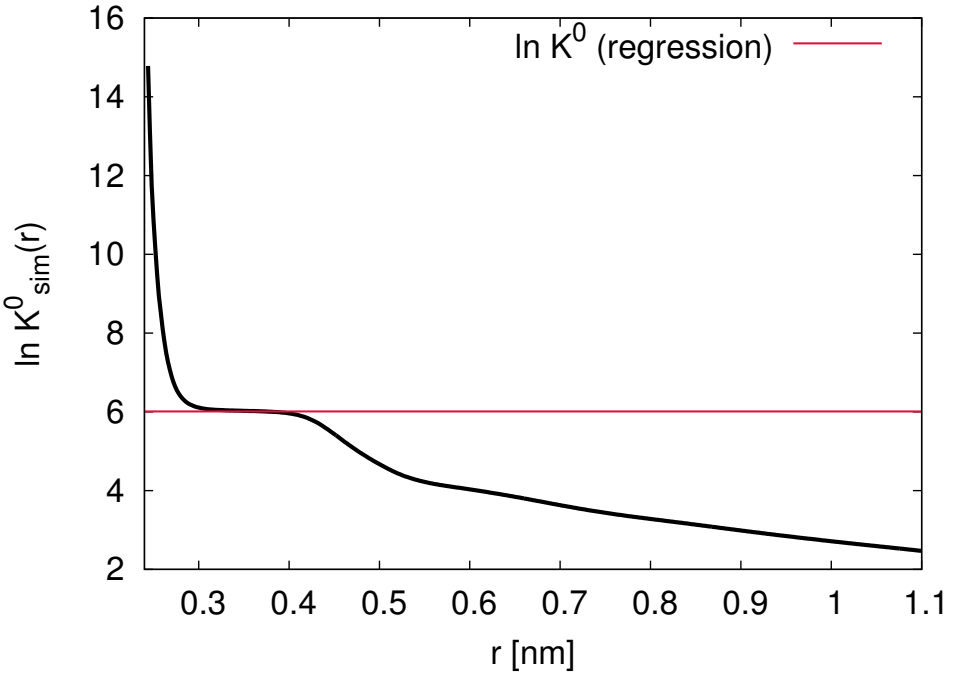

Fig. A.2 Values of $\ln K^0_{\mathrm{sim}}(r)$ in accordance with Eqn. (A.2) and Eqn. (A.3) for sodium-chloride pairing in pure water ($x_{\mathrm{DMAc}} = 0$). The red solid line denotes the value $\ln K^0 = 6.01$ as obtained by linear regression analysis of the corresponding m-values in the main text.

$r \leq 0.3$, whereas a constant value for 0.3 nm $< r <$ 0.45 nm can be observed, which is followed by a sharper (0.45 nm $\leq r <$ 0.52) and a moderate decrease at $r \geq 0.52$ nm.
In consequence, the association constant changes rapidly for $r \leq 0.3$, which also denotes the

distance of the contact ion pair (*cf.* Fig. (A.1)). Hence, ion association in pure water (and in presence of DMAc) is mostly dominated by contact ion pairs, whereas the contributions from 1SP and 2SP to $\ln K^0$ are less pronounced. This conclusion is also supported by the value $\ln K^0 = 6.01 \pm 0.59$ as evaluated by linear regression analysis (main text). The corresponding value agrees nicely with the value of $\ln K^0_{\text{sim}}(r)$ at $r = 0.3 - 0.42$ nm, which thus highlights the dominance of contact ion pairs as already discussed in section A.2.

A.4 Analysis of m-value for different associated ion pair reference states

As it was outlined in the main text, the *m*-value can be evaluated by

$$m = \left(\frac{\partial \ln K_{\mathrm{app}}}{\partial \rho_3} \right)_{T,p} = \frac{a_{33} \Delta \nu_{23}}{\rho_3} \tag{A.4}$$

in which a_{33} denotes the derivative of the chemical activity for DMAc in water/DMAc solution without ions, ρ_3 the bulk number density of DMAc, and $\Delta \nu_{23}$ the difference in the preferential binding coefficients with regard to the dissociated and the associated ion state, as obtained from the constrained MD simulations. In the main text, we mainly focused on the preferential binding coefficient to the contact pair state with an ion distance of 0.25 nm. Here, we also study the value of $\Delta \nu_{23}$ for an intermediate state at 0.32 nm (IS), and a solvent-shared state (1SP) at 0.44 nm in comparison to the dissociated ion state with an ion distance of 1.3 nm (*cf.* Fig. (A.1)). In consequence, we performed additional constrained MD simulations for the IS and 1SP state in analogy to the CP state. Due to a missing clear signature of the associated 2SP state, we ignore it as a well-defined reference state.

As can be seen in Fig. A.3, the *m*-values, when calculated by Eqn. (A.4), vary only slightly for the different associated ion pair states (CP, IS and 1SP). With regard to these results, it can be concluded that the differences in the preferential binding coefficient $\Delta \nu_{23}$ with regard to distinct associated ion pair states only slightly modify the value of *m* in accordance with Eqn. (A.4), as long as these states significantly differ from the dissociated ion state.

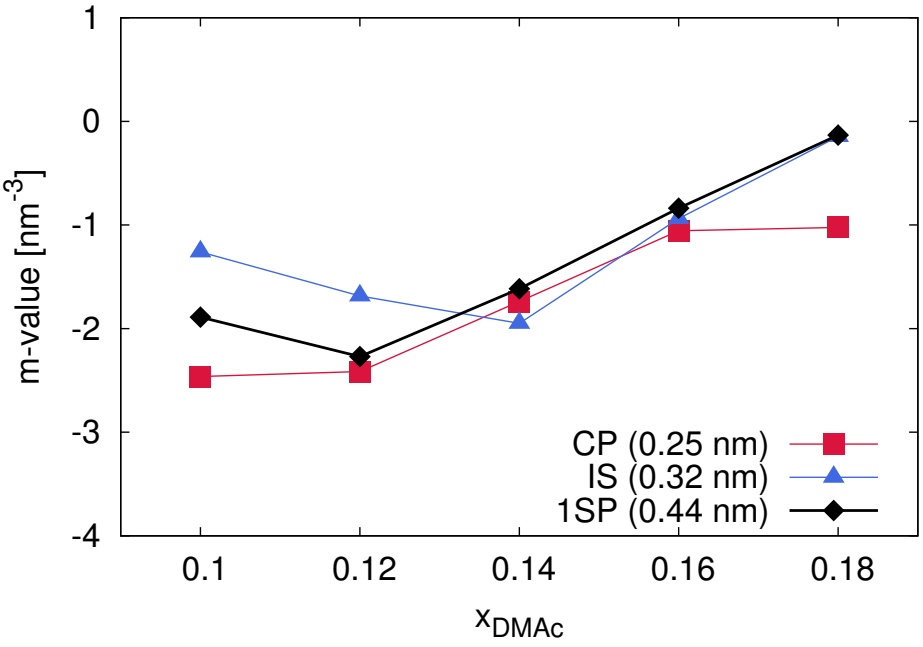

Fig. A.3 Values of *m* in accordance with Eqn. (A.4) for different mole fractions of DMAc and with regard to different associated ion pair reference states (CP, IS and 1SP) as denoted in the legend. More details can be found in the text.

A.5 Analysis of the derivative of the chemical activity for different associated ion pair reference states

The values of the chemical activity can be either calculated in terms of a Kirkwood-Buff approach

$$a_{33}(\mathrm{KB}) = \left(\frac{\partial \ln a_3}{\partial \ln \rho_3}\right)_{T,p} = \frac{1}{1+\rho_3(G_{33}-G_{31})} \tag{A.5}$$

for water/DMAc mixtures without ions, and equivalently by

$$a_{33} = \frac{\ln(K_{\mathrm{cs}}/K^0)}{\Delta\nu_{23}} \tag{A.6}$$

in terms of a linear regression analysis with the ion association constant in pure water $\ln K^0$, and in presence of co-solutes $\ln K_{\mathrm{cs}}$, and with the corresponding differences in the preferential binding coefficients $\Delta\nu_{23}$. More details on the corresponding analysis can be found in the main text, where the contact ion pair (CP) and the dissociated ion pair were chosen as reference states. Here, we explicitly focus on IS and 1SP instead of CP as corresponding associated ion pair reference states in order to study the robustness of Eqn. (A.6) with regard to different reference states and different values of $\Delta\nu_{23}$ (more details on the ion states can be found in section A.2). For the corresponding analysis, we performed additional constrained simulations with fixed ion pair distances of 0.32 nm (IS) and 0.44 nm (1SP). As association constant in pure water, we chose $\ln K_0 = 6.01$ in agreement with the results in the main text (linear regression analysis), and the corresponding values for $\ln K_{\mathrm{cs}}$ were evaluated for all ions within a distance of 1.1 nm as it was also discussed in more detail in the article.
The corresponding values in accordance with Eqn. (A.5) and Eqn. (A.6) are shown in Fig. A.4. As can be seen, the corresponding values for distinct reference states highlight a good agreement between a_{33} and $a_{33}(\mathrm{KB})$ for values $a_{33}(\mathrm{KB}) \leq 2$. In fact, non-ideal effects, as discussed in the main text, become more pronounced for less stable associated ion pair states (1SP and IS vs. CP) as can be seen for $a_{33} = 3.6$ corresponding to $\mathrm{x}_{\mathrm{DMAc}} = 0.3$.

A.6 Polyion-solvent and polyion-counterion coordination numbers

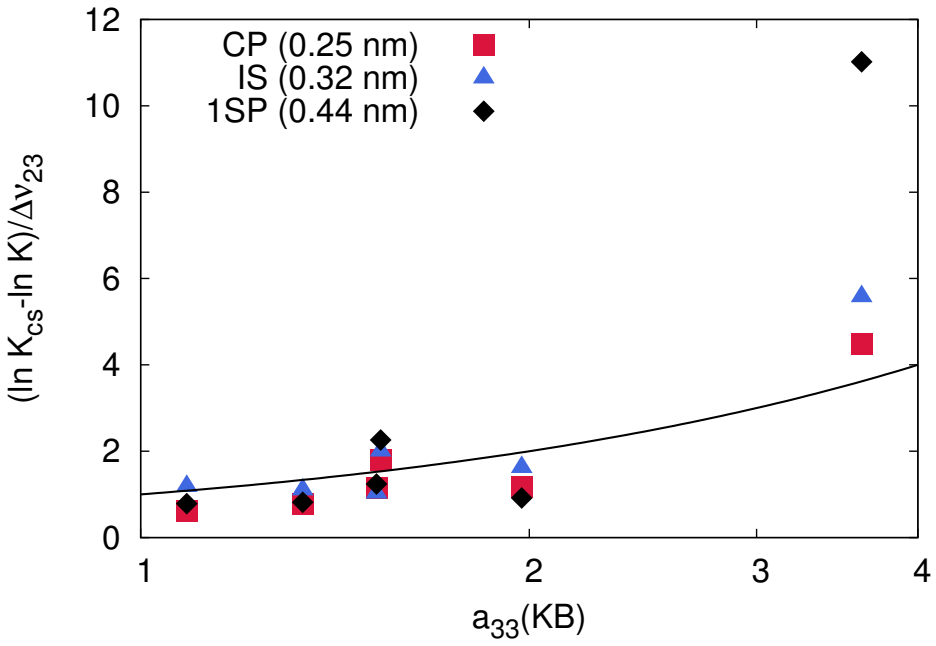

Fig. A.4 Values for the derivative of the chemical activity $a_{33}(\mathrm{KB})$ (KB approach with Eqn. (A.5)) in comparison to the values for a_{33} as obtained by linear regression (Eqn. (A.6)) for DMAc mole fractions between $x_{\mathrm{DMAc}} = 0.08 - 0.3$. The black solid line corresponds to an exact agreement with slope equals unity on a logarithmic scale.

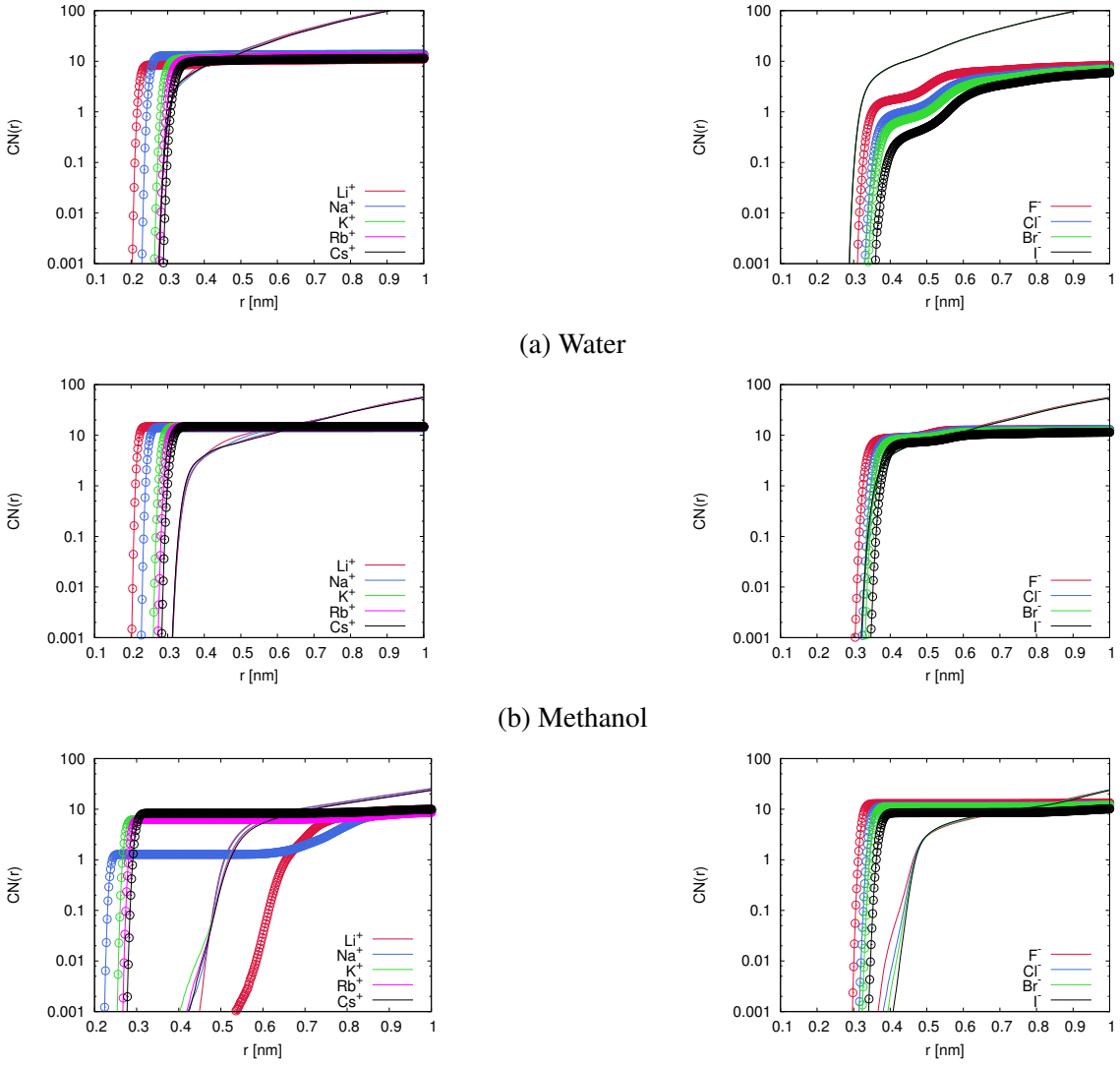

(a) Water

(b) Methanol

(c) DMAc

Fig. A.5 Coordination numbers CN(r) between polyion and solvents (solid lines) and between polyion and counterions (lines with datapoints). The left side shows the results for the cations and on the right side the results for the anions are presented. The results for water are shown in the top, methanol in the middle and DMAc in the bottom.

A.7 Potential of mean force between ions and solvent molecules

The potentials of mean force[173] are calculated by $\Delta_{\mathrm{PMF}}(r) = -k_B T \ln(g_{\pm s}(r)/g_{\pm s}(\infty))$ where $g_{\pm s}$ denotes the radial distribution function between ions and solvent molecules.

A.8 Total energies: ion-solvent and ion-polyelectrolyte interactions

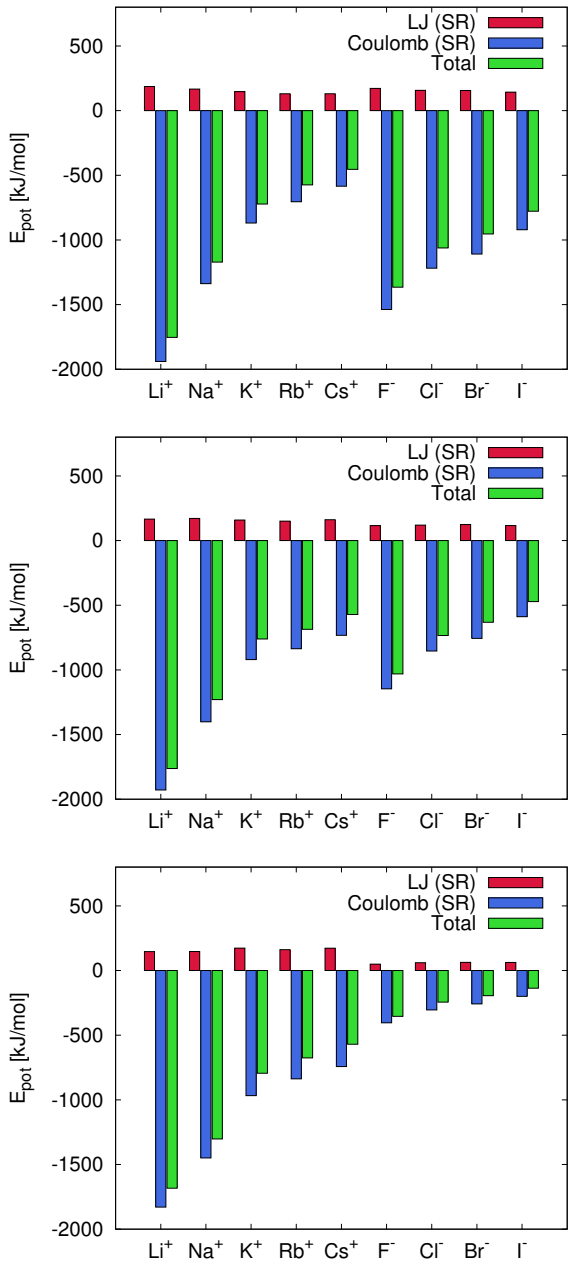

Fig. A.6 Sum of Lennard-Jones short-range (LJ (SR)) and Coulomb short-range (Coulomb (SR)) energies between ions and polyelectrolyte and ions and solvent in water (top), in methanol (middle) and in DMAc (bottom).

A.9 Interaction energies between ions

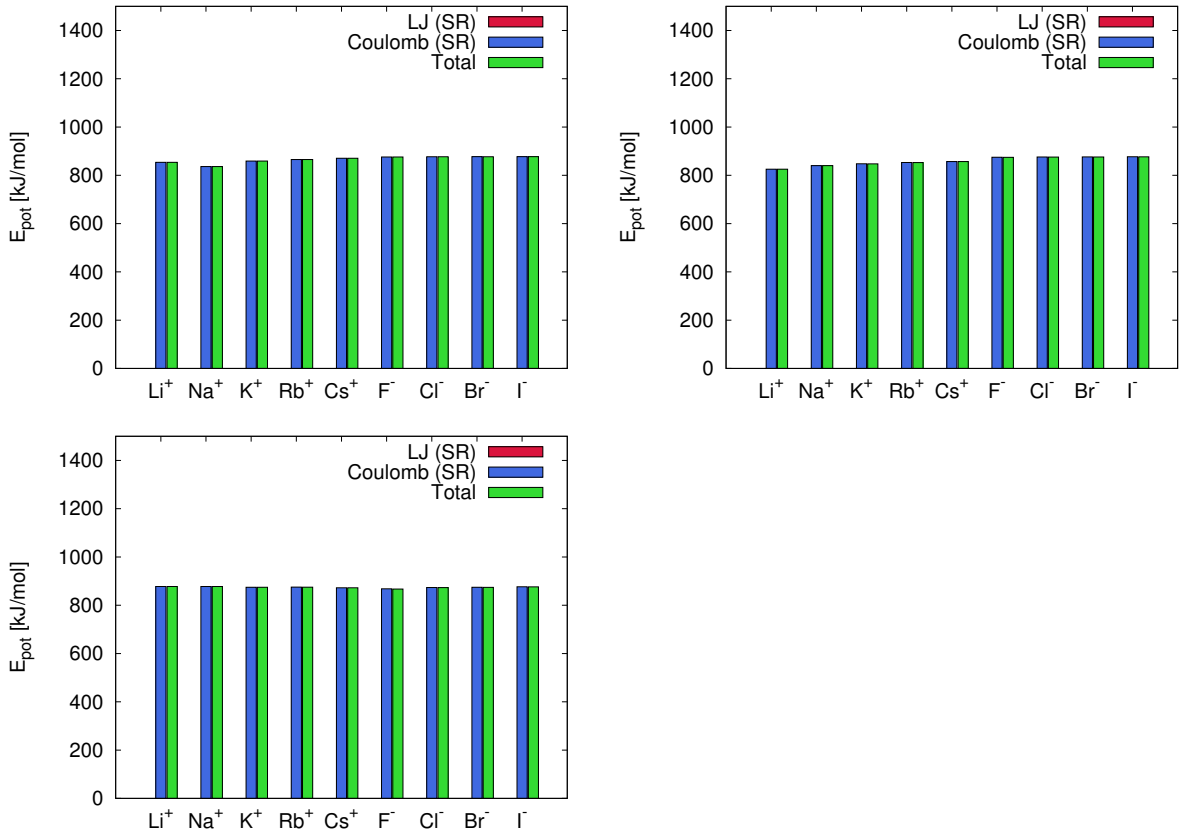

Fig. A.7 Lennard-Jones short-range (LJ (SR)) and Coulomb short-range (Coulomb (SR)) energies between ions in water (top), in methanol (middle) and in DMAc (bottom).

A.10 Ratio between LJ and electrostatic energies including ion-polyelectrolyte and ion-solvent interactions

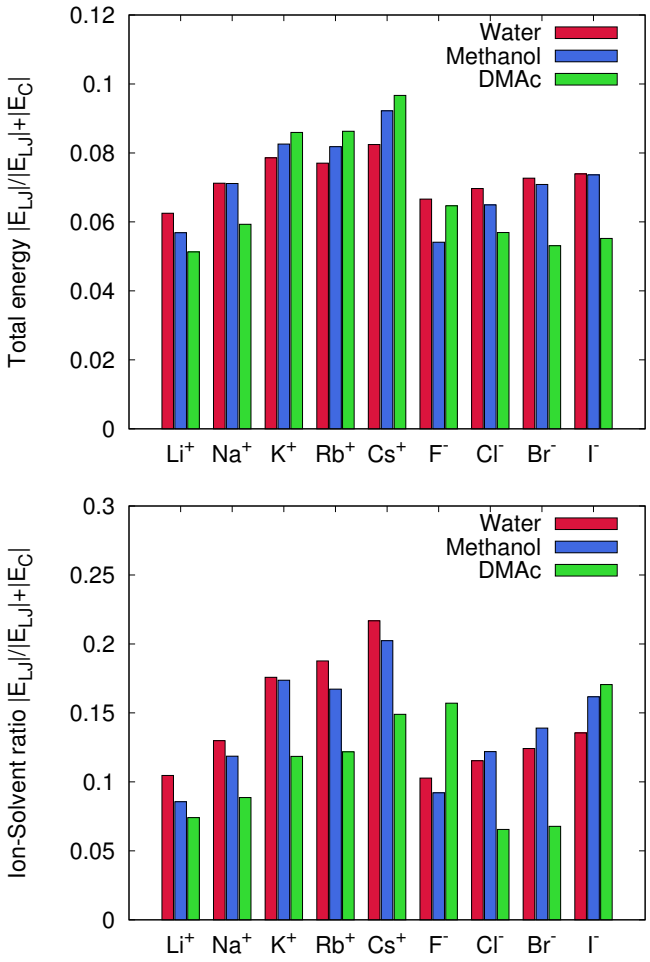

Fig. A.8 Ratio of Lennard-Jones to electrostatic interactions concerning the total interaction energy of the ions, including ion-solvent, and ion-polyelectrolyte interactions (top), and between the ions and the solvent molecules (bottom).

Table A.2 Diameters (taken from Ref. 57) for all ion species [57].

Ion	d_0 [nm]
Li^+	0.182
Na^+	0.245
K^+	0.334
Rb^+	0.362
Cs^+	0.413
F^-	0.370
Cl^-	0.440
Br^-	0.476
I^-	0.535

A.11 Closest contact distance between ions and polyion

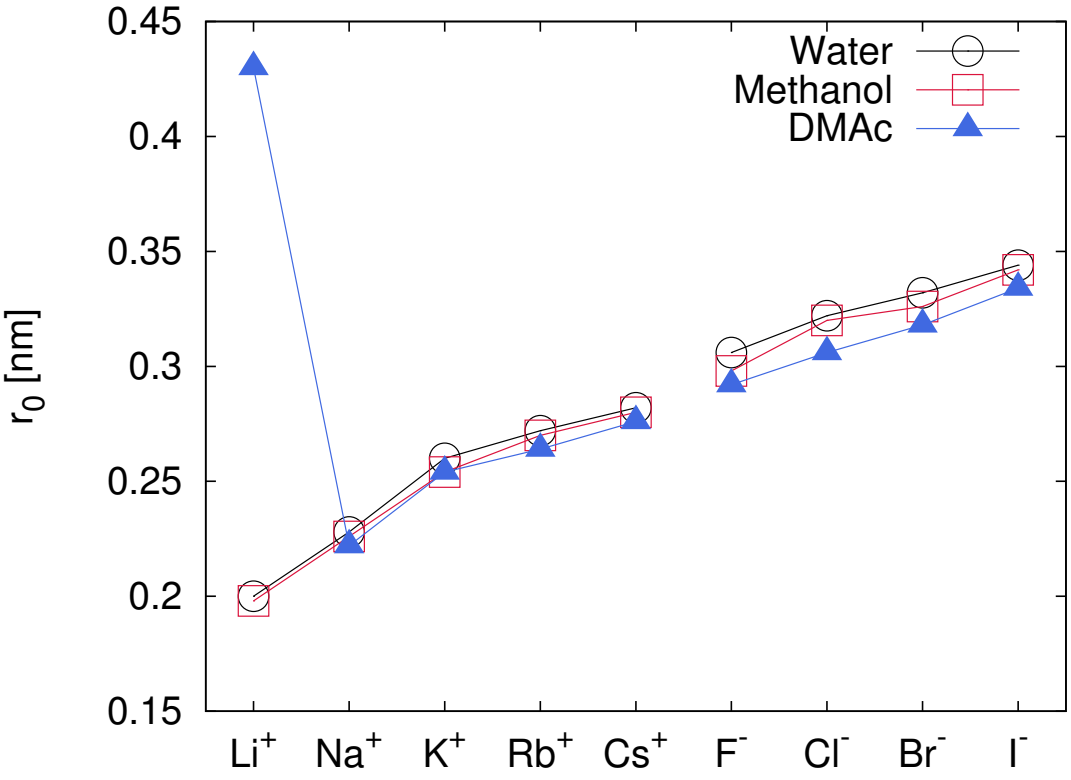

Fig. A.9 Closest contact distance r_0 between ions and polyions for all solvents and all ion species.

A.12 Closest contact distance between ions and solvent molecules

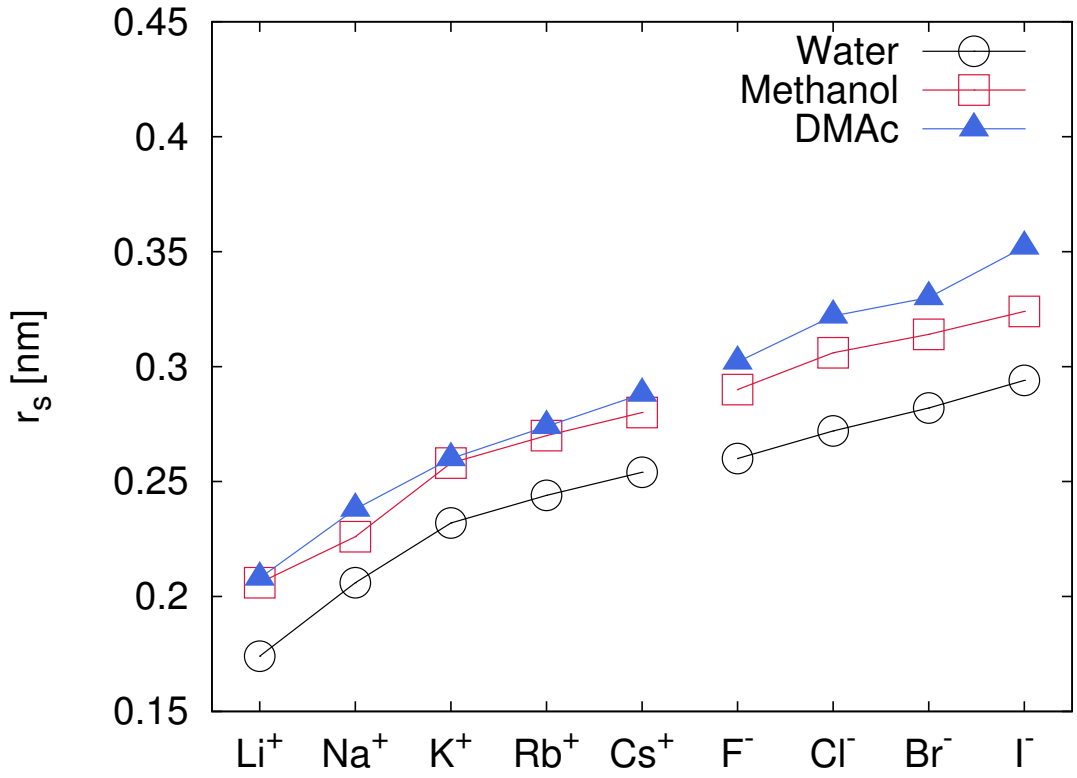

Fig. A.10 Closest contact distance r_s between ions and solvent molecules for all solvents and all ion species.

Appendix B

Additional Information

B.1 CHELPG partial charges for atoms of adiponitrile

Table B.1 shows the CHELPG partial charges for atoms of adiponitrile with regard to quantum chemical calculations as described in the main article. All other parameters (bonded and non-bonded interactions) are identical to the corresponding atom types defined in the OPLS/AA force field [82].

B.2 Mass densities: experimental and simulation results

Table B.1 CHELPG partial charges for atoms of adiponitrile. All other parameters are identical to Ref. 82.

Atom types	Partial charges $q\,[e]$
N	-0.53
C(N)	0.48
C3	-0.35
C(alkyl)	0.10
H(C3)	0.13
H(alkyl)	0.02

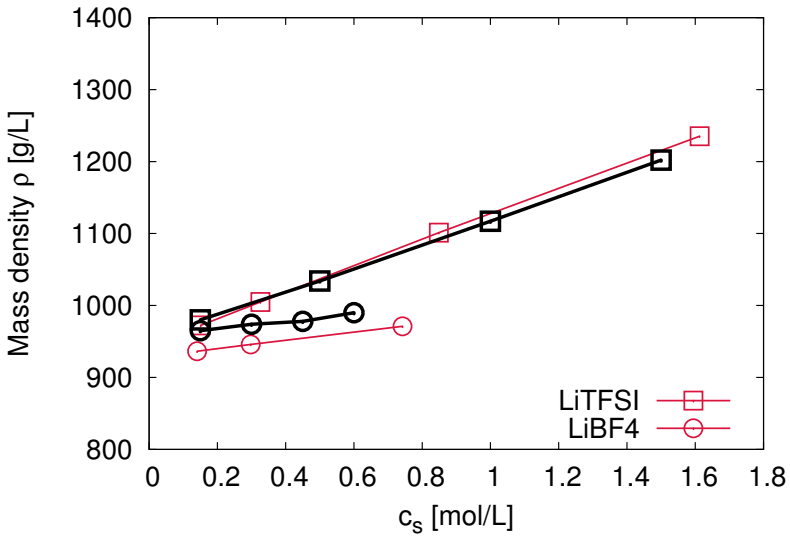

Fig. B.1 Mass densities of all simulated adiponitrile-lithium salt electrolyte formulations. Black symbols represent experimental results, whereas red symbols indicate simulation outcomes. The values for LiTFSI and LiBF4 electrolyte solutions with different salt concentrations c_s are marked as squares and circles, respectively.

B.3 Coordination number of adiponitrile molecules around lithium ions

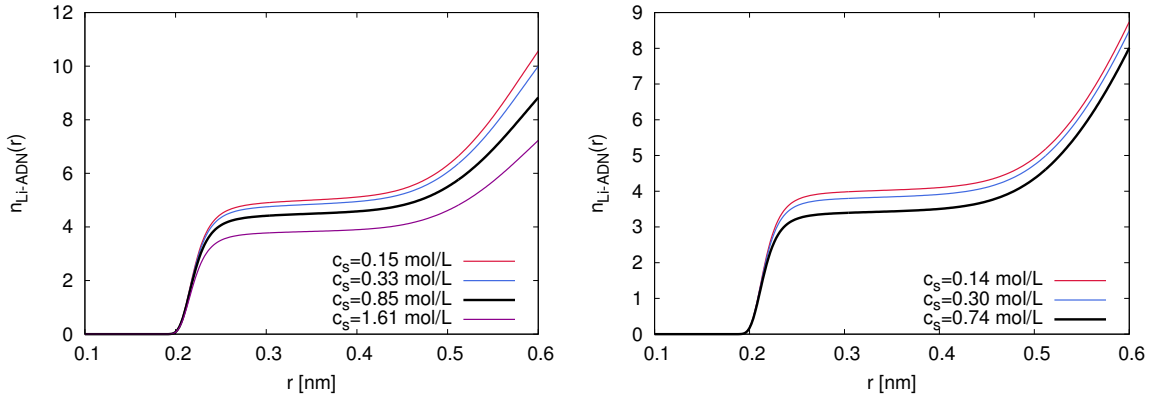

Fig. B.2 Left side: Coordination number of adiponitrile molecules $n_{\text{Li-ADN}}(r)$ around lithium ions for various salt concentrations of LiTFSI. Right side: Coordination number of adiponitrile molecules $n_{\text{Li-ADN}}(r)$ around lithium ions for various salt concentrations of $LiBF_4$.

B.4 Center-of-mass radial distribution functions between lithium ions and anions

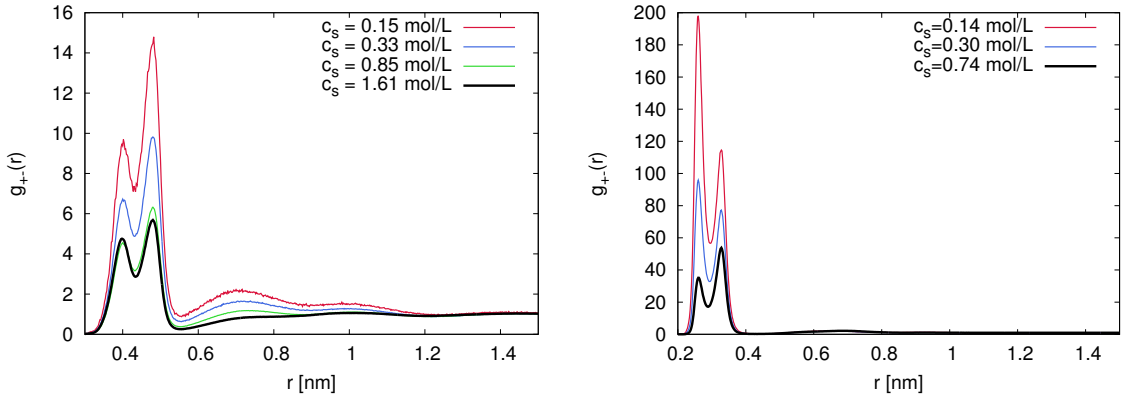

Fig. B.3 Left side: Center-of-mass radial distribution functions between lithium ions and TFSI anions for different salt concentrations c_s of LiTFSI in adiponitrile. Right side: Center-of-mass radial distribution functions between lithium ions and BF_4^- anions for different salt concentrations c_s of $LiBF_4$ in adiponitrile.

B.5 Radial distribution functions for LiTFSI: lithium ions and nitrogen atoms of $TFSI^-$ and adiponitrile

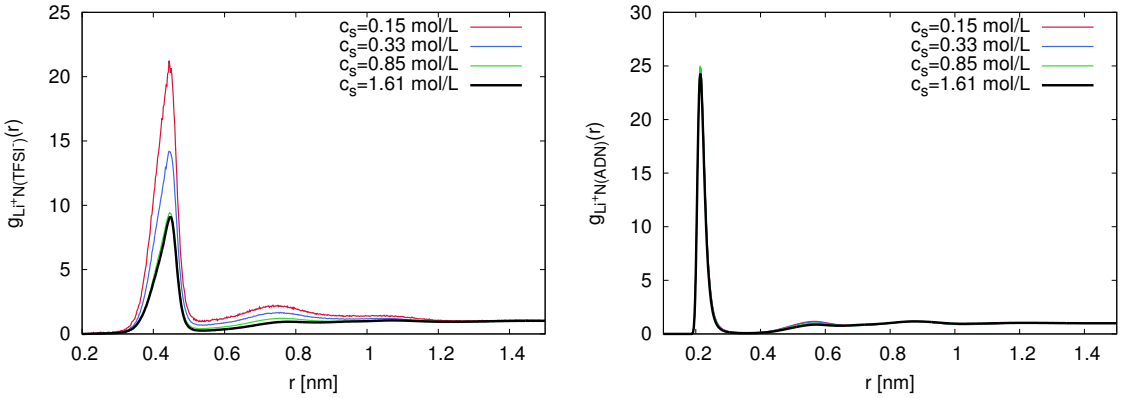

Fig. B.4 Left side: Atomic radial distribution functions between lithium ions and nitrogen atoms of TFSI anions for different salt concentrations c_s of LiTFSI in adiponitrile. Right side: Atomic radial distribution functions between lithium ions and nitrogen atoms of adiponitrile for different salt concentrations c_s of LiTFSI in adiponitrile.

B.6 Radial distribution functions for $LiBF_4$: lithium ions and fluorine atoms of BF_4^- and nitrogen atoms of adiponitrile

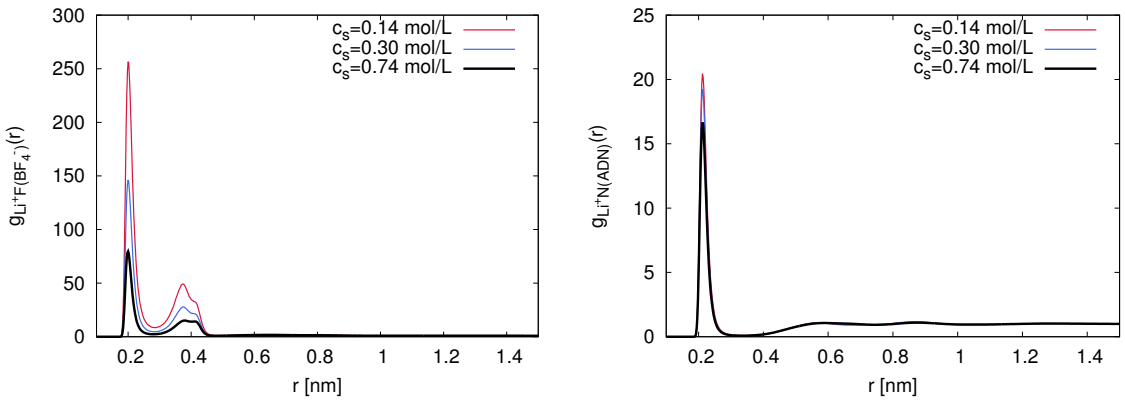

Fig. B.5 Left side: Atomic radial distribution functions between lithium ions and fluorine atoms of BF_4^- anions for different salt concentrations c_s of $LiBF_4$ in adiponitrile. Right side: Atomic radial distribution functions between lithium ions and nitrogen atoms of adiponitrile for different salt concentrations c_s of $LiBF_4$ in adiponitrile.

B.7 Relative coordination numbers in $LiBF_4$-ADN mixtures: local environment around lithium and BF_4^- ions

The relative coordination number around lithium and BF_4^- ions is defined as $n_{(+/-)j}(r) = n_j(r)/n_{\mathrm{tot}}(r)$, where $n_{\mathrm{tot}}(r)$ denotes the total coordination number of all species around the corresponding reference ions. The results for $LiBF_4$ are shown in Fig. B.6.

B.8 Relative coordination numbers in LiTFSI-ADN mixtures: local environment around lithium and $TFSI^-$ ions

The relative coordination number around lithium and $TFIS^-$ ions is defined as $n_{+/-}(r) = n_j(r)/n_{\mathrm{tot}}(r)$, where $n_{\mathrm{tot}}(r)$ denotes the total coordination number of all species around the correspondng reference ions. The results for LiTFSI are shown in Fig. B.7.

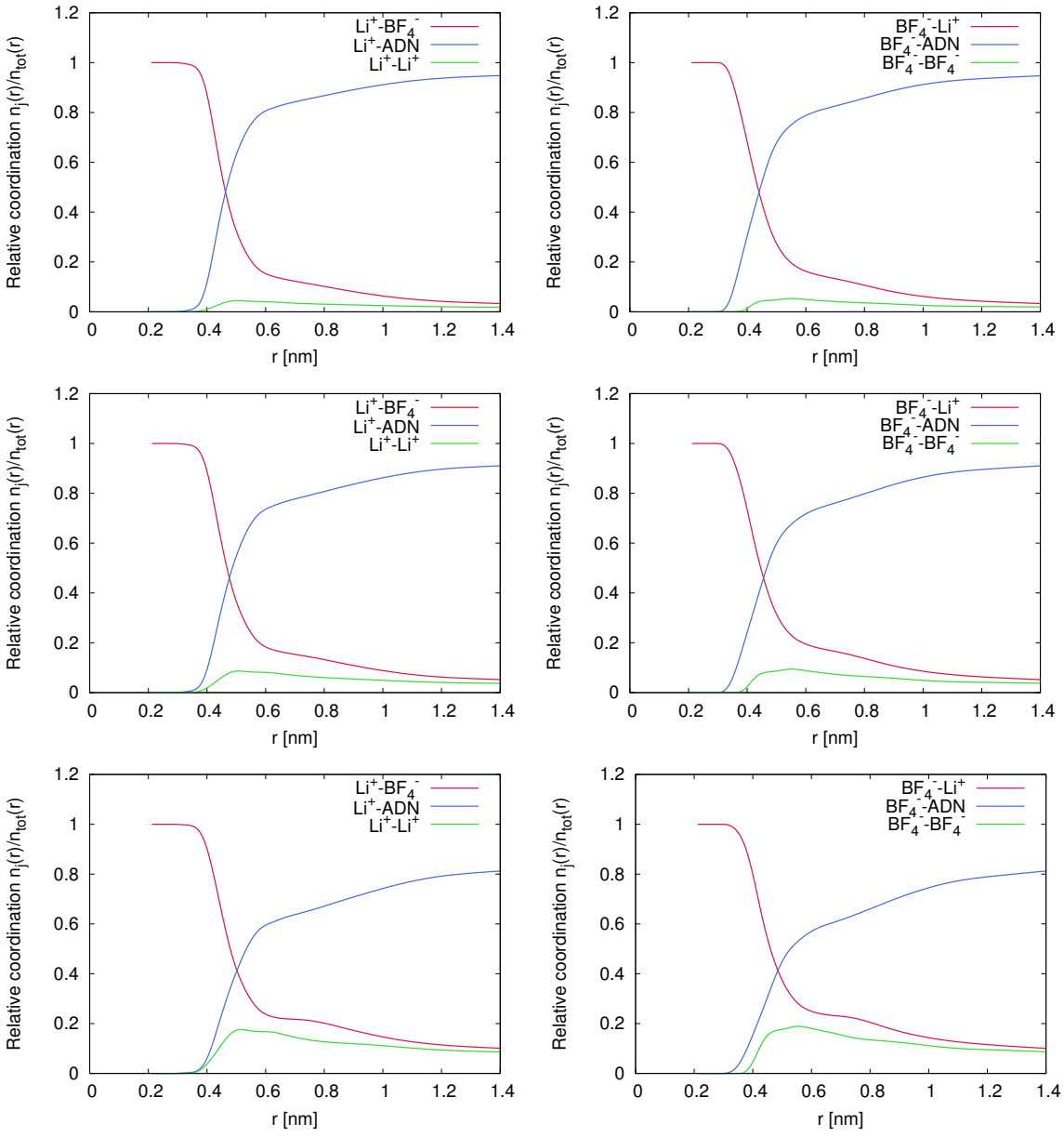

Fig. B.6 Relative coordination number for species $n_j(r)/n_{\text{tot}}(r)$ as denoted in the legend for different LiBF4 concentrations of $c_s = 0.14$ mol/L (top), $c_s = 0.30$ mol/L (middle), and $c_s = 0.74$ mol/L (bottom) around lithium (left side) and BF_4^- ions (right side).

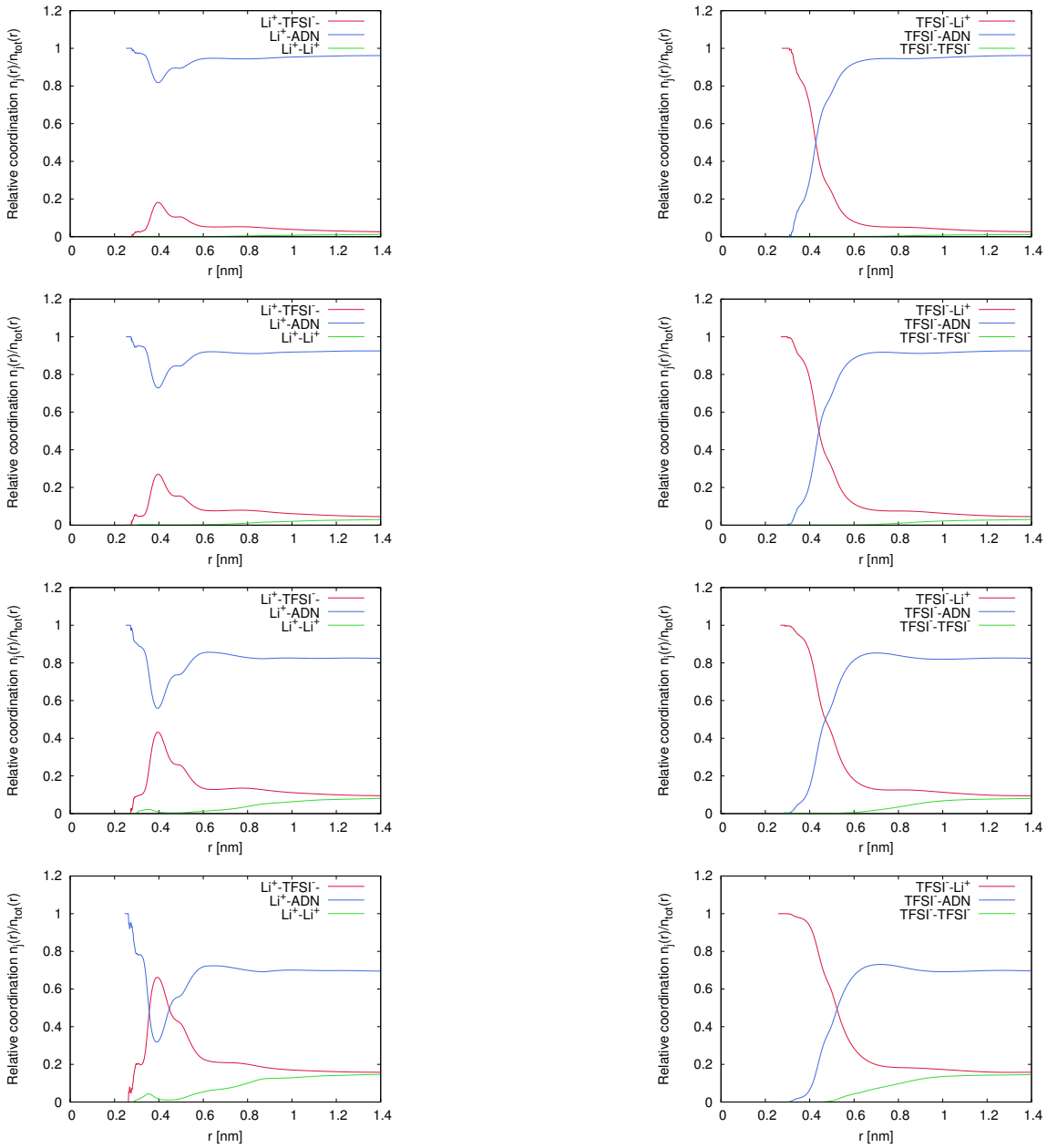

Fig. B.7 Relative coordination numbers for species $n_j(r)/n_{\text{tot}}(r)$ as denoted in the legend for different LiTFSI concentrations from top to bottom with $c_s = 0.15$ mol/L, $c_s = 0.33$ mol/L, $c_s = 0.85$ mol/L, and $c_s = 1.61$ mol/L around lithium (left side) and BF_4^- ions (right side)

B.9 Potentials of mean force between ions

Potentials of mean force (PMF) between the lithium ions and the corresponding anions were calculated in accordance with

$$\Delta_{\mathrm{PMF}} = -k_B T \ln g_{+-}(r) \tag{B.1}$$

where $g_{+-}(r)$ denotes the radial distribution function between Li^+ and anions (Ref. [33]).

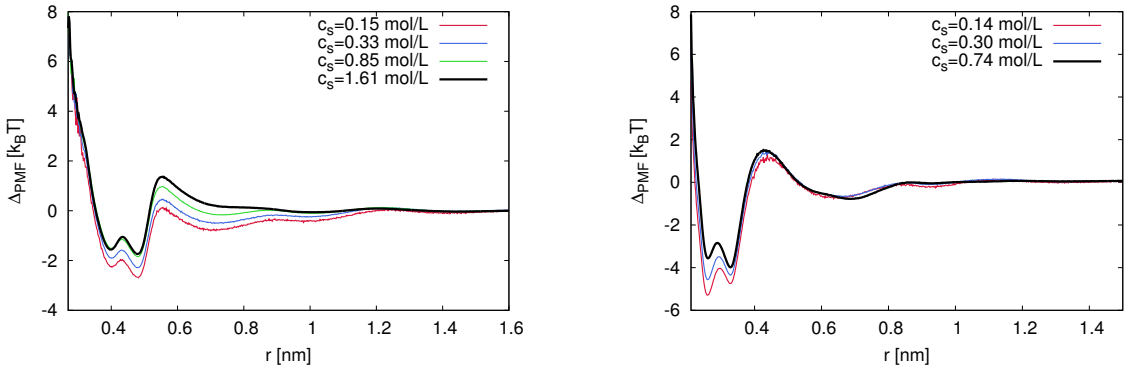

Fig. B.8 PMF values Δ_{PMF} between lithium ions and anions for different concentrations c_s of LiTFSI (left side) and $LiBF_4$ (right side).

B.10 Ion self-diffusion coefficients

B.11 Correlation between relaxation time scales

The relaxation times τ_{TST} for ion species are calculated in accordance with Eqn. 29 in the main text (values from Fig. 4). The ion relaxation times are calculated according to the values shown in Tab. 3 in the main text. All values are shown in Tab. B.2.

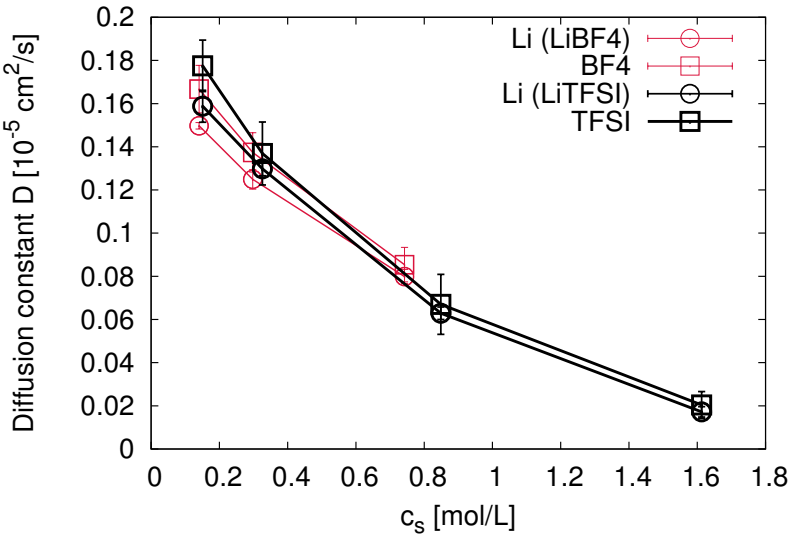

Fig. B.9 Self-diffusion coefficients for all ions at various salt concentrations c_s. The values for lithium ions are shown as circles (red color for lithium ions of LiTFSI and black color for lithium ions of $LiBF_4$). The corresponding results for the anions are shown as squares. The lines are just guides for the eye.

Table B.2 Relaxation τ_{TST} and corresponding ion correlation times τ for distinct concentrations c_s of LiTFSI and $LiBF_4$ in adiponitrile.

Salt	Concentration c_s [mol/L]	τ_{TST} [ns]	τ [ns]
LiTFSI	0.15	0.005	0.319
LiTFSI	0.33	0.003	0.454
LiTFSI	0.85	0.001	2.169
LiTFSI	1.61	0.001	80.002
$LiBF_4$	0.14	0.036	6.653
$LiBF_4$	0.30	0.101	6.653
$LiBF_4$	0.74	6.292	24.644